修士学位論文

論　　文　　題　　名

IMPACT OF TRACTOGRAPHY PARAMETERS ON BRAIN STRUCTURAL NETWORKS; THE CONNECTOME MAPPER

CONNECTOME MAPPER を用いた脳構造ネットワーク解析における TRACTOGRAPHY パラメータの影響

（西暦）　2018 年 07 月 06 日　提出

首都大学東京大学院

人間健康科学研究科 博士前期課程 人間健康科攻

放射線科学域

学修番号：16897617

氏　名：Wanni Arachchige Pradeepa Ruwan

（指導教員名：妹尾淳史）

修士学位論文

論　　文　　題　　名

IMPACT OF TRACTOGRAPHY PARAMETERS ON BRAIN STRUCTURAL NETWORKS; THE CONNECTOME MAPPER

CONNECTOME MAPPERを用いた脳構造ネットワーク解析におけるTRACTOGRAPHYパラメータの影響

（西暦）　　2018　年　07月　06　日　提出

首都大学東京大学院

人間健康科学研究科 博士前期課程 人間健康科学専攻

放射線科学域

学修番号：16897617

氏　名：Wanni Arachchige Pradeepa Ruwan

（指導教員名：　妹尾淳史）

別紙様式３（修士申請者用）

（西暦）　2018　　年度　博士前期課程学位論文要旨

YEAR　ABSTRACT OF MASTER'S THESIS

学位論文題名（注：学位論文題名が英語の場合は和訳をつけること）
IMPACT OF TRACTOGRAPHY PARAMETERS ON BRAIN STRUCTURAL NETWORKS; THE CONNECTOME MAPPER
CONNECTOME MAPPER を用いた脳構造ネットワーク解析における TRACTOGRAPHY パラメータの影響

学位の種類：　修士（放射線学）
Type of Degree: Master of Science in Radiological Sciences
首都大学東京大学院
Tokyo Metropolitan University
人間健康科学研究科　博士前期課程 人間健康科学専攻　放射線科学域
The Graduate School of Human Health Sciences, Master's Course
The Department of Radiological Sciences
学修番号/Student ID No.16897617
氏　名/Name　：WANNI ARACHCHIGE PRADEEPA RUWAN
（指導教員名/Supervisor：　PROF.ATSUSHI SENOO）

**Note: The abstract should be one to two A4 pages long. (One page should be around 300 words.)*

The process of reconstructing the white matter tracts using Diffusion Tensor Imaging (DTI) refers to tractography which is a key to structural connectivity since it is the best non-invasive technique to investigate brain networks. The structural networks which generate from diffusion may influence by tractography parameters. Thus, examine the optimum parameters can be beneficial as it helps to create better connectomes. In this study, we examine the tractography parameters of the Connectome Mapper. We aimed to optimise parameters including the number of seeds, step size and turning angle in tractography of the Connectome Mapper (www.cmtk.org) which is a combination of sophisticated neuroimaging tools. Therefore, we could be able to use a better choice of tractography parameters in future clinical studies.

DTI and T1 images of ten healthy subjects (3.0T, Philips, Achieva) were processed to construct connectivity matrices using the Connectome Mapper. The graph theory analysis was applied on connectivity matrices using Brain Connectivity Toolbox. Connectivity measures of five different number of seeds per voxel (15, 25, 35, 45, 55), step sizes (0.1 mm, 0.5 mm, 1 mm, 1.5 mm, 2 mm) and turning angles (40^0, 50^0, 60^0, 70^0, 80^0) were analysed for whole brain connectivity by estimating mean network measures including degree, betweenness centrality, local efficiency, cluster coefficient, eccentricity, strength, small-worldness and characteristic path length.

Our study emphasised that more connections can be obtained when increasing the tractography parameters. We suggested that given parameters are not any more

optimal than another in term of the number of seeds, turning angles or step size. While some cases showed drastic points that were not significant in many cases suggesting that the default values of tractography parameters would be appropriate to use in future studies. Moreover, future studies should give careful consideration to the choice of tractography parameter based upon the network measure that will be analysed.

Table of Contents

CHAPTER 1

Introduction

1.1 Background of the Research

Magnetic Resonance Imaging (MRI) is a widely available neuroimaging method that offers sophisticated structural and diffusion MRI (dMRI), in particular providing connectivity information in brain networks. Construction of structural brain connectivity based on dMRI which enables white matter structure analysis *in vivo* [1]. The novel advances in MRI such as Diffusion Tensor Imaging (DTI), tractography and Fractional Anisotropy (FA) maps have been evolving to analyse more complex brain networks using excellent brain mapping tools and protocols. Technological advancements in neuroimaging are increasingly combined with powerful network constructing tools in which is the basis of understanding the structural connectivity through the comprehensive map of anatomical regions of the human brain [2]. DTI provides microstructural details in the white matter fibre tracts using its application and advances technical methods which can cause to improve many investigations in neuroimaging than the conventional approach. Understanding Structural and functional networks are the essential development that has been gained using MRI and neuroimaging analysis tools in the past decade.

The concept of the brain networks of interconnected neurons has a far history in neurosciences. However, modern neuroimaging technology allows mapping of brain networks with interconnecting anatomical regions and pathways at microstructural resolution. The connectome derives from large-scale networks and provides a detailed description of structural connectivity in the brain [2]. The connectome is a network that made of nodes to represent anatomical brain regions and edges that can quantify the structural brain connectivity. Therefore, connectome is an abstract representation of neural connections. Generally, connectome creation based on fibre tracking algorithms which estimate trajectories to capture the orientation of maximal diffusion that could be a real representation of fibre tracts that shows the linking of various brain regions. Thus Tractography is key to connectivity analysis which needs to use diffusion information from tractography [3].

In general, mapping brain connectivity is crucial for the understanding of the function of the human brain [3]. Structural connectivity refers to anatomical connections which linking a set of neural elements. The primary concern of these connections is the white matter links with cortical and subcortical brain regions. Functional connectivity describes a pattern of statistical dependencies and effective connectivity explains casual effects of neural elements. Graph theory is used to interpret brain networks which consist of nodes to represent neural elements and edges to represent their mutual connections [2].

Tractography-based DTI data is widely used in studies of structural connectome. However, the reliability of DTI with its resolution and accuracy is not much apparent. Tractography allows to create trajectories of a fibre bundle in the white matter *in vivo* and extract the connectome of the brain [4]. Also, constructing structural and functional connections in the connectome is a challenging task when extracts the relevant aspects of

brain networks [2]. This challenge guides to apply modern network modelling, numerous tools and algorithms in neuroimaging [2] [4].

In the field of modern neurosciences, there are numerous state-of-the-art packages available freely. However, these tools can have some of the limitations and disadvantages at the practical level when using for the brain mapping. Therefore, the validation of technical parameters in some stages of the connectome creation can help to avoid issues arising in neuroimaging tools. On the other hand, results of the connectome analysis largely depend on tractography which based on a selection of parameters and algorithms of tractography [5]. Therefore, a comparison between different groups of parameters may have a possibility to alter network structures.

This study mainly designed with two tools including the Connectome Mapper Toolkit and the graph theory-based tool, Brain Connectivity Toolbox (BCT). The Connectome Mapper is a user-friendly software package that including dedicated neuroimaging tools together. The aim of creating the Connectome Mapper was to support researchers through the full processing pipeline for connectome creation using dMRI [2]. Graph theory analysis was applied on connectivity matrices which have obtained using the Connectome Mapper pipeline. In response, this work aims to investigate about parameters of tractography that can make changes on the graph theory analysis.

The Connectome Mapper performs full processing pipeline and creates connectivity matrices using dMRI data. The workflow of the Connectome Mapper depends on few stages and user is able to control parameters that provided in each stage at any time. The connectome analysis application can be used for various investigation particularly for brain plasticity after stroke. In addition, comparison of structural connectivity in two groups of pathological conditions is also possible with the connectome analysis [3].

Construction of connectomes and graph theory analysis has become a robust approach to understanding structural connectivity and functional connectivity as well. Tractography identifies the pathways of the white matter with anatomical regions and their networks. Therefore, this combination of graph theory and connectome creation through tractography could use to investigate some findings in neurological disorders and to deduce the relationship between structures and functions. The graph theory is applied while nodes define using anatomical parcellation, the edges define by tractography of the white matter for identifying white matter pathways which connect through brain regions [4]. Graph theory comprises various network measures to describe local and global connectivity in networks. These networks are also categorised as weighted and binary and directed and undirected networks. Therefore, network measures are used to illustrate these various representations of networks. The value of network measure is usually affected by characteristics of networks such as the number of nodes and edges [6].

1.2 Objectives

The objectives of this research were to understand the impact of tractography parameters on structural network measures using healthy subjects and to optimise tractography parameters related to the Connectome Mapper. Thus, we could be able to use

these optimal parameters in future clinical studies when constructing the connectomes using the Connectome Mapper.

1.3 Outline of the Thesis

Chapter 1

This chapter introduces the background of the research, objectives and design of the thesis briefly.

Chapter 2

Chapter 2 explains the theoretical background of the MRI with basic pulse sequences.

Chapter 3

The main content of chapter 3 is the theoretical concept of DWI including DTI and tractography.

Chapter 4

The concept of graph theory is described in this chapter by introducing network measures to describe brain connectivity.

Chapter 5

Chapter 5 presents the description of brain mapping and the descriptive information of the Connectome Mapper.

Chapter 6

Chapter 6 describes the tractography parameters.

Chapter 7

Chapter 7 describes the research content and provides the discussion, conclusion and present and future directions.

Chapter 8

Chapter 8 is a summary of the research.

CHAPTER 2

Basics of Magnetic Resonance Imaging

2.1 History of MRI

The physical principles of MRI underlie Nuclear Magnetic Resonance (NMR) which is an analytical chemistry technique based on spin and electrical charge of nuclei. The NMR phenomenon rapidly allowed development of clinical applications in medicine. The first successful demonstration of NMR was conducted in 1946, simultaneously by two American scientists, Felix Bloch and Edward Purcell with two different concepts. Bloch's observation was based on water molecule and Purcell studied with paraffin wax. Both Bloch and Purcell were jointly awarded the Nobel Prize for physics in 1952 [7].

In 1973, Paul Lauterbur invented that Magnetic Resonance can be used to create an image. Sir Peter Mansfield developed the utilisation of gradients in the magnetic field. Both, Lauterbur and Sir Peter Mansfield were awarded the Nobel Prize in Physiology and Medicine in 2013 for their concerns of discovering MRI. Raymond Damadian discovered the principles of MRI as a diagnostic tool in 1970 and published a paper in the journal Science in 1971, and a patent was granted in 1974. Raymond reported that NMR can be used distinguished tumours and normal tissues *in vivo*. However, construction of MRI was completed by 1977. Since then, the medical use of MRI was developed rapidly. In 1975, phase and frequency encoding were proposed by Richard Ernst and Ljunggren, and Twieg introduced k-space. The first MRI images in clinical were available in 1980. Since then MRI is widely available and serves as the primary imaging modality for many clinical issues [7].

2.2 Physics Overview of MRI

MRI is based on magnetisation properties of nuclei which consist of protons and neutrons. In the clinical MRI, Hydrogen (^1H) nuclei are used because of its composition of the body such as abundance in water and fat. When an external magnetic (B0) field placed across protons, they can be aligned with the magnetic field. Nuclei are randomly oriented in the absence of magnetic field. Nuclei such as ^1H and ^{13}C are nuclear spins (I) which can behave as a tiny magnetic bar either parallel or antiparallel to the magnetic when presence an external magnetic field. This alignment of the ^1H is known as magnetisation which can be caused by the precession of the proton. The Larmor equation defines the frequency of precision.

$$f_0 = \gamma B_0 \tag{2.1}$$

f_0 denotes precession frequency, B_0 denotes Strength of the external magnetic field and γ is the gyromagnetic ratio which is a constant for a specific nucleus or particle. For example; γ of ^1H is 42.57MHz/T.

The moment of the parallel and antiparallel nuclei is the net magnetisation vector which perturbs with radiofrequency (RF) pulses. RF pulse causes the net magnetisation to create a certain angle with the main magnetic field and produce two magnetisation components, longitudinal and transverse magnetisation. RF pulse usually lasts in

microsecond after applying, and nuclei absorb RF energy. Nuclei return to the resting alignment through relaxation process and generate free-induction decay (FID) signals. Tissues have different relaxation which refers to nuclei returns to thermal equilibrium after absorbing energy from RF pulses. There are two kinds of relaxation, longitudinal relaxation (T1) and transverse relaxation (T2) describe according to the time constant. During longitudinal relaxation, spins release energy to the surrounding lattice is also known as spin-lattice relaxation and spins are getting out of phase due to redistribution of energy within the spin system in T2 relaxation which is also known as spin-spin relaxation [8].

2.2.1 T1 Relaxation Time

Spin-lattice relaxation which is also known as T1 relaxation or longitudinal relaxation measures how quickly net magnetisation vector recovers to the ground state with the direction of B0. In this relaxation, spins return from high energy to low energy level with releasing energy to the surrounding nuclei as spins return to longitudinal magnetisation (Mz) exponentially. The rate is governed by the time of T1 which is the time takes to spin recovers 63% of its maximum magnetisation (Figure 2.1).

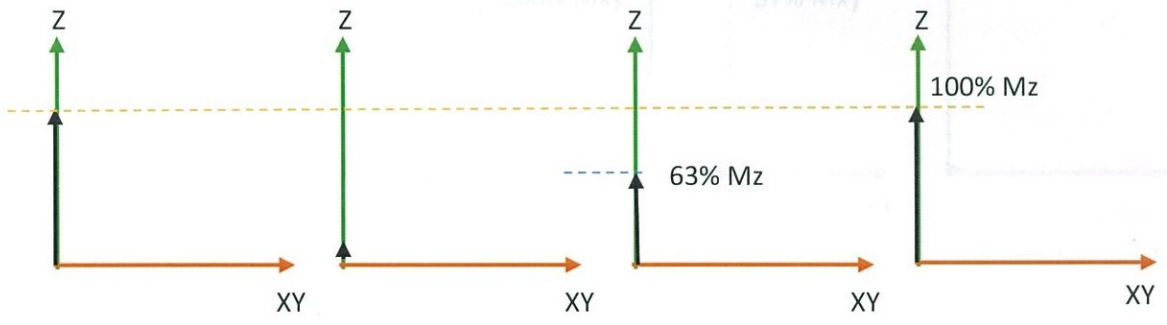

1. Mz is 100% before applying the pulse
2. Mz is 0 after applying the pulse
3. Mz slowly recovers to 63%
4. Mz continues to recover until the stating value of 100%

Figure 2.1 Longitudinal relaxation

2.2.2 T2 Relaxation Time

T2 relaxation is also known as spin-spin relaxation time or the transverse relaxation (Mxy) time. T2 relaxation describes the loss of phase in the transverse plane (Figure 2.3). Spins rotate around the z-direction in phase when RF pulse is placed. However, resulting from intrinsic effect and magnetic field inhomogeneity (T2*) (Figure 2.2) spins lose their coherence, and net magnetisation decreases to zero. T2 relaxation depends on field strength, temperature, microviscosity and presence of large molecules.

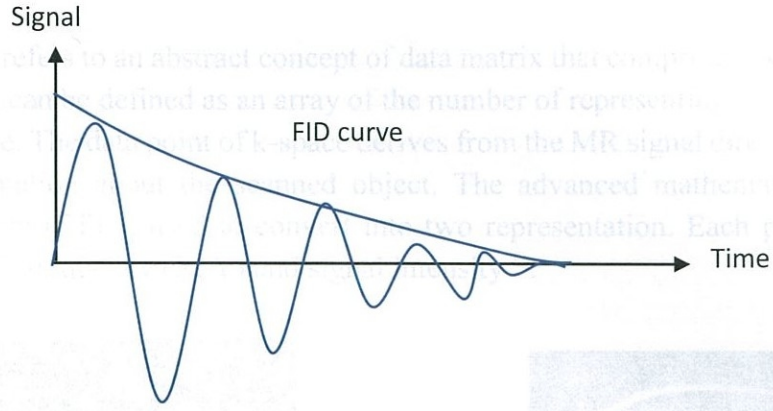

Figure 2.2 Free Induction Decay

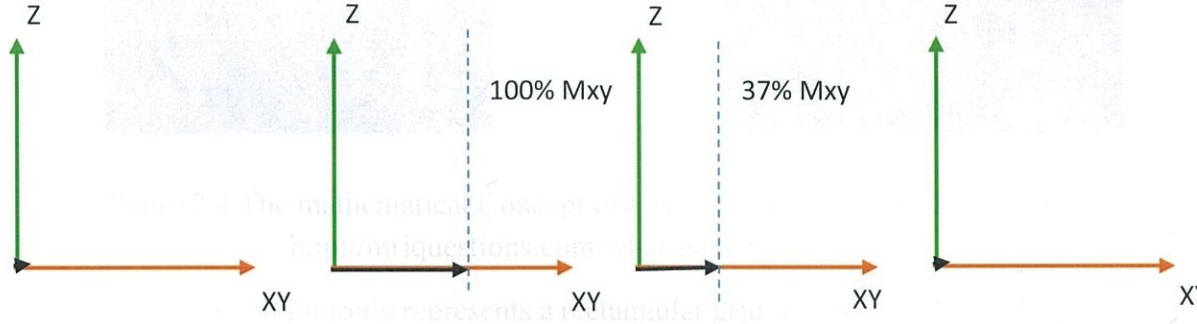

1. Mxy is 0 before applying 90 pulse
2. Mxy becomes 100% after applying 90
3. Mxy slowly decays to 37% and that time is a constant
4. The Mxy continues decaying until 0

Figure 2.3 Transverse Relaxation

2.2.3 Repetition Time and Echo Time

Repetition Time (TR) and Echo Time (TE) are basic parameters in MRI pulse sequences. TE is the time from the centre of the RF pulse to the centre of echo. TR is the length of time between consecutive pulses and echoes. TE controls the amount of T2 relaxation, and TR determines how much longitudinal magnetisation recovers between each pulse.

2.2.4 Flip Angle

The amount of rotation the net magnetisation (M) shifts when applying the RF pulse is known Flip angle. On the other hand, flip angle describes by the axis of hydrogen proton shifts from longitudinal plane Z axis to its transverse plane of XY by while excitation with RF pulses.

2.2.5 *k*-Space

k-space refers to an abstract concept of data matrix that comprises the raw MRI data. *k*-space of MRI can be defined as an array of the number of representing spatial frequencies in the MR image. The data point of k-space derives from the MR signal directly and contains identical information about the scanned object. The advanced mathematical technique, Fourier transform (FT) is used to convert into two representation. Each point of *k*-space contains specific frequency (X, Y) and signal intensity [8].

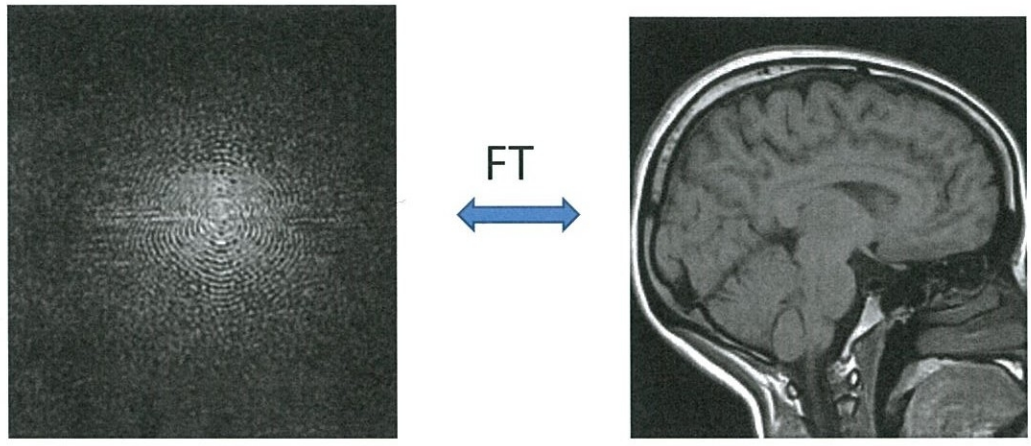

Figure 2.4 The mathematical Concept of *k*-space (Source: Reproduced from http://mriquestions.com/what-is-k-space.html)

The *k*-space commonly represents a rectangular grid with axes of Kx and Ky (Figure 2.5) which are corresponded to the horizontal x-axis and vertical y-axis in the image. However, this Kx and Ky do not represent individual pixel values. Each pixel of an image is the weighted sum of all the distinct points in the *k*-space. Generally, central regions of the *k*-space represent contrast information, and peripheral regions of the *k*-space encode spatial resolution.

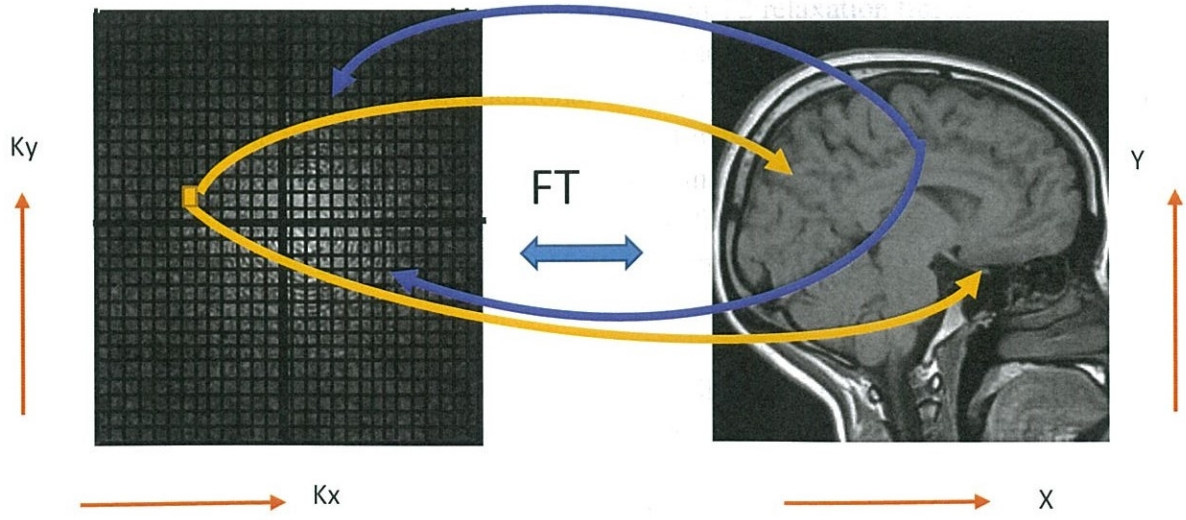

Figure 2.5 The representation of *k*-space (Source: Reproduced from http://mriquestions.com/what-is-k-space.html)

2.2.6 Free Induction Decay

Free induction decay (FID) is a short-lived sinusoidal electromagnetic signal which appears immediately after 90^0 pulse. The amplitude of the FID signal decreases when net magnetisation returns to equilibrium. FID signal decays rapidly with a time constant T2 which is much shorter than T2 (Figure 2.2).

2.3 MRI Pulse Sequences

MRI pulse sequence describes as a preselected set of RF and gradient pulse, generally, repeated many times during a scan. The time interval between two pulses, the amplitude and the shape of the gradient can manipulate MRI signal acquisition, and those may affect the features of the MR images. These pulse sequences are computer programs that control hardware aspect of the MRI measurements. Generally, parameters such as TR, TE, TI or flip angle describe pulse sequence. In MRI, the most common sequences are T1 weighted imaging and T2 weighted imaging. Broadly, spin echo, inversion recovery, diffusion-weighted, echo planar imaging and gradient echo pulses are commonly used in the field of MRI. Specifically, selection of pulse sequence depends on magnetic field strength, MRI manufacturer and the pathological conditions [8].

2.3.1 T1 Weighted Imaging

T1 weighted image is one of the primary pulse sequences in MRI. T1 weighted imaging refers to longitudinal relaxation of a tissue's net magnetisation vector. Basically, spins are aligned with the external magnetic field (B_0) by RF pulses and slide back towards the original equilibrium of B_0. However, all tissues do not get back to equilibrium equally. Therefore, T1 reflects the portion of time spins realign with the B_0 main magnetic field. Generally, T1 weighted images have short TE and TR.

2.3.2 T2 Weighted Imaging

T2 weighted imaging is also the main pulse sequence in MRI. These images have long TR, and long TE. T2 weighted imaging is based on T2 relaxation time of tissues. Each tissue belongs to inherent T2 value. However, magnetic field inhomogeneity can increase the T2 relaxation time. $T2^*$ is also an additional effect of T2 weighted imaging. T2 weighted image depends on the transverse relaxation of the net magnetisation vector. Spins undergo relaxation from the transverse plane towards the main magnetic field B_0 in the T1 weighting and at the same time spins are experienced decay from the aligned precession in the transverse plane thus the difference in this decay is captured in T2 weighting.

2.3.3 Spin Echo Sequence

The Spin Echo (SE) sequence is one of the earliest developed and commonly used pulse sequences. SE is made in series of pulses of 90^0 pulse and 180^0 rephasing pulses at TE/2. signals are read at TE. SE pulse includes a slice selective 90^0 pulse after 180^0 rephasing pulses. Figure 2.6 shows the arrangement of 90^0 pulse and 180^0 pulse at TE/2.

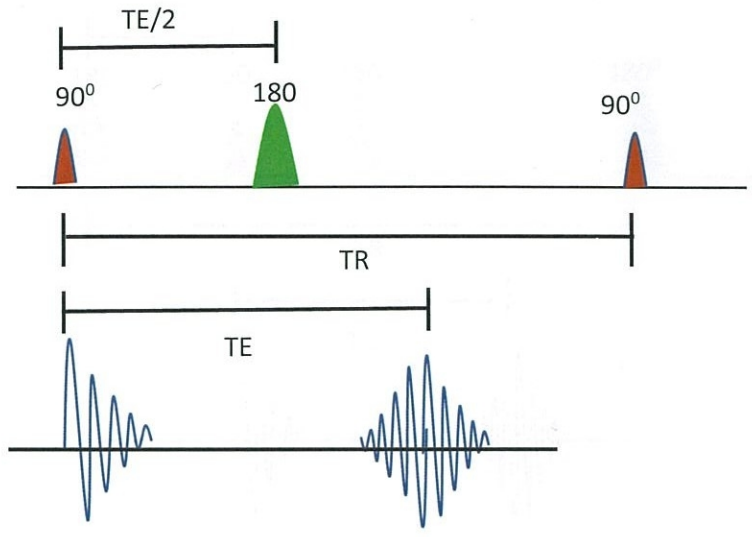

Figure 2.6 The arrangement in the RF pulses in SE

2.3.4 Inversion Recovery Pulse Sequence

Inversion recovery (IR) is a conventional SE which preceding an 180^0 inverting pulse. For instance, 90 -180 and echo can be written. Figure 2.7 shows this arrangement of RF pulses in IR. The inversion time can be defined as the time between, 180^0 inverting pulse and 90^0 pulse. The purpose of inverting pulse is to flip the initial longitudinal magnetisation, M_z of tissues in the image slices into –z direction which is opposite to the main magnetisation B_0 while inversion time interval of the magnetisation of tissues increases under T1 relaxation towards the +z direction. Therefore, tissues passing through zero will not generate a signal and effectively suppress the signal. This point is called nulled which is occurred when TI at 0.69 x T1 in generally. IR has some advantages compared to SE due to several reasons; longer scan time, flow-related artifacts can emerge, and signal to noise can decrease due to tissue suppression.

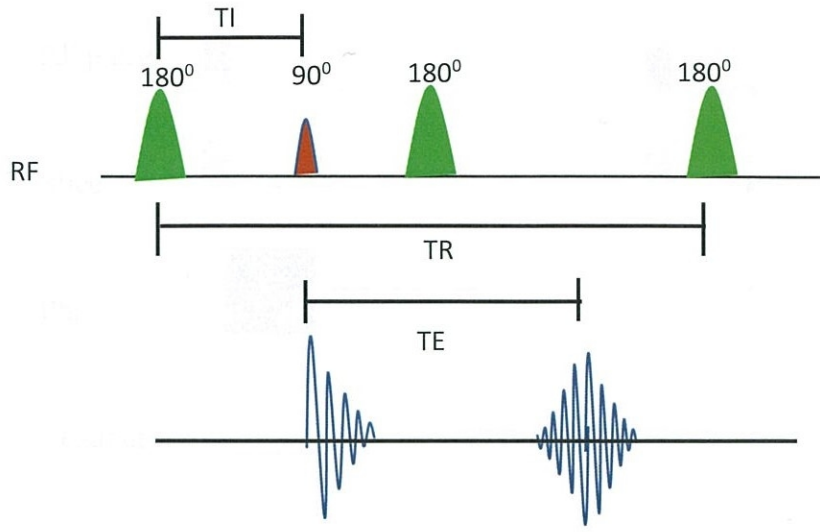

Figure 2.7 The arrangement of RF pulses in IR

2.3.5 Gradient Echo Pulse Sequence

Gradient echo (GRE) is the simplest pulse sequence, basis of many applications of modern MRI. Gradient echo pulse sequence differs from SE in two reasons; utilisation of gradient fields to generate transverse magnetisation and a flip angle is less than 90^0 in GRE. The gradient echo that generate by the frequency-encode gradient can be used in succession and opposite directions. The gradient echo is used in reverse at first to enforce transverse dephasing of spins and the right after, as a readout gradient to realign dephased spins. GRE consists of a series of excitation pulses and each pulse separated by a repetition time (TR). Figure 2.8 a) shows the arrangement of RF pulses in GRE. These RF pulses are usually chosen less than 90^0. A signal can be acquired at some characteristic time after applying excitation pulses. Signals from free induction decay (FID) is generated in GRE immediately after applying each RF pulse.

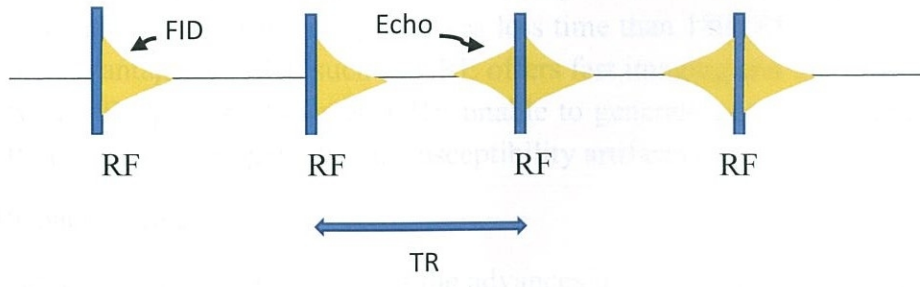

(a)

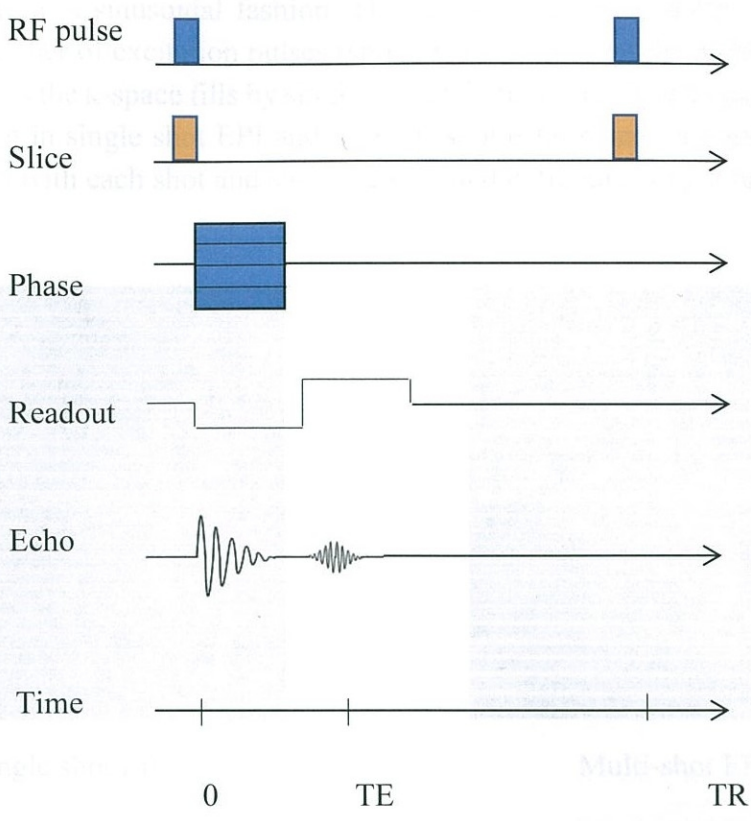

(b)

Figure 2.8 (a) Series of excitation pulse of GRE (b) Gradient application and signal formation of GRE

A bipolar readout gradient is needed to generate echo as a gradient echo which has no 180^0 pulses. Therefore, dephasing gradient is applied before the readout gradient. The reason for applying dephasing gradient is to obtain an echo as readout gradient is applied and data are acquired. Figure 2.8 b) shows the gradient application and signal formation of the GRE.

In gradient echo, spins are refocused by reversing the direction of the spin rather than flipping spins. Gradient refocusing of spins takes less time than 180^0 RF pulse refocusing. There are some advantages of GRE such as GRE offers fast imaging and use low flip angle with less powerful RF pulses. However, GRE unable to generate good T2 contrast, since GRE is sensitive to B0 inhomogeneity and susceptibility artifacts can emerge feasibly.

2.3.6 Echo Planar Imaging

Echo Planar Imaging (EPI) is one of the advances in MRI gradient pulse sequences. EPI enables to obtain individual MR slices in the time frame of 50-100 msec, and this is beneficial for minimising the effect of patient motion. EPI can perform with multiple echoes of a different phase in steps which are obtained using rephrasing gradients instead of series of 180^0 RF pulses following 90^0 and 180^0 in a spin echo sequence. Here EPI uses rapidly

reversing readout gradients or frequency-encoding gradients. This switching or reversing readout is done in a sinusoidal fashion. The image acquisition of EPI can be completed providing a number of excitation pulses (shots) which represent the number of TR periods. Figure 2.9 shows the k-space fills by single shot and multi-shot. The k-space data is acquired by a single shot in single shot EPI and in multi-shot echo planar, a portion of the k-space data is required with each shot and shots are repeated until collecting a full set of data.

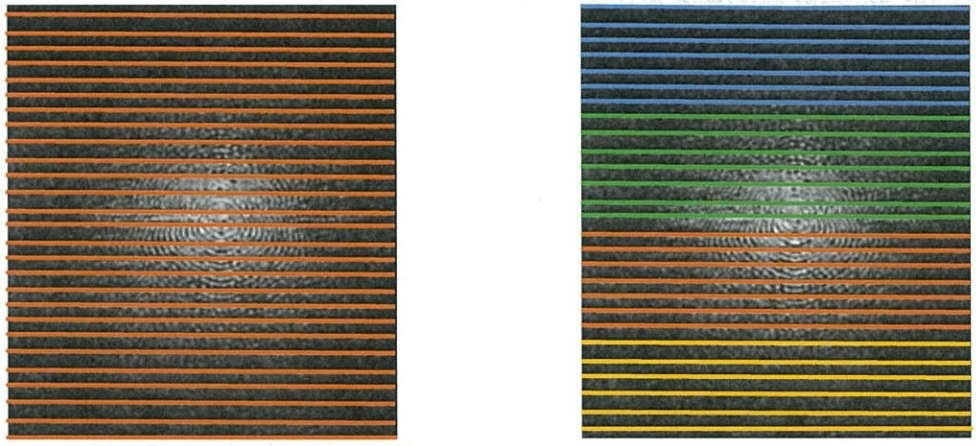

Single shot EPI Multi-shot EPI

Figure 2.9 Single shot EPI and multi shot EPI (Source: Reproduced from http://mriquestions.com/echo-planar-imaging.html)

EPI has advantages such as sensitivity to off-resonance effect is increased, T2 T2* imaging and sectional efficiency are improved, and snapshot imaging is possible. Most clinical application of EPI is imaging brain that EPI based diffusion imaging is used for investigating cerebral ischemia and stroke [8].

CHAPTER 3

Diffusion MRI

3.1 Diffusion Weighted Imaging

Diffusion refers to the random movement of water or nano molecules due to the thermal collision. DWI examines the random motion of water molecules in tissues. Diffusion is also known as the Brownian motion which is investigated by Scottish botanist Robert Brown. Brown observed spontaneous vibration of pollen particles through the microscope in 1827.

Since its inception in 1985, Diffusion Weighted Imaging (DWI) has been continuously evolved in MRI to scrutinise microscopic motion of water molecule known as Brownian motion in tissues. However, the first DWI pulse sequence was determined by Stejskal and Tanner in early 1965 [9]. DWI is an excellent method to evaluate tissue functions in many specific organs including the brain, cartilages and liver, kidney and breast.

3.2 Principles of DWI

The human body is approximately 60%-70% composed of water. Diffusion refers to the Brownian motion which is driven by the thermal energy of water molecules [10]. Diffusion of the particular tissue depends on the temperature and microstructural architecture which diffusion takes place. For example, Diffusion in the cerebrospinal fluid (CSF) is different from intracellular and intercellular space. These differences can be used to produce the appropriate contrast in MR images by changing the MR sequences [11]. The microstructural architecture changes when physiological factors occur such as destruction or regeneration of tissues that may influence on the diffusion of water molecules within the tissue [9].

The movement of water molecules in biological tissues can have barriers due to interaction with cell membrane and macromolecules. The basic foundation of Diffusion MRI is Einstein's diffusion equation, and distribution of diffusion obeys the Gaussian law. DWI uses the self-diffusion of water molecules is also known as a self-diffusion coefficient, which is around 3.0×10^{-9} m^2/s at 37° C. In biological tissues, self-diffusion is lower than the actual value. However, diffusion-based displacement of water molecules is used to encode MRI signals in order to generate DW images [12].

3.3 DWI Pulse Sequences

DWI generates with the readout signals depend on diffusion gradients. Currently, single-shot gradient, EPI is the most common gradient scheme in DWI. EPI pulse sequence in DWI enables to detect ischemic changes in tissues rapidly after imaging. For example, in an ischemic attack, cells absorb water molecules and diffusivity decreases. Motion Probing Gradients (MPG) are applied on EPI to detect the level of diffusivity decreases in tissues.

DWI generates using two gradients with magnitude, G. Therefore, one gradient causes to dephasing and another one is a rephrasing opposite gradient which is applied symmetrically to the 180^0 RF pulse [13]. The Stejskal-Tanner equation describes the signal attenuation of DWI.

Stejskal-Tanner equation:

$$\boldsymbol{S(b) = S_0 e^{-bD}} \tag{3.1}$$

S (b) refers to the signal received for that particular gradient value (or b-value 'b'), S_0 is the signal strength without any diffusion weighting, and D denotes diffusion.

The following equation defines the b value in dMRI.

$$\boldsymbol{B = \gamma^2 G^2 \delta^2 \{\Delta - \delta \backslash 3\}} \tag{3.2}$$

γ is the gyromagnetic ratio of hydrogen proton, a constant, given as 42.58 MHz/T, G is the magnitude of applied gradient, δ is the duration of gradient and Δ is the time between the applications of the two gradients. The unit of b value is s/mm^2.

MPGs are also applied to visualise the degree of diffusivity in different directions. MPGs usually detect motion and enhance signal by dephasing moving molecules. In tissues, stable molecules rephase at the time of echo. Therefore, tissues with lower diffusivity due to pathological condition visualise with higher signal intensity, and healthy tissues observe with lower signal intensities. The degree of motion in DWI scan depends on b-factor which is determined by the characteristics of MPGs. Figure 3.1 shows the application of gradient in DWI to obtain signals.

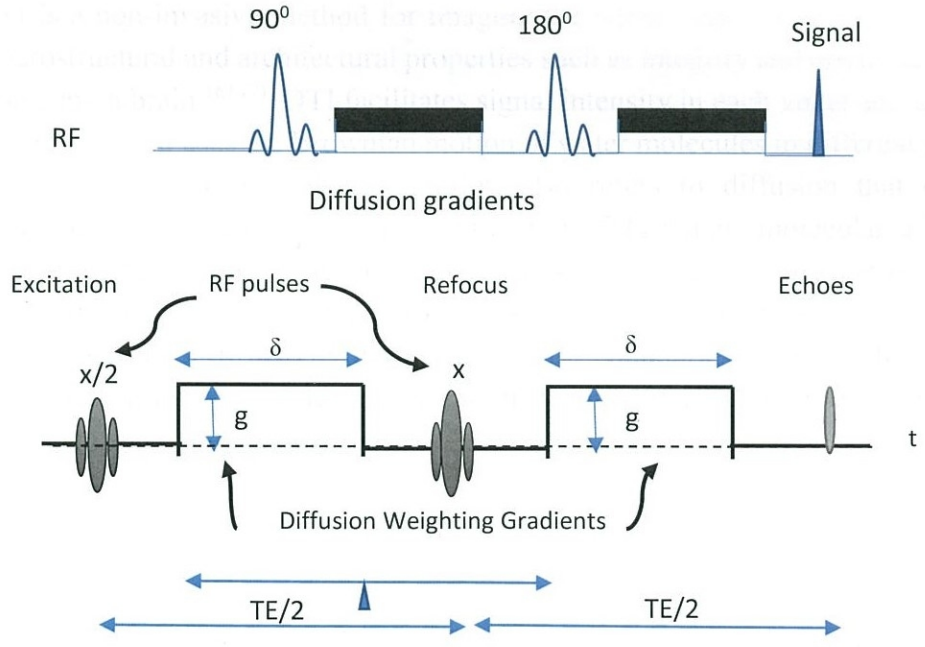

Figure 3.1 Application of gradient for diffusion weighted images

Pulse gradient Spin Echo sequence for diffusion weighted images. G represents gradient intensity δ represents gradient duration and Δ represents gradient spacing

Generally, DWI scans are performed with at least two b values. The more considerable b value determines, the higher degree of signal attenuation from water molecules. DWI is usually acquired with a lower b value of b=0 s/mm2 without gradient

application [13]. Hence image is equal to T2 image contrast that does not carry diffusion details and a high b value of 1000 s/mm^2 [14]. DWI is a modified image sequence with T1 and T2 contrast in addition to the diffusion contrast. This high T2 signals can bring hyperintensity signal on diffusion image, is called T2 Shine-through effect.

3.4 Apparent Diffusion Coefficient maps

Apparent Diffusion Coefficient (ADC) is referred to measuring the magnitude of diffusion of water molecules in tissues. Diffusion images are usually in two types, DWI and ADC calculated images.

The concept of ADC was introduced to avoid misinterpretation of hyper-intensities due to shine through effect from T1 and T2 contrast with the diffusion MRI [15].

$$\boldsymbol{ADC} = \frac{ln\left(\frac{S_0}{S_1}\right)}{(b_1 - b_0)} \tag{3.3}$$

S_0 and S_1 are the signal intensity obtained with the b_0 and b_1 values.

Usually, ADC values are automatically calculated with the MRI system. The units of ADC is mm^2/s.

3.5 The Fundamentals of DTI

DTI is a non-invasive method for imaging the white matter in vivo and allows to explore microstructural and architectural properties such as integrity and orientation of fibre tracts in the human brain [16] [17]. DTI facilitates signal intensity in each voxel and directional detail (tensor) in which uses the Brownian motion of water molecules in different directions to reconstruct images. The Brownian motion also refers to diffusion that occurs in microscopic molecular motion due to thermal energy. DTI pursue molecular diffusion to probe microstructural properties of biological tissues [18]. Figure 3.2 shows microstructural properties of different tissues related to diffusivity details in ellipsoids and tensors. Moreover, restrictions of diffusivity in microstructural boundaries such as cell membranes or myelin sheaths in neurons yield anisotropic diffusion which can be used to distinguish the pathological tissues and healthy tissues [19].

Diffusion trajectory	Diffusion ellipsoids	Diffusion tensor
 Isotropic unrestricted diffusion (Free water)	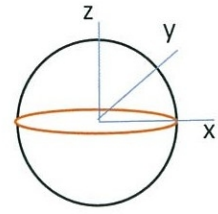	$\begin{pmatrix} D & 0 & 0 \\ 0 & D & 0 \\ 0 & 0 & D \end{pmatrix}$
 Isotopic restricted diffusion (Random barriers present)	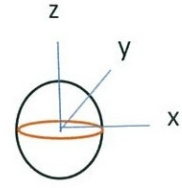	$\begin{pmatrix} D_{eff} & 0 & 0 \\ 0 & D_{eff} & 0 \\ 0 & 0 & D_{eff} \end{pmatrix}$
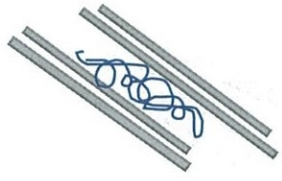 Anisotropic restricted diffusion (Axonal Bundle)	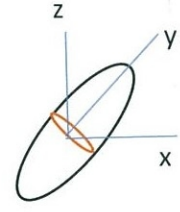	$\begin{pmatrix} D_{xx} & D_{xy} & D_{xz} \\ D_{yx} & D_{yy} & D_{yz} \\ D_{xz} & D_{yz} & D_{zz} \end{pmatrix}$

Figure 3.2 Diffusivity of water in microstructural boundaries (Source: Reproduced from Mukherjee P et al. 2008)

In pure water, molecules move as free motion in all directions which is called unrestricted isotropic diffusion, and restricted isotropic occurs with random barriers present in organs. The CSF in the brain can have isotropic diffusion. When the mobility of water molecules are not equal in all direction, molecules have anisotropic diffusion [16]. For example, the white matter owns anisotropic diffusion due to cellular membranes, myelination and the packing of axons [20].

DWI is acquired after applying diffusion gradients in any number of directions to measure the water diffusion in the particular tissue. DWI is performed before use of DTI by applying diffusion gradients along three orthogonal directions of X, Y, and Z. The diffusion tensor illustrates the diffusivity of water molecules with a Gaussian model. This three-dimensional Gaussian distribution of the matrix is proportional to the displacement of the

molecule [20]. Generally, a tensor is a mathematical model with a 3 x 3 matrix of the vector that contains information of maximum diffusivity (Figure 3.3). The direction of maximum diffusivity corresponds with the orientation of fibre tracts.

$$D = \begin{pmatrix} D_{XX} & D_{XY} & D_{XZ} \\ D_{YX} & D_{YY} & D_{YZ} \\ D_{ZX} & D_{ZY} & D_{ZZ} \end{pmatrix}$$

Figure 3.3 Maximum diffusivity

DTI uses the shape of three-dimensional tensors and degree of diffusion to analyse three-dimensional structure with three kinds of diffusivities, known as eigenvalues of λ1, λ2, λ3 associated with perpendicular directions, known as eigenvectors of v1, v2, and v3 [21,22] (Figure 3.4).

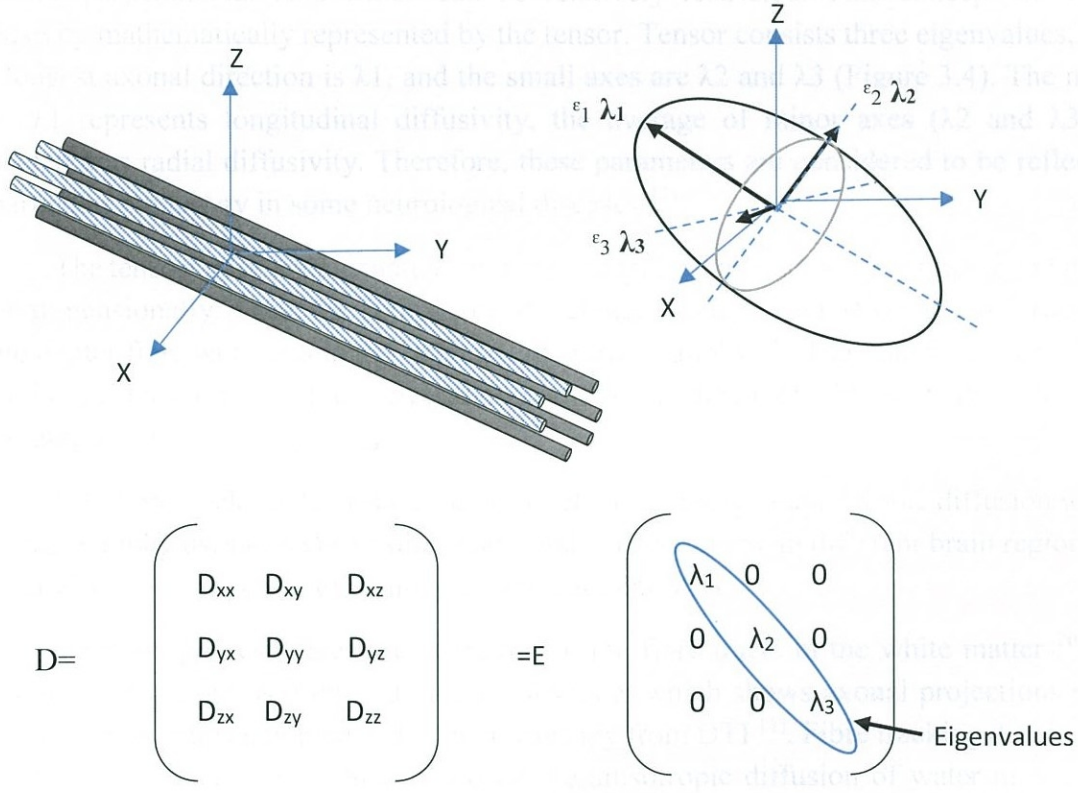

Figure 3.4 Orientation of eigenvalues corresponded to X, Y, Z axis (Source: Reproduced from Jellison BJ et al. 2004)

The largest eigenvector is termed primary eigenvector which associates with λ1 to indicate the direction of magnitude of largest water diffusion. This λ1 is also known as longitudinal diffusivity. The second and third eigenvectors are associated with eigenvalues of λ2 and λ3. The mean of λ2 and λ3 is termed as radial diffusivity [20].

The mean of the three eigenvalues illustrates the diffusivity (D_{av}) of water within a particular voxel. Anatomic features in DTI can be measured by parameters such as fractional anisotropy (FA), mean diffusivity (MD) and axial diffusivity.

$$D_{av} = \frac{\lambda 1 + \lambda 2 + \lambda 3}{3} \tag{3.4}$$

The degree of directionality is measured by the Fractional Anisotropy (FA)

$$FA = \frac{\sqrt{(\lambda 1-\lambda 2)^2+(\lambda 2-\lambda 3)^2+(\lambda 1-\lambda 3)^2}}{\sqrt{2}\sqrt{\lambda 1^2+\lambda 2^2+\lambda 3^2}} \tag{3.5}$$

3.6 The Basics of Tractography

In the white matter, directionality or anisotropy of water establishes with axonal alignment. Generally, water diffuses parallel along the longitudinal axis of the axon rather than the perpendicular axis which can be relatively restricted. This concept of water diffusivity mathematically represented by the tensor. Tensor consists three eigenvalues, and the longest axonal direction is λ1, and the small axes are λ2 and λ3 (Figure 3.4). The main axis, λ1 represents longitudinal diffusivity, the average of minor axes (λ2 and λ3) is considered as radial diffusivity. Therefore, these parameters are considered to be reflected in particular pathology in some neurological diseases [23].

The tensors of the white matter can be reconstructed in macroscopic fibre orientation, three-dimensionally. Thus, the computerised technique in diffusion MRI to reconstruct the white matter fibre pathways in the brain is called tractography [24]. The transformation of the axes in the tensor into fibre trajectories could be attained by different algorithms in tractography [23].

DTI fibre tracking determines inter-voxel connectivity of anisotropic diffusion water [18]. Tractography uses to identify fibre tracts and connections with different brain regions *in vivo* in which is impossible to identify in conventional MRI.

Tractography estimates the trajectory of the fibre tracts in the white matter [20]. In addition, tractography is a three-dimensional model which shows axonal projections non-invasively with information on diffusion anisotropy from DTI [11]. Fibre tracking determines the intravoxel connectivity which based on the anisotropic diffusion of water molecules. DTI fibre tracking includes functional and high-resolution information of the white matter [16].

3.6.1 Technical Considerations of Tractography

In tractography, there is some vital consideration including data acquisition, fibre modelling, fibre reconstruction and the number of seeds. The b-value and number of gradients are crucial points during DWI acquisition. The b-value represents the amount of diffusion weighted and time and strength of gradients. Generally, application of the number of directions are 30 or fewer, and b-value is about 1000s/mm^2 in the field of diffusion [25].

The other important consideration is the method of fibre tracking. There are two methods of DTI fibre tracking; 1. deterministic tractography 2. probabilistic tractography. Deterministic tracking is continuous tracking which starts from user-defined voxels and streamline follows primary eigenvector voxel wise in three-dimensionally. The direction of tracking changes when the trajectory is taken place an edge of the voxel and match the eigenvector of next voxel [19]. Deterministic tractography can be visualised as a curve line which is the streamline. The output of probabilistic tractography is a map of connection probabilities. Tract seeding, tract selection and, stopping threshold are also useful to interpret tractography [25].

The deterministic tractography has various method in the seeding method. The most popular seeding method is Fibre Assignment by Continuous Tracking (FACT) which is able to track high-resolution three-dimensional tracking of axonal projections. FACT method starts with a seed voxel and steps in principle directions until voxel edge which is known as variable step size [26]. This process repeats until stopping criteria is met. Euler introduced another method that is constant step starts the path in principle direction at a seed, interpolating a new tensor at path endpoint. Therefore, next step based on interpolation. Figure 3.5 shows the difference between these two seeding methods.

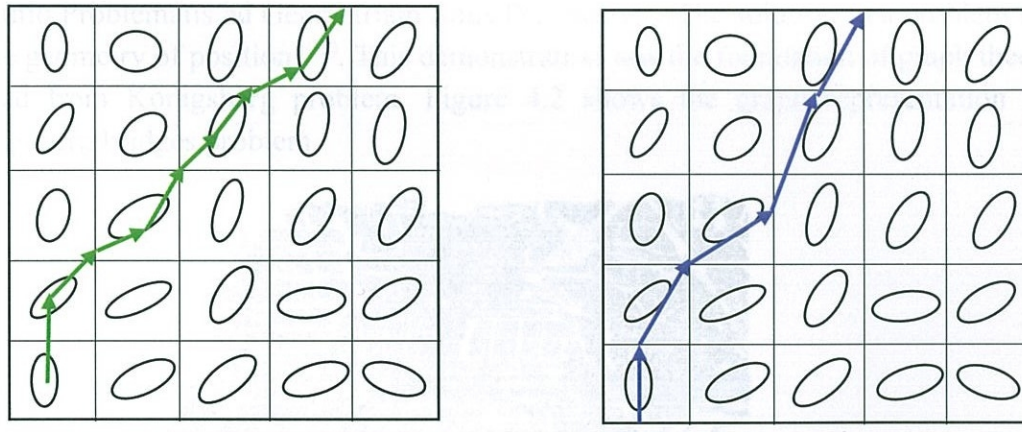

Euler's Method (Constant step) FACT (Variable step)

Figure 3.5 Deterministic tractography techniques (Source: Reproduced from http://dsi-studio.labsolver.org/course/fiber-orientation-distribution)

3.6.2 Stopping Criteria of the Tractography

In a deterministic tractography, the outcome of tracking depends on certain parameter including the curvature change threshold (turning angle), anisotropy threshold and anatomical criteria. The tracking processes stops when certain criteria are met in the tractography. Turning angle avoids crossing of boundaries and bended trajectories which enable to impose smoothness criterion. The anisotropy threshold may avoid propagating in a region where is meaningless and anatomical criteria stop seeding after reached to the grey matter boundary. The choice of stopping criteria is crucial to avoid stepping outside the bundle in the white matter [27].

CHAPTER 4

Graph Theory

4.1 History of Graph Theory

The concept of the network has become popular in many research fields such as engineering, social sciences and, neuroscience. This network theory is a part of the mathematical concern of analysis of graphs which are a mathematical abstraction of networks [28]. The graph theory concept began with the Leonhard Euler's original publication in 1736 in which based on one of the particular puzzles related to the problem of the Konigsberg bridges. The basic concepts of graph theory were involved in the solutions to this problem [29].

The old city of Konigsberg in Eastern Prussia had the river of Pregal (Figure 4.1) which flowed through the city seven bridges were connecting to different lands in the city. It is said that people in Konigsberg used to wonder that possible to find across each of seven bridges exactly once. These attempts were failed many times, and people used to believe that task was impossible. Leonhard Euler, one of the mathematicians at that time involved with the Konigsberg problem and gave some general solutions [30]. Euler's first mathematical demonstration of Konigsberg was presented to the Petersburg Academy, named with "Solutio Problematis ad Geometriam Situs Pertinentis" (The solution to a problem relating to the geometry of position) [31]. This demonstration was the foundation of graph theory that started from Konigsberg problem. Figure 4.2 shows the graph representation for the Konigsberg bridges problem.

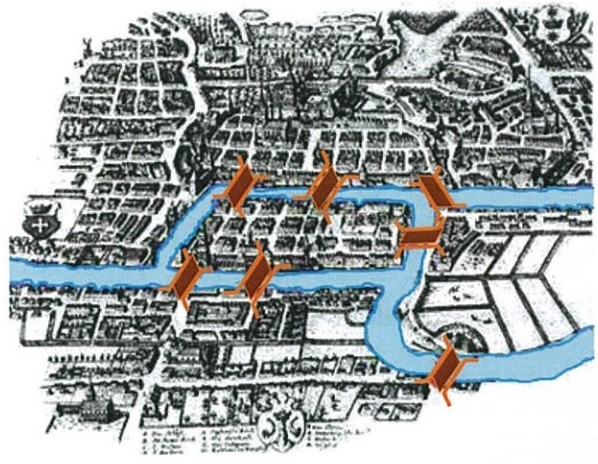

Figure 4.1 Seven bridges in Konigsberg (Source: Reproduced from Wikipedia)

Although the roots of graph theory based on Euler's theory, a crucial step forward ensued after random graphs were discovered. There were many vital theories were proven under the phenomenon of random graphs which is termed random nets [32] [33]. However, in 1988 Duncan Watts and Steven Strogatz turned out to a new page in graph theory by proposing an elementary model of a one-dimensional network on a ring. Furthermore, the discovery of small world networks based on their study [33] [34]. This study illustrated many theories of graph theory such as clustering coefficient and path length. Barabasi and Albert

discovered another important measure, the scale-free networks such as the World Wide Web and networks of airports in 1999 [32) 35)]. These advancements of graph theory cause to inspire novel applications in neuroscience [32)].

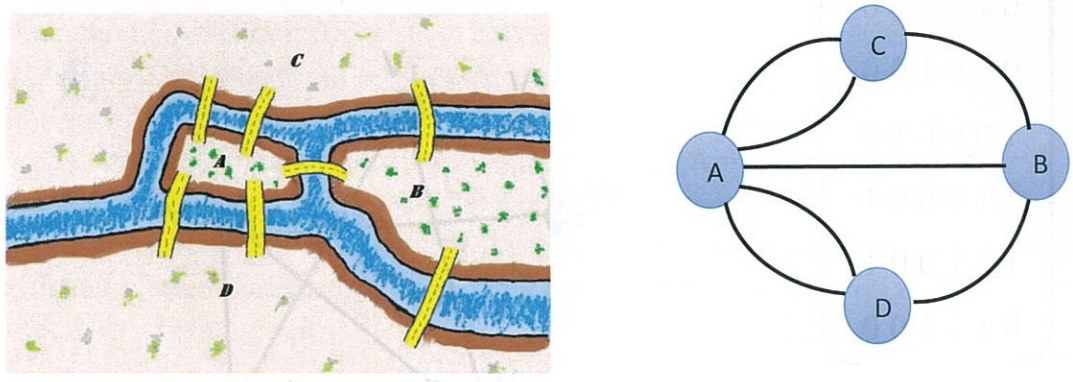

Figure 4.2 Graph representation of Konigsberg bridges (Source: Reproduced from https://medium.freecodecamp.org)

4.2 Definition of Graph Theory

Graph (G) is a mathematical theory which represents networks. (Figure 4.3) A graph consists of a group of vertices or nodes (V) and a set of edges (E). In a network, a node can have interaction with another node when the presence of an edge between two nodes [32)].

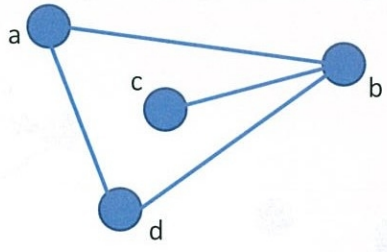

Figure 4.3 Graph representation

G=(V,E)

V={a,b,c,d}

E={{a,b},{b,c},{b,d},{a,d}}

Graphs represent as N x N connection matrix where N is the number of nodes in which termed the adjacency matrix (A). The adjacency matrix consists information connectivity in the graph. Figure 4.3 shows the representation of graph. For example, Graph (G) has v1, v2, v3 ….vn and adjacency matrix of N x N matrix (A) whose (*i, j*) entry denotes by this:

$$[A]_{i,j} = \begin{cases} 1 \text{ if vi and vj adjacent} \\ 0 \text{ if not} \end{cases}$$

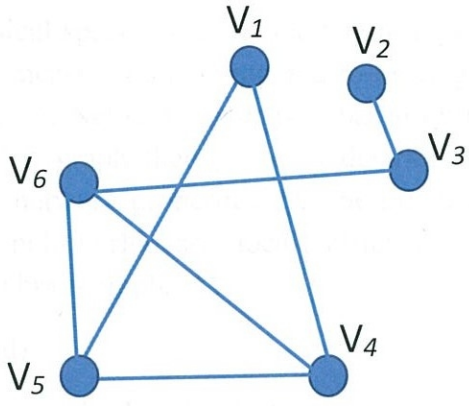

$$A = \begin{pmatrix} 0\,0\,0\,1\,1\,0 \\ 0\,0\,1\,0\,0\,0 \\ 0\,1\,0\,0\,0\,1 \\ 1\,0\,0\,0\,1\,1 \\ 1\,0\,0\,1\,0\,1 \\ 0\,0\,1\,1\,1\,0 \end{pmatrix}$$

Figure 4.4 Connectivity Matrix representation by a graph

Graphs can have variations such as undirected and directed graphs, weighted and unweighted graphs. Figure 4.5 shows a directed and an undirected graph. When information flows through both directions along the edges which is termed undirected, and when information flow through one direction, called directed graphs. Graphs which have the same significance is termed unweighted graphs, and weighted graphs refer to when weights are not the same significance, and each edge is assigned the weights in the graph [32].

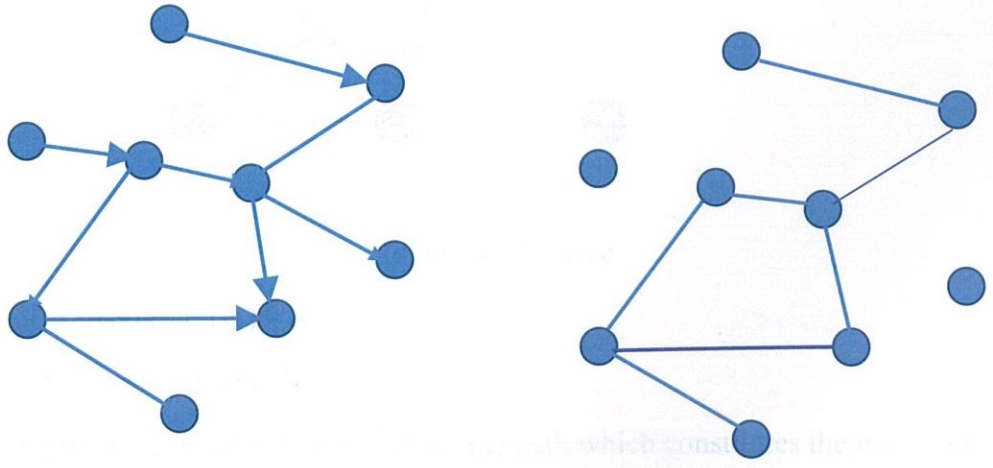

Directed graph Undirected graph

Figure 4.5 Directed and Undirected graph

4.3 Graph Theory Measures

The human brain consists of networks which have anatomical connections to linking the neural elements. With the complexity of the brain, neural networks and functions have not been fully understood. Therefore, scientists have been focusing on graphs which are an abstract model with information about brain networks. Graphs compose nodes and edges to represent physical space and network role in topological space. Topological properties of graphs can be measured and compared to other graphs which derive from neural or non-neural systems [36]. Network analysis is based on mathematical principles of graph theory and measures of graph theory use to determine the neurobiological interpretation and measure brain network properties [37]. The graph theory measures such as degree, cluster coefficient, small-worldness, local efficiency determine structural and functional connectivity in brain graphs [36].

4.3.1 Degree (d)

The degree is the simplest measure among graph theory topological measures. Degree determines the number of edges (E) which connected to the particular node. (V) The degree is also known as degree centrality which is used to determine that nodes are well connected through links in networks. Nodes with high degree play a significant role in a network to increase connectivity and flow of information through networks [36].

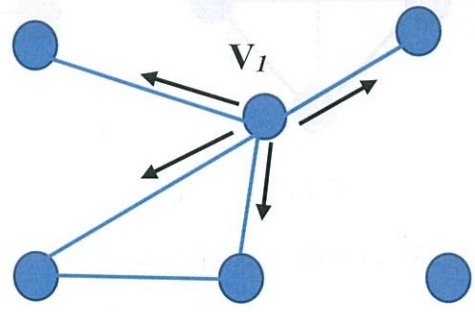

Figure 4.6 Degree

Degree of A denotes d (v_1) = 4

4.3.2 The Shortest path length

In graph theory, the shortest path is the path which constitutes the minimum number of edges in a network graph.

4.3.3 Betweenness Centrality (BC)

Betweenness centrality can be used to measure the extent to which a vertex lies on a path between other vertices. For instance, vertices with high betweenness would have considerable influence within a network of information passing between different regions or vertices [37].

Betweenness centrality of a node refers to the ratio of the shortest paths between all other nodes that pass through a particular node. Therefore, betweenness centrality quantifies the control of a node on the communication between other nodes.

$$C_B\,(\mathbf{V}) = \sum_{s \neq v \neq t} \frac{\delta_{st}\,(V)}{\delta_{st}} \tag{4.1}$$

Here, s, t, δ_{st}, δ_{st} (V) denote, source, destination, number of the shortest path between (s, t) and that pass through V respectively.

4.3.4 Clustering Coefficient (C)

Local connectedness in a network is measured by clustering coefficient that is a measure of the degree to which nodes in a graph tends to cluster each other. This proportion of a number of nodes are connected to each node is defined as clustering coefficient. Clustering coefficient can be varied between 0 and 1. High clustering coefficient determines that nodes are well connected to each other in a network [38].

Clustering coefficient (C) of a node is calculated by the ratio between the number of closed triplets which observed and the maximum possible closed triplets in the graph.

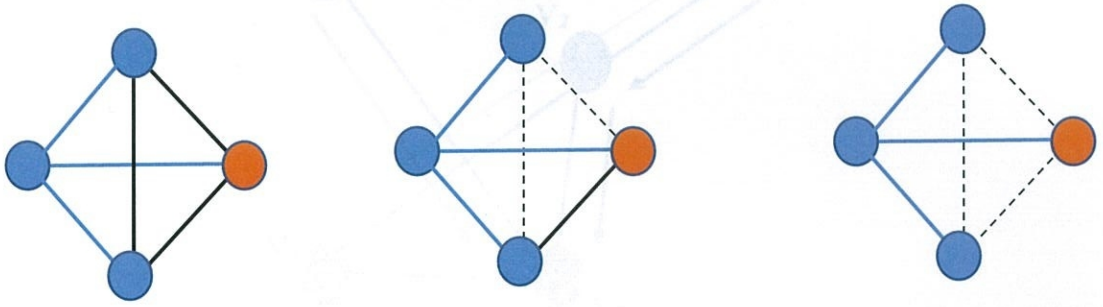

C=1 C=1/3 C=0

Figure 4.7 Cluster coefficient (Source: Reproduced from Wikipedia)

Clustering coefficient is calculated using following equation

$$C_{v1} = \frac{2L}{deg_{v1}}\,(deg_{v1} - 1) \tag{4.2}$$

Here L is number edges between (v_1) neighbours of node.

Example;

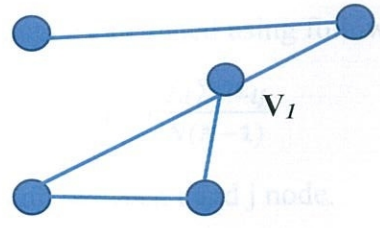

Figure 4.8 Example of cluster coefficient

For this example deg (v_1) = 3 L =1

$C\ (v_1) = 3 / 3\ (3\text{-}1) = 0.5$

The Average clustering coefficient in the total graph can be illustrated as

$$\mathbf{C} = \frac{\mathbf{1}}{\boldsymbol{N}} \sum_{\boldsymbol{C=1}}^{\boldsymbol{N}} \boldsymbol{C(v1)} \tag{4.3}$$

4.3.5 Characteristic Path length (L)

The characteristic path length (L) indicates the integration of a network and flow of information within the network. The distance of the shortest path (σ) between two nodes is the length of the path with the minimum number of connections. Therefore, the characteristic path length of a network is the average minimum number of connection between two nodes in the network. The characteristic path length is used to quantify global efficiency [38].

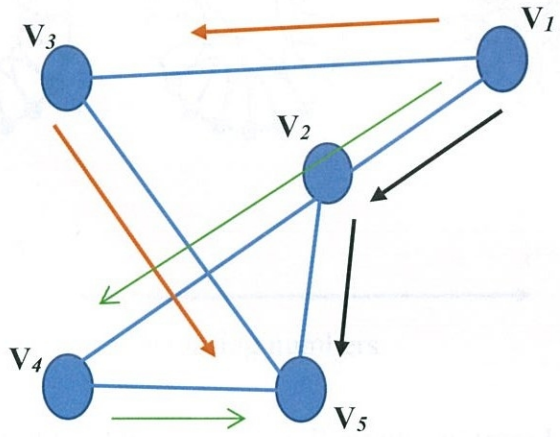

Figure 4.9 Characteristic path length

This figure 4.9 shows three different paths between V_1 and V_5, but the shortest path is 2, indicates by black arrows.

The characteristic path length refers to the shortest path length between two nodes averaged over all pairs of nodes.

The characteristic path length can be calculated using following formula.

$$\boldsymbol{L} = \frac{\sum_i \sum \boldsymbol{j}\, \boldsymbol{L_{ij}}}{\boldsymbol{N(N-1)}} \tag{4.4}$$

L_{ij} denotes the shortest path length between i and j node.

The network is more likely to be linear, as the network has higher characteristic path length and lower characteristic path length would be showed a more compact network.

4.3.6 Small-Worldness (SW)

The concept of Small-worldness (SW) network was introduced by Watts and Strogatz in 1998 [34]. The regular network consists of nodes which are only related to neighbour nodes and the random network consists of nodes which are related randomly [39]. Figure 4.10 shows the arrangement of interconnected nodes in the regular network, small world and random network. The concept of small-world consists of clustering which defines the extent to which the neighbour nodes are interconnected [40]. Small world network has shorter characteristic path length than regular networks [38]. A small-world network characterises by high local clustering and low minimum path length between a pair of nodes.

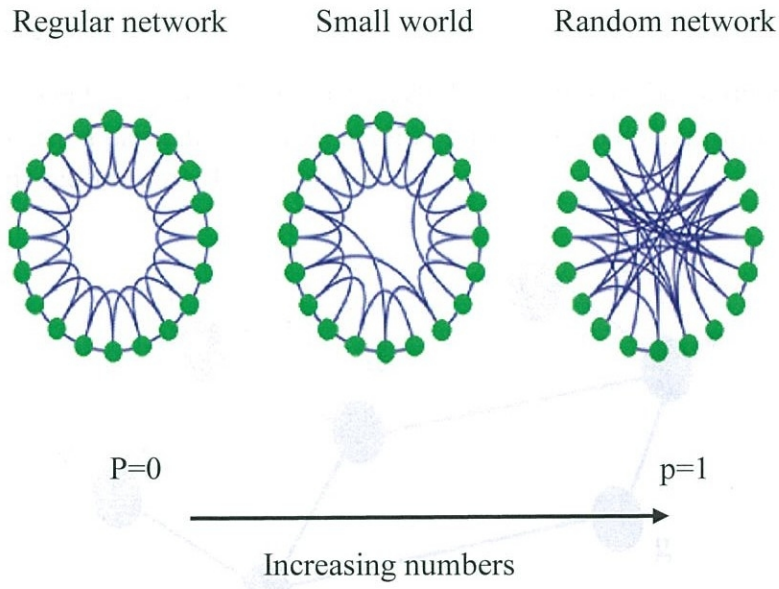

Figure 4.10 Small-worldness (Source; Reproduced from Liao X et al., 2017)

SW is calculated using following formula.

$$\boldsymbol{SW} = \frac{\boldsymbol{C/C_{rand}}}{\boldsymbol{L/L_{rand}}} \tag{4.5}$$

Here C is cluster coefficient and L is characteristic path length in the tested network C_{rand} and L_{rand} are cluster coefficient and path length respectively in a random network. Generally, small-worldness is less than 1.

4.3.7 Network Efficiency

The efficiency of a network defines how efficiently information exchange between nodes [42]. This efficiency can be applied to both local and global scales in a network.

Global efficiency in a graph of G is measured as

$$\boldsymbol{E_{glob}(G)} = \boldsymbol{1/N(N-1)} \sum_{i \neq j \in} \boldsymbol{G} \frac{\boldsymbol{1}}{\boldsymbol{d_{ij}}} \tag{4.6}$$

Here d_{ij} denotes the shortest path length between node I and j in the G graph.

The local efficiency is defined as follows.

$$E_{loc}(G) = \frac{1}{N}\sum_{i\in G} E_{glob}\,(G_i) \tag{4.7}$$

E_{glob} is the global efficiency in the graph and G_i denotes the subgraph composed of neighbours a node of i.

4.3.8 Eccentricity

The eccentricity ($e_{(v)}$) of a connected network can be defined as the maximum distance between a particular node to another node. The diameter of the graph is termed as the maximum eccentricity of a node [43].

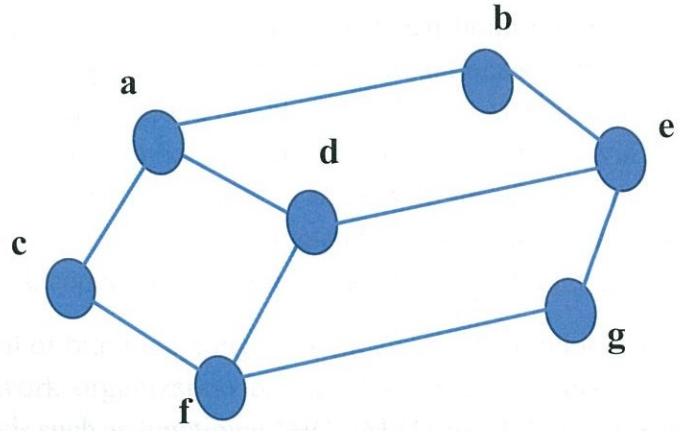

Figure 4.11 Eccentricity

In the figure 4.11 graph, the eccentricity of 'a' is 3 because the maximum distant of the graph is 'a' to 'g'. From a to b = 1, a to c is 1, a to d= 1, a to e = 2, a to f = 2, a to g = 3

4.3.9 Strength (S)

In a weighted network, strength (S) is defined as the mean of all weights of edges. Therefore, the strength of a graph (G) with N number of nodes, from I to j distinct nodes is calculated as below. W_{ij} denotes the connection weights of all edges [44].

$$\mathbf{S(G)} = \frac{1}{N}\sum_{i\neq j\in G}^{N_M} w_{ij} \tag{4.8}$$

CHAPTER 5

The Connectome Mapper

5.1 Brain Mapping

The brain is the most complex organ with 85 to 100 billion neurons [45] in the human body with multiple connections from webbing in every possible direction, forming the vast brain networks. These huge number of neurons are interconnected anatomically and functionally. The abstract version of networks called connectome refers to connection matrix of the brain that describes interconnectivity patterns at multiple levels. Recently, researchers use connectome in order to understand functional brain states through interconnections in neuroscience [46, 47]. The connectome can provide crucial neuroinformatics resources that cause to development of neuroscience in theory and experiments [47].

Brain connectivity derives from anatomical, functional and effective connectivity. Anatomical and functional connections between brain regions have organised in order to process information optimally. Functional interactions synchronise activities between brain regions not only local regions but also peripheral. Anatomical connectivity which is also known as structural connectivity creates the connectome via synaptic contacts among neurons. The white matter consists of the whole set of fibre tracts in the brain. Functional connectivity illustrates statistical dependencies between anatomically separated brain regions. Effective connectivity refers to the influence of one neural system over another [46].

The goal of brain mapping is to understand hierarchical and complex structural and functional network organization of the brain. With the evolution of non-invasive brain imaging methods such as functional MRI (fMRI) and dMRI, many neuroscientists have been focusing on mapping a detailed picture of brain structural and functional architecture. Brain mapping enables to improve understanding of brain connectivity [45].

Structural connectivity can be better understood using dMRI which provides essential information on structural connectivity *in vivo*. Diffusion MRI helps to investigate complex microstructural information of the white matter in the brain. Although dMRI can provide valuable information on structural connectivity, information is not adequate to understand brain connectivity. Functional connectivity provides the information of directionality, and fMRI can be used to extract complementary information to the better understanding of brain connectivity [45]. Since structural connectivity in the brain is the basis of functional connectivity, linking these two need to be address quantitatively.

5.2 The Connectome Mapper

The evolution of MRI has opened up new directions towards studying the structure and functions in the brain for neurosciences. MRI allows investigating much invaluable information in the brain non-invasively. However, understanding of the brain connectivity is a challenge to neuroscientist with its complexity. Both dMRI and fMRI are two main techniques in investigating interactions and interconnections between brain regions [3]. Mainly dMRI allows the white matter in the brain with the demonstration of the location

and trajectory of neuronal tracts *in vivo* [22]. White matter tractography is a useful advancement in dMRI to understand many neurological diseases including stroke, dementia, traumatic brain injuries and Alzheimer disease. A connectome is a neural connection that can be seen as a network. Generally, connectome represents by adjacency matrix which is known as connectivity matrix.

The Connectome Mapper is a unique software that can use to understand the brain connectivity by creating connectivity matrix [3]. The Connectome Mapper is an open source software and a user-friendly pipeline that comprises a combination of various state-of-art neuroimaging software packages which are freely available. Usually, researchers should use these software packages separately, or they have to write their own script to use a combination of all software packages for the fulfilment of data processing. Therefore, the Connectome Mapper aimed to resolve this kind of inconvenience in neuroimaging in term of diffusion pipeline processing. In the field of neurosciences, there could be a very few software tools which have been combined several dedicated tools to perform diffusion pipeline. The main goal of the Connectome Mapper was to provide some guide and support to researchers through all the stages together which are needed for construction of connectome. Also, this tool provides custom processing workflow to fulfil specific needs in connectome creation. Moreover, pipeline processing is simplified that may cause researchers to understand the organisation, image processing and analysis of the data. The Connectome Mapper can be used with wide variety of MRI data such as DTI, Q-Ball imaging, Diffusion Spectrum and fMRI as well.

The Connectome Mapper belongs to the Connectome Mapping Toolkit (CMTK) (http://www.connectomics.org/). This tool is written in Python program. The Connectome Mapper is sophisticated software that can be compatible with much state-of-art software in the neuroscience field. The workflow of the Connectome Mapper is the basis on a wide range of software packages including FSL (www.fmrib.ox.ac.uk/fsl), FreeSurfer (surfer.nmr.mgh.harvard.edu), and Diffusion Toolkit (www.trackvis.org/dtk) etc. The Connectome Mapper owns processing stages and specific task of the workflow with a feasible graphical user interface (GUI). Figure 5.1 shows the GUI of the Connectome Mapper.

5.3 Processing Stages of the Connectome Mapper

The Connectome Mapper is a combination of neuroimaging tool including FSL (https://fsl. fmrib.ox.ac.uk/fsl/fslwiki/FSL), FreeSurfer (https://surfer.nmr.mgh.harvard.edu/), and Diff usion Toolkit (DTK) (http://trackvis.org/dtk/). Stages of the Connectome Mapper are, pre-processing, segmentation, parcellation, registration, fibre tracking and connectome creatin g.

The minimum requirement to implement the Connectome Mapper for structural connectivity is diffusion image series and T1 weighted image series which can be in Digital Imaging and Communication in Medicine (DICOM) or Neuroimaging Informatics Technology Initiative (NIfTI) format. However, DICOM images are internally converted into NIfTI format while processing at the beginning of the workflow.

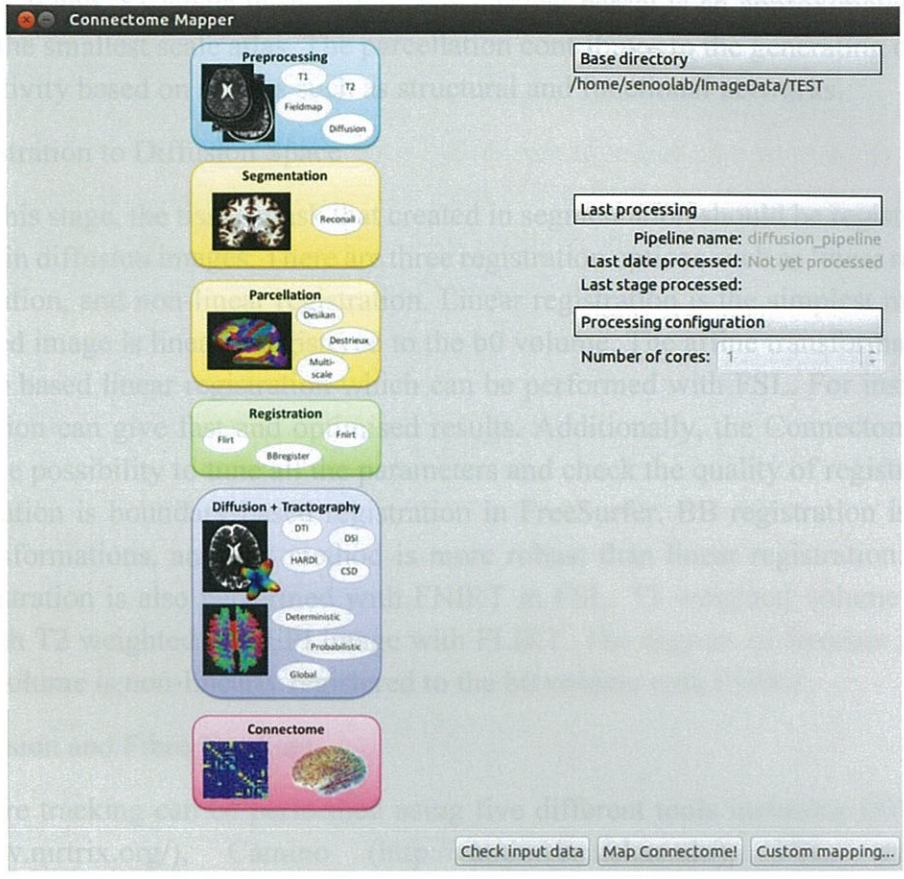

Figure 5.1 The Connectome Mapper GUI

5.3.1 Pre-processing

Diffusion images are more vulnerable to geometric distortion from EPI readout. DTI images are distorted by eddy current as well. Pre-processing enables to avoid eddy current distortion and motion artifacts. In the connectome mapper pre-processing is supported by FUGUE tool of FSL. The correction of non-linear distortions can be performed by additional scan called field maps. However, when a user is unable to obtain field maps, linear registration would still be improved with the T2 weighted non-EPI acquisition.

5.3.2 Segmentation and Parcellation

The pipeline processing in the Connectome Mapper starts with the segmentation of the white matter. In the stage of segmentation, T1 weighted images are processed to extract white matter from grey matter, and CSF. The extracted white matter areas are labelled as nodes in the connectome later on in the parcellation stage. The segmentation is usually performed by FreeSurfer tool, and custom segmentation is also available when user holds a custom atlas. The default tool of the parcellation is NativeFreesurfer. Additionally, Lausanne2008 or custom options are also available at this stage. FreeSurfer creates brain structures and labels based on anatomical atlases which are Desikan-Killiany, and Destrieux. The parcellation starts with the Desikan-Killiany atlas and cortical surface further divides into parcels using the two-phase portioning technique to form multi-scale parcellation of the

cortex. The Connectome Mapper uses five different subject-specific atlases to create 1015, 463, 234, 129 and, 83 labels in the brain. The cortical parcel is an approximately 1.5 cm^2 surface in the smallest scale atlas. The parcellation contributes to the generating of nodes in the connectivity based on studies such as structural and functional networks.

5.3.3 Registration to Diffusion Space

In this stage, the tissue mask that created in segmentation should be registered to the b0 volume in diffusion images. There are three registration options such as linear registration, BB registration, and non-linear registration. Linear registration is the simplest method that T1 weighted image is linearly registered to the b0 volume. The affine transformation refers to intensity based linear registration which can be performed with FSL. For instances, the FLIRT option can give fast and optimised results. Additionally, the Connectome Mapper provides the possibility to tune all the parameters and check the quality of registration. The BB registration is boundary-based registration in FreeSurfer. BB registration is based on linear transformations, and this method is more robust than linear registration. The non-linear registration is also performed with FNIRT in FSL. T1 weighted volume should be aligned with T2 weighted non-EPI image with FLIRT. The degrees of freedom are 6^0. T2-weighted volume is non-linearly registered to the b0 volume with FNIRT.

5.3.4 Diffusion and Fibre Tracking

Fibre tracking can be performed using five different tools including DTK, MRtrix (http://www.mrtrix.org/), Camino (http://camino.cs.ucl.ac.uk/), FSL, and Gibbs (http://docs.mitk.org). MRtrix, Camino, and FSL perform probabilistic tractography, DTK, and Gibbs perform only deterministic streamlines, MRtrix and Camino can perform both tractography methods.

The deterministic streamline with DTK is the most common and easier tractography method in the Connectome Mapper which offers parameters such as the number of seeds, step size, and turning angle that user is able to choose the value of those. The default number of seeds, step size, and turning angle are respectively 32, 1 mm, and 60. Tracking is stopped once streamline criteria is met such as after streamline reached the boundary of grey matter or not sync with the diffusion direction with nearby voxels. The spline function provides filtering which is the basis of fibre length or smoothing to enhance the quality of streamlines. Deterministic tractography is more likely to be sensitive to the noise. To overcome this limitation, the Connectome Mapper has alternative approaches such as global or probabilistic tractography.

In the fibre tracking stage, the Connectome Mapper implements either deterministic, probabilistic or global tractography and each tool provides different seeding technique. For instance, default streamline tracking tool, DTK enables to perform deterministic tractography with randomly chosen N seed points per voxel. MRtrix performs both deterministic and probabilistic tractography, and it uses N, seed points per seed mask. In the probabilistic tractography, tracking starts from the selected ROI and N seeds points per region can be randomly selected. However, global tractography does not have seeding strategy.

5.3.5 Connectome Creation

The final stage in the Connectome Mapper is connectome creation. The connectome is constructed by combining results of tractography with segmentation results. The Connectome Mapper uses Python package of NETWORKX (networkx.lanl.gov) to create a connectome. NETWORKX is a powerful Python package that can be used to create and manipulate complex networks. The final result of Connectome Mapper is a connectivity matrix. The Connectome Mapper offers various options to store results in different formats such as MAT-file, Python pickle, and CFF or graphml files.

The fibre trajectory that reconstructed in this stage is intersected to the boundary of the white matter and grey matter which used to assign a pair of anatomical connections R_i and R_j. This trajectory is represented by a cell C_{ij} in the connectivity matrix.

5.3.6 The Execution Time of the Connectome

The execution time of the Connectome Mapper is varied accordingly for each algorithm in different stages. Generally, the full processing time is about 12 to 72 hours per a subject on an ordinary workstation on the Linux platform. Additionally, segmentation takes 12 to 24 hours. While fibre tracking needs up to 48 hours in probabilistic tractography with default parameters, deterministic tractography takes only a few minutes to complete the task.

5.3.7 Limitations of the Connectome Mapper

The Connectome Mapper has mainly experimented with GE and SIEMENS MRI images. However, pipeline of the Connectome Mapper cannot be implemented when MRI image header stores incorrect information.

5.4 Literature Review of the Connectome Mapper

With the revolution of MRI, neuroscience researchers endeavour to understand brain networks and neurophysiological mechanism. MRI is a non-invasive imaging modality that offers advanced modalities for investigating detailed information of the brain with the new perspective. In the field of neuroimaging, dMRI and fMRI are useful imaging technique to study how brain regions are interconnected. The advanced technique such as DTI helps to map the neuron axonal structure through fibre tracking [3]. Brain mapping is a vital method for understanding the molecular, cellular and functional mechanism particularly after rehabilitation of stroke patients [48]. A connectome is a network that can describe as a comprehensive map of neural connections of the brain. The Connectome Mapper is a novel and useful tool for creating a connectome. The development in the analysis of complex networks in the brain mainly based on graph theory. Graph theory illustrates features of the complex, local and global network measures in the whole brain scale of a human [49].

Some researchers have conducted brain mapping researchers using this dedicated pipeline software. Elda and Emma conducted a study to investigate brain networks characterisation of high-risk preterm school-age children. In their study, the Connectome Mapper pipeline was used to process DWI and T1 weighted images. DWI images were pre-

processed to correct eddy current and head motion using FSL. In the Connectome Mapper pipeline process, registration was accomplished using BB registration tool from FreeSurfer, and white matter extraction was performed using FreeSurfer. Tractography was performed by the inbuilt method in the tool. Graph theory measures of degree, strength, clustering coefficient and local efficiency were analysed [50].

Fischi-Gomez et al. have researched on structural brain connectivity in school-age infants for the impaired network for cognitive skills and social cognition. In this study connectomes were created using the CMTK. DWI and high-resolution T1 weighted images were used to create streamline tractography in FreeSurfer. In this study, local and global connectivity measures were analysed to investigate cognitive functions of children by the new approach of whole brain connectome analysis [51].

Szalkai et al. have found that small brains showed lack of connectivity and large brains in females have the deep connectivity. In this study, graphs were created using the CMTK. FreeSurfer has been applied for parcellation with Desikan-Killiany anatomical atlas with multi-scale parcellation like 83,129, 234, 463, and 1015. Deterministic tractography was performed using MRtrix tool [52]. In our study, deterministic tractography was performed using Diffusion Toolkit, and 83 brain regions were analysed for graph measures.

Kerepesi et al. have conducted a study on mapping the brain to investigate connections between the regions of the brain using CMTK for brain segmentation, parcellation, and creation of connectomes. Parcellation was performed for 1015 brain regions including cortical and subcortical regions which based on Desikan-Kiliany atlas in FreeSurfer. Tractography was performed using the deterministic streamline in MRtrix process [53]. In our study, parcellation was fulfilled for 83 brain regions and deterministic tractography was performed in DTK. According to the results of their study, frontal lobes were conservative and superior temporal, and postcentral gyri were diverse.

Szalkai et al. have conducted another study on graph theory analysis to investigate that women's brains are better connected than Men's Brains. Connectomes were constructed using CMTK. The parcellation was performed for 83, 129 and 234 cortical and subcortical brain regions which were based on Desikan-Kiliany brain atlases using FreeSurfer. This research concluded that female connectomes have more edges than males' connectomes [54].

Kim et al. have shown structural connectivity difference between healthy controls and Parkinson's disease patients using CMTK for DTI and T1 weighted images. The Connectome Mapper pipeline was implemented for pre-processing the DTI. Registration was done using non-linear registration using FSL. Tractography was performed for fibre assignment by continuous tracking from DTK. Structural connectivity of 8 brain regions was compared between healthy controls and Parkinson patients [55].

CHAPTER 6

Tractography

6.1 Introduction to Tractography

DTI delineates the white matter microstructure in the brain by tracking the diffusion of water in neurons. This technique known as tractography has become an important biomarker in the neurodevelopment because it allows white matter structure to examine *in vivo*. In tractography, visualisation and segmentation of these fibre tracts are the most useful aspect of clinical neuroscience [56]. Tractography is a key in neuroimaging since it is the only non-invasive clinical method of reconstructing the white matter to illustrate and visualise the brain wiring system in structural connectivity [24].

Diffusion anisotropy of the water in the white matter based on three axonal alignments. Diffusion of the water more likely to be aligned along the axon and relatively limited to be aligned with the perpendicular axis which is called ellipsoid or a tensor. The method of translation of the longest axis of the tensor into trajectories are achieved by different kind of tractography algorithms such as deterministic or probabilistic tractography. We focused on deterministic tractography in the present study which is clinically more common in the neuroscience [23].

Tractography assumes that each voxel is represented by single fibre orientation. Mathematically this fibre orientation is considered as a three-dimensional vector field is known as streamline.

$$dr\,(s)/\,ds = v[r(s)] \tag{6.1}$$

r (s) is 3D position along the streamline and v is the 3D vector field.

$$r\,(s) = \int s_0\, v[r(s)]ds \tag{6.2}$$

$r\,(s_o) = r_o$ represent the starting point of the streamline which is called as a seed point. This process of streamline integrates the streamline which is referred to as streamline tracking [57].

Generally, two basics tractography approaches are widely applied in clinical and research settings; deterministic and probabilistic tractography. The deterministic tractography constructs white matter tracts which based on user-specified seed points, the principal eigenvector of diffusion and user-specified thresholds that can limit the trajectory. Most typical instances are user-specific curvature threshold and the local FA. Deterministic streamline is the relatively simpler approach, estimating the fibre tract orientation at every voxel is rarely accurate. The deterministic approach considers the mean distribution of orientation of fibre tracts. The probabilistic tractography estimates the entire distribution of possible orientation of fibre tracts which emerge from the specified seed point in all voxels. For instance, if the vast number of tracts are crossing each voxel when probability map derives in the streamline, voxels with the most number of tracts passing through include in the probability tractography. Broadly, the probabilistic approach is more sophisticated and robust, but also harder to compute streamlines compared to deterministic streamlines [56].

Figure 6.1 shows the difference between deterministic tractography and probabilistic tractography.

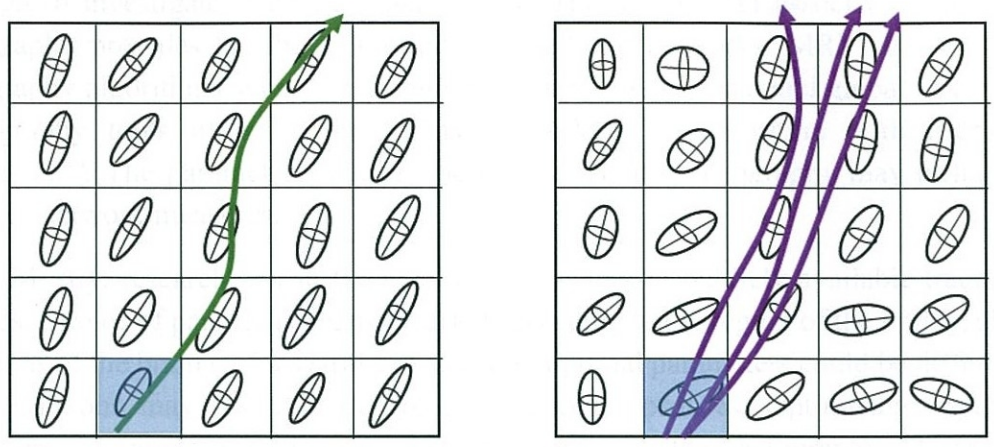

Deterministic tractography Probabilistic tractography

Figure 6.1 Visual representation of deterministic tractography and probabilistic tractography (Source: Reproduced from Rodrigues NB et al. 2017)

The ability of fibre tracking in dMRI to reconstruct the white matter pathways has raised possibilities for numerous clinical applications and offers potential studies in structural and functional aspects [57]. In diffusion, tractography is the only method that can identify and measure the connections and pathways non-invasively.

Tractography is one of the essential steps of construction of connectivity matrix as it can extract fibre bundles in the white matter in order to investigate features of brain networks. Besides, features of structural networks may depend on important tractography parameters such as the number of seeds, turning angle, step size or algorithm. Brain networks can be analysed using methodology such as graph theory using various network parameters including degree, strength, betweenness centrality, local efficiency and cluster coefficient. The global network parameters such as characteristics path length and small-worldness also can be estimated using graph theory. Brain networks describe a graph which consists of a set of nodes and edges that are connected to each node. The main tractography techniques are based on the fixed parameters, and the curvature of streamline and the scale can be varied in each anatomical region. Therefore, optimal tracking parameters also vary with the Region of Interest (ROI). Thus, interpretation of connectivity profiles may become more complicated with slightly different parameters [24].

Tractography has some limitation that has not yet been validated. Moreover, fibre tracking has a significant limitation that fibre tracking unable to accurately delineate tracts within a single voxel due to fibre orientation such as kissing, crossing, converging and diverging [56]. However, probabilistic tractography approach has less risk to bring underestimation of fibre bundles in the brain [23].

6.2 Tractography Parameters

The combination of connectome analysis and graph theory becomes a powerful approach to investigate structural connectivity. The use of DTI associated white matter tractography provides an ability to study about brain networks. MRI has a number of tractography algorithms such as deterministic, probabilistic, local and global tractography. Tractography tools offer the possibility to choose the algorithm with user-defined parameters [5]. The parameters that can be used to create tractography may influence the results of network measures.

Mostly, researchers use fixed set of parameters in publicly available tractography methods. Choice of parameters can be varied according to the region of the brain, subject or conditions of the brain such as stroke. Therefore, optimal parameters could be different and, these variations may result in different connectivity profiles. Optimising tractography parameters are crucial since they may impact on output of the tractography. Therefore, it is essential to investigate the features of the parameters of streamline tractography. Besides, each technique has its array of parameters that should be adjusted with care, depending on the pathological conditions in the study. For instance, the parameters which use for healthy subjects may differ from patients with various pathological conditions [24].

In this study, we briefly reviewed the impact of the number of seeds per voxel, step size, and turning angle of tractography related to the Connectome Mapper. These three parameters are mainly used in streamline tractography and review how variations would lead to different output in graph theory measures.

6.2.1 Turning Angle

Stopping criteria uses turning angle to terminate the fibre tracking when stepping outside the bundle of the white matter. The angular threshold is the maximum bending angle that allows for a streamline trajectory. Generally, the angular threshold for deterministic tractography is 45^0, and probabilistic tractography mostly implements with turning angle of 80^0 [58]. The maximum turning angle of tractography is calculated as follows.

$$\alpha = 2 \arcsin (\text{step}/ 2\ \text{curvature}) \qquad (6.3)$$

In the equation, α denotes maximum turning angle and once after establishing the step and curvature, α can be calculated.

6.2.2 The Number of Seeds

Two types of seeding methods are available in tractography. 1. ROI seeding and 2. Complete seeding. In the ROI seeding method, the user can select the starting ROI and initiates from the voxel that the same ROI located. The complete seeding method refers to track from anywhere in the tracking mask. Thus, it is highly depended on resolution and number of seeds are placed in a voxel. The features of the tractography such as geometry, length, location, and pathology can be affected by the best choices of parameters [24]. The selection of the number of seeds per voxel satisfies the threshold in the initial tracking, and each seed will start to track fibres. Thus, higher number of seeds per voxel will generate

more fibres in the brain. However, the number of seeds depends on the size of the voxel size. For instance, with the large voxel size, more seeds have to be chosen [59].

6.2.3 Step Size

Step size is an important parameter as it can affect highly curved regions. The primary advantage of choosing the correct step size is creating long fibre trajectories by linking fibre orientation in each voxel in the brain [57]. Although there is no standard in the optimal value of step size, the even small alteration may bring an important effect on fibre tracking process. For instance, the too large step size can step outside the bundle, and smaller step size can have numerical errors [24].

6.3 Literature Review for Optimisation of Tractography Parameters

Bastiani et al. have compared tractography algorithms and parameter to evaluate the changes in connectivity matrices using FA and maximum angle between two consecutive steps. The voxel size set as 5 x 5 x 5, and the step size set as 1mm to perform to local tractography, and the graph-based algorithm has been performed with varying the step sizes. Two angular thresholds 30^0 and 90^0 which is a common choice in deterministic tractography were used in the study [60].

In neurosciences, a variety of tractography algorithms are widely used to calculate streamlines through different tractography principles. The selection of probabilistic and deterministic tractography, local and global tractography are included different reconstruction trajectories which based on diffusion signals. Each trajectory can have some advantages and disadvantages as well. Moreover, any tractography method needs an optimal set of parameters which is essential to obtain maximum and minimum fibre length, seed selection and termination of stopping criteria. Thus, the minimum radius curvature would allow streamline to build a better connectome. However, parameters cannot be optimal across all conditions [27].

Chamberland et al. have mentioned that tractography studies mostly conduct with a fixed set of parameters. However, the scale and curvature of fibre bundles can vary from region to region and pathology of the ROI. The various parameters that use to track the white matter may result in different connectivity profiles, and interpretation of the result can be varied dramatically. Therefore, Chamberland et al. have reported that investigating optimal parameters would be extremely advantageous as it may bring more sensitive streamline features through potential converge on optimal setting for the connectome analysis [24].

The reliability of tractography for mapping the brain is limited by technical factors which can affect the final results of connectome. Therefore, Thomas et al. have conducted a study to investigate the anatomical accuracy of the brain connections derived from tractography. This study has been focused on possible limitations in the gold standard tractography techniques. Moreover, the effect of angular threshold and composition of the seed ROI were estimated using DWI data from a rhesus macaque brain *ex vivo* with different

MRI imaging techniques to obtain tractography. Specificity and sensitivity of the tractography method were calculated in the precentral gyrus using Youden index [61].

Cheng et al. have reported optimisation of seed density in DTI tractography for structural networks. This study examined the impact of the number of seeds in tractography on a variance of structural connectivity. They have used as a specific standard to measure the noise of the image. This research was a comparison of the number of random seeds from 1 to 40. For instance, tractography was constructed using the number of seeds such as 1, 5, 10, 15, 20, 25, 30, 35, and 40. The effect of the number of seeds was explored using a set of network measures including degree, betweenness centrality, strength, cluster coefficient, and small-worldness [62].

CHAPTER 7

Impact of Tractography Parameters on Brain Structural Networks; The Connectome Mapper

7.1 Background and Objectives

DTI is one of the promising and non-invasive techniques in the MRI that can assess the microstructural features of the white matter pathways. Mainly, the process of reconstructing the major white matter tracts is called tractography, allows mapping the brain structural connectivity *in vivo*. Despite, these advanced MRI techniques, recent studies on brain connectivity have proposed that whole-brain white matter networks can be analysed using deterministic or probabilistic tractography [63]. Tractography creates the axonal fibre bundles that connecting anatomically separated brain regions once after estimating fibre directions [60].

In neurosciences, reconstructing the macro scale connectome, to mapping structural connections has increasingly become popular in the recent years. Modelling the whole brain of the human as a large-scale network is so-called connectome [58]. The connectome delineates graph which comprises a set of nodes which represent parcellation of brain regions and edges to derive their connections [60]. Comprehensively, three steps are required to compute a connectome from DTI images; 1.A high-resolution T1 image is used to segment and obtain the white matter, 2. Neuronal fibre bundles are extracted in tractography, 3. Reconstructing connectivity matrix by registering T1 images into diffusion image and then intersecting the fibre trajectories with segmented brain regions pair-wise [3].

Brain networks derive from anatomical or physiological observations which can be termed as structural and functional networks. Brain connectivity consists of three kinds of connectivity such as structural connectivity, functional connectivity and effective connectivity. Structural connectivity refers to anatomical connections which link a set of neural elements. In the brain, these connections represent links between cortical and subcortical brain regions. Generally, structural connectivity is estimated as a set of undirected links. Functional connectivity is referred to as the statistical dependence of neuronal elements. Effective connectivity represents casual interactions between neural elements. Our study based on structural connectivity since this study utilised only DTI images [2].

The connectome can be seen as adjacency matrix which is possible to analyse using graph theory and network analysis [60]. Graph theory analysis examines the white matter networks and topological properties such as path length, degree, betweenness centrality, cluster coefficient and small-worldness [63]. Construction of graphs utilises tractography results with node parcellation and connectivity matrix [64]. The degree is the simplest approach of graph theory which is the number of edges connected to a node. The strength is the sum of neighbouring link weights of a node. The betweenness centrality refers to all shortest paths in the network that pass through a particular node [62]. Also, global networks properties include cluster coefficient, characteristic path length and small-worldness is one of the most ubiquitous properties in graph theory [64]. The analysis of brain networks is made

feasible by developing novel imaging methods combined with tools to perform graph theory such as Brain Connectivity Toolbox [2].

Many researchers utilise multiple applications to analyse connectome which are needed to be sophisticated and reliable to obtain excellent features in graphs. The Connectome Mapper is a useful tool for neuroimaging community since the Connectome Mapper incorporates state-of-the-art tools that can use to study brain wiring system. In the tool, each stage provides additional options and possible custom functionalities to facilitate a flexible, user-friendly environment for connectome reconstruction. The Connectome Mapper mainly tested for MRI data from SIEMENS and GE without any issues, except that, it allows a user to control parameters and manually correct and modify intermediate data such as brain mask. In addition, if something goes wrong, the Connectome Mapper GUI can help to tune the parameters and re-process the particular step that gives erroneous results [3].

Diffusion tractography can be influenced by various conditions such as anatomical preparations, diffusion acquisition, data processing, tractography algorithms and tracking parameters. More importantly, tractography profiles can be varied with parameters such as streamline numbers, step size, curvature, fibre orientation, and whole brain versus ROI seeding [58]. Moreover, optimal tracking parameters can be varied dramatically concerning the area of interest or subject or pathological conditions. Thus, the different parameter may bring different connectivity profiles. The reliability of connectivity matrices highly depends on tractography techniques and parameters. Therefore, setting these parameters of tractography is a challenge in order to obtain optimal results in clinical studies.

In neurosciences, scrutinising the impact of tractography parameters on connectivity analysis has gained much attention because currently, there is no gold-standard set of parameters [1]. DTI based tractography may have various tracking parameters such as tracking mask, step size, interpolation, turning angle, and seeding strategy [24]. We examined three parameters including seeds per voxel, turning angle and step size used in deterministic tractography of the Connectome Mapper using DTK. Although a few studies have been addressed the optimisation parameters in tractography, previous literature has not been found related to the tracking parameters in the Connectome Mapper to date. Most users have performed tracking stage of the Connectome Mapper with randomised seeding and default step size and turning angle which are 1 mm and 60^0 respectively.

We aimed to understand the optimal parameters in fibre tracking that can impact on the network measures in structural connectivity since optimising parameters in tractography highly beneficial in future studies with the Connectome Mapper. To achieve this goal, we used DTI and high-resolution T1 data of 10 healthy subjects. The Connectome Mapper creates connectivity matrices, and graph theory computes network measures, the combination was used to examine tractography parameters using network measures. We examined the effect of three tractography parameters with five number of values in each on the network measures including degree, betweenness centrality, cluster coefficient, eccentricity, local efficiency, strength, characteristic path length and small-worldness. In addition, we investigated the relationship of tracking parameters corresponding to the network measures.

7.2 Materials and Methods

7.2.1 MRI Acquisitions

Ten healthy subjects (Age; 43 ±15 years) participated in this study. All Subjects were healthy volunteers with no history of neurological or psychiatric disorders. MRI data were acquired on a 3.0T Philips Achieva scanner (Kikyogahara Hospital, Nagano, Japan). DTI images were acquired with b=800 s/mm^2 and 34 directions over a matrix 128 x 128 x 55, voxel resolution= 1.75 x 1.75 x 3 mm^3 and TE=70 ms, TR=5038 ms. High-resolution T1-weighted MRI data were obtained using following parameters; TE= 3ms, TR= 6 ms with a matrix size of 240 x 240 x 120 and voxel resolution 1 x 1 x 1.5 mm^3.

7.2.2 Image Processing

The whole-brain structural connectomes were extracted using CMTK, a Python-based software (www.cmtk.org) [3]. Figure 7.1 shows the stages of creating connectome matrix in the Connectome Mapper. Motion corrections and eddy current corrections were performed in the pre-processing using an inbuilt method of the Connectome Mapper. The high-resolution T1 image was segmented to extract the white matter from the grey matter and CSF using FreeSurfer tool. Parcellation of cortical and subcortical structures was performed using nativeFreeSurfer tool based on two anatomical atlases, Desikan-Killiany and Destrieux. Eighty-three brain regions were further parcels in this stage. T1 weighted image was registered to the non-diffusion weighted image, b0 volume using linear registration in FSL. Deterministic tractography was performed with FACT algorithm using DTK. In the Connectome Mapper, tractography was performed with regulating turning angle, the number of seeds per voxel and step size. Connectomes were created with altering the turning angles of 40^0, 50^0, 60^0, 70^0, and 80^0, the number of seeds 15, 25, 35, 45, and 55 and step sizes of 0.1 mm, 0.5 mm, 1 mm, 1.5 mm and 2 mm. Connectivity matrices were obtained in the connectome stage as the MAT-file format in MATLAB.

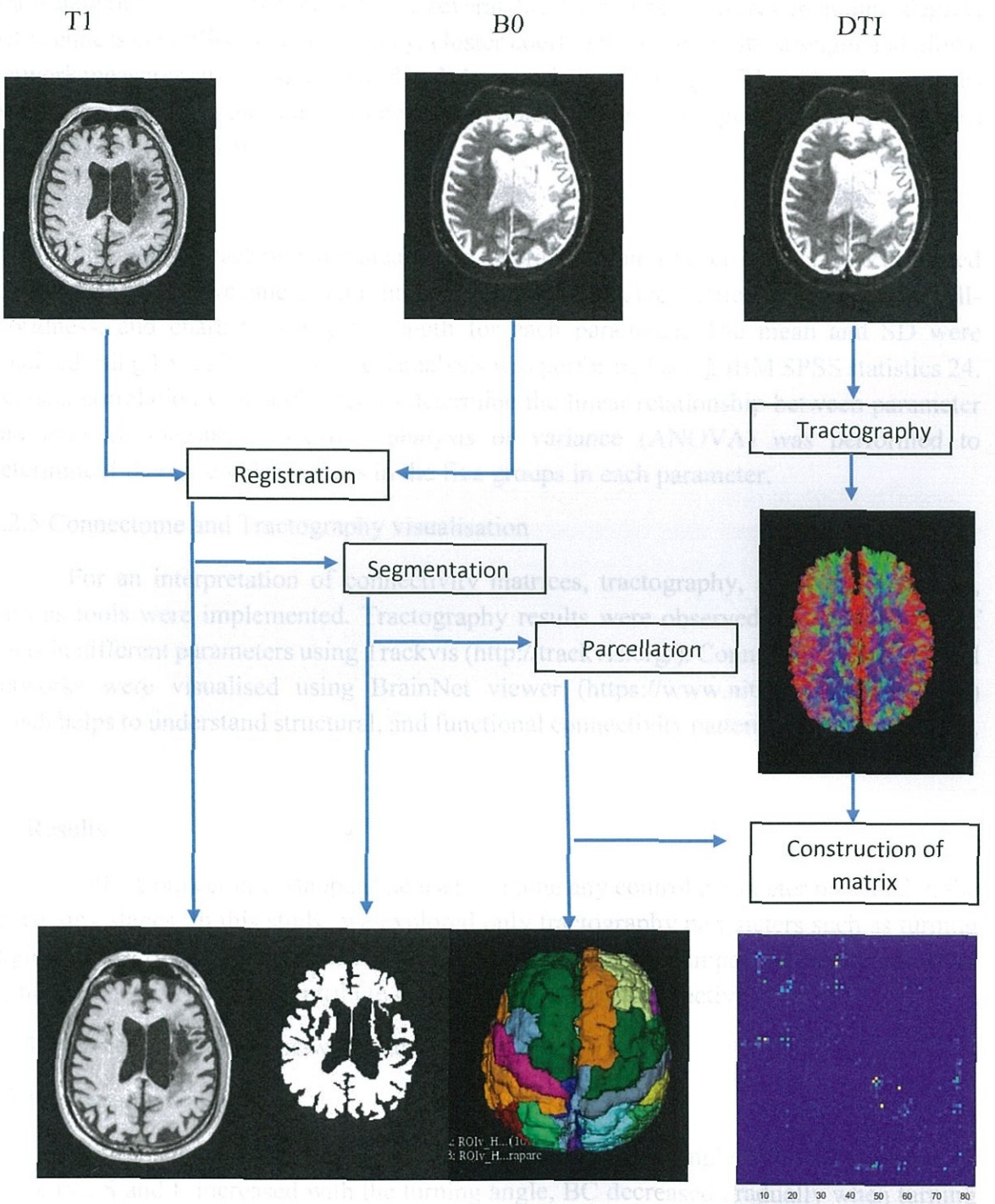

Figure 7.1 Image processing in the Connectome Mapper

7.2.3 Application of Graph Theory

Structural connectomes can be seen as connectivity matrices that are used to define brain networks. Graph theory belongs several local network measures including degree, betweenness centrality, local efficiency, cluster coefficient, eccentricity strength and global network measures such as small world and characteristic path length. The network measures were computed using the Brain Connectivity Toolbox (https://sites.google.com/site/bctnet/) on MATLAB (R2017b).

7.2.4 Data Analysis

The mean of each network measure in 83 brain regions of each subject was calculated to obtain degree, betweenness centrality, cluster coefficient, local efficiency, strength, small-worldness, and characteristic path length for each parameter. The mean and SD were obtained using Excel 2016. Statistical analysis was performed using IBM SPSS statistics 24. Pearson correlation was performed to determine the linear relationship between parameter and network measures. One-way analysis of variance (ANOVA) was performed to determine if there were differences in the five groups in each parameter.

7.2.5 Connectome and Tractography visualisation

For an interpretation of connectivity matrices, tractography, and brain networks, various tools were implemented. Tractography results were observed for examination of tracts in different parameters using Trackvis (http://trackvis.org/). Connectivity matrices and networks were visualised using BrainNet viewer (https://www.nitrc.org/projects/bnv/) which helps to understand structural, and functional connectivity patterns of brain networks.

7.3 Results

In the Connectome Mapper, the user can tune any control parameter provided in the processing stages. In this study, we explored only tractography parameters such as turning angle, number of seeds per voxel and step size to investigate the impact of these parameters on network properties that contribute to describe structural connectivity.

7.3.1 The mean and SD of network measures

7.3.1.1. Turning Angle

Table 1 shows the mean of network measures in turning angle. While the mean d, C, E_{loc}, e (v), S and L increased with the turning angle, BC decreased gradually when turning angle increases. The mean SW increased from 40^0 to 50^0 and after that decreased as turning angle increases. Thus, the largest SW belonged to 50^0.

Turning Angle	mean ± SD				
	40°	50°	60°	70°	80°
d	13.20± 0.70	17.18±0.75	20.14± 0.75	23.14± 0.77	26.53±0.77
BC	254.79±11.24	229.04±16.57	223.18±8.75	203.66±5.85	187.38±7.25
C	43.09±8.29	78.36±14.56	110.56±20.86	132.36±25.27	151.84±31.92
E_{loc}	84.98±15.58	147.79±25.37	202.34±34.52	239.91±41.58	271.13±50.45
e(v)	1061.21±2013.91	1725.56±306.09	2328.31±400.92	2949.96±498.54	3557.82±589.66
S	2701.71±532.52	5039.25±930.02	7454.73±1294.82	9977.93±1689.29	12826.25±2142.48
SW	2.32± 0.14	2.42± 0.28	2.35± 0.17	2.28± 0.25	2.11± 0.27
L	32.95±6.16	61.45±10.78	90.91±14.98	121.68±19.54	156.42±24.77

Table 1 Mean of network measures in five groups of the turning angle for 10 subjects

d = Degree, BC = Betweenness Centrality, C = Cluster Coefficient, E_{loc} = Local Efficient, e(v) = Eccentricity, S = Strength, SW = Small-Worldness, L = Characteristics Path Length

7.3.1.2. The Number of Seeds per Voxel

The mean values of network measures in the whole brain, degree, local efficiency, cluster coefficient, eccentricity, strength and characteristic path length increased as the number of seeds per voxel increases. Table 2 shows the results of d, C, E_{loc}, e (v), S, and L increased when the number of seeds per voxel increases. The BC increased when the number of seeds changes from 15 to 45 and slightly dropped when seeds per voxel at 55. SW only slightly altered while the number of seeds per voxel increased from 15 to 55. However, SW was slightly lower in 35 seeds per voxel.

Number of seeds	mean ± SD				
	15	25	35	45	55
d	18.90±0.63	19.77±0.67	20.33±0.62	20.72±0.73	21.04±0.66
BC	213.99±8.64	218.78±12.56	219.06±12.08	226.70±5.62	225.14±11.74
C	59.53±10.38	91.39±16.56	118.87±23.79	145.94±30.75	173.52±36.37
E_{loc}	108.85±17.39	166.17±27.70	217.49±39.17	268.45±50.16	318.54±60.08
e(v)	1153.58±196.13	1848.72±319.04	2530.74±439.13	3202.23±556.68	3870.21±677.25
S	3703.09±597.19	5928.42±976.19	8102.49±1343.81	10254.6±1701.25	12837.77±2067.21
SW	2.30±0.19	2.39±0.20	2.36±0.24	2.45±0.19	2.48±0.33
L	45.16±7.28	72.29±11.90	98.81±16.39	125.06±20.75	151.07±25.21

Table 2 Mean of network measures in five groups of the number of seeds per voxel for 10 subjects

d = Degree, BC = Betweenness Centrality, C = Cluster Coefficient, E_{loc} = Local Efficient, e (v) = Eccentricity, S = Strength, SW = Small-Worldness, L = Characteristics Path Length

7.3.1.3. Step Size

Table 3 shows the mean of d, and S increased while BC, C, E_{loc} and SW decreased when step size increases. The mean S did not show linear increment, and the rate of increment was lower by 2 mm step size.

The mean SW showed a steep drop from 0.1 mm to 0.5 mm, and the rate of decrement was lower after 0.5 mm. interestingly, e (v) peaked at 1 mm step size and decreased by 1 mm. The mean L increased when step size increases from 0.1 mm to 1.5 mm and decreased by 2 mm step size.

Step Size (mm)	mean ± SD				
	0.1	0.5	1	1.5	2
d	13.18±0.48	17.24±0.67	20.14±0.75	23.01±0.71	25.91±1.06
BC	309.70±22.06	257.49±9.98	222.56±9.04	195.63±8.07	174.46±7.96
C	129.79±16.36	121.08±20.11	110.56±20.86	99.48±17.76	86.56±16.31
E_{loc}	234.73±30.51	221.10±35.51	202.34±34.52	183.03±29.91	161.05±26.68
e(v)	2035.20±330.08	2306.62±399.17	2328.31±400.92	2290.27±387.73	2195.25±366.80
S	5892.54±855.74	7071.77±1174.49	7454.74±1228.37	7689.80±1258.88	7703.41±1289.28
SW	3.06±0.23	2.53±0.16	2.35±0.17	2.25±0.24	2.08±0.19
L	71.86±10.44	86.24±14.32	90.91±14.98	93.77±15.35	93.44±15.72

Table 3 Mean of network measures in five groups of step size for 10 subjects

d = Degree, BC = Betweenness Centrality, C = Cluster Coefficient, E_{loc} = Local Efficient, e (v) = Eccentricity, S = Strength, SW = Small-Worldness, L = Characteristics Path Length

7.3.2 Pearson correlation test results

The Pearson correlation was carried out to look for the relationship between parameters and network measures. Table 4 shows the results of the Pearson correlation test in each parameter. The results suggested that correlation between the turning angle and degree, betweenness centrality, cluster coefficient, local efficiency, eccentricity, and characteristic path length were statistically significant and $p < 0.01$, two-tailed and correlation between turning angle and small-worldness was statistically significant and $p < 0.05$. The correlation between the number of seeds per voxel and all the network measures except small-worldness were statistically significant at $p < 0.01$, two-tailed and correlation between the number of seeds and small-worldness was significant at $p<0.05$, two-tailed. The correlation between step size and all the network measures except eccentricity were significant at $p < 0.01$ and correlation of step size and eccentricity was not statistically significant. The correlation between the turning angle and small-worldness ($r = -0.317$, $p= 0.025$) was moderate and the number of seeds was weakly related to small-worldness ($r=0.244$, $p=0.088$). The step size is weakly correlated to eccentricity ($r= 0.099$, $p = 0.493$) and the correlation between the step size and strength ($r= 0.434$, $p=0.002$) and characteristic path length ($r= 0.434$, $p = 0.002$) were moderate.

Parameters		d	BC	C	E_{loc}	e(v)	S	SW	L
Turning Angle [degree]	Pearson Correlation	.986**	-.896**	.864**	.872**	.901**	.934**	-.317*	.934**
	Sig. (2-tailed)	0.000	0.000	0.000	0.000	0.000	0.000	0.025	0.000
Number of seeds per voxel	Pearson Correlation	.735**	.373**	.844**	.870**	.898**	.906**	0.244	.906**
	Sig. (2-tailed)	0.000	0.008	0.000	0.000	0.000	0.000	0.088	0.000
Step size [mm]	Pearson Correlation	.979**	-.944**	-.640**	-.639**	0.099	.434**	-.793**	.434**
	Sig. (2-tailed)	0.000	0.000	0.000	0.000	0.493	0.002	0.000	0.002

** Correlation is significant at the 0.01 level (2-tailed)

* Correlation is significant at the 0.05 (2-tailed)

Table 4 The results of Pearson correlation test for total sample (N= 50)

d = Degree, BC = Betweenness Centrality, C = Cluster Coefficient, E_{loc} = Local Efficient, e (v) = Eccentricity, S = Strength, SW = Small-Worldness, L = Characteristics Path Length

7.3.3 One-way ANOVA test results

7.3.3.1Turning Angle

Table 5 shows the ANOVA test results in turning angle. There was significant difference between groups in turning angle as determined by one-way ANOVA in all the network measures except small-worldness ($F(4, 45) = 2.277$, $p = 0.076$).

Network measures	F	Sig.
d	430.611	0.000
BC	52.488	0.000
C	35.544	0.000
E_{loc}	39.034	0.000
e(v)	48.788	0.000
S	77.344	0.000
SW	2.277	0.076
L	77.344	0.000

Table 5 The one-way ANOVA results of the turning angle ($p<0.05$)

d = Degree, BC = Betweenness Centrality, C = Cluster Coefficient, E_{loc} = Local Efficient, e (v) = Eccentricity, S = Strength, SW = Small-Worldness, L = Characteristics Path Length

7.3.3.2 The number of seeds per voxel

Table 6 shows the one-way ANOVA results which determined that there was no statistically significant difference between the number of seeds per voxel and betweenness centrality ($p=0.084$) and small-worldness ($p=0.506$).

Network measures	F	Sig.
d	14.608	0.000
BC	2.199	0.084
C	27.953	0.000
E_{loc}	35.089	0.000
e(v)	47.039	0.000
S	51.499	0.000
SW	0.842	0.506
L	51.499	0.000

Table 6 The one-way ANOVA results of the number of seeds per voxel ($p<0.05$)

d = Degree, BC = Betweenness Centrality, C = Cluster Coefficient, E_{loc} = Local Efficient, e (v) = Eccentricity, S = Strength, SW = Small-Worldness, L = Characteristics Path Length

7.3.3.3 Step size

Table 7 shows the One-way ANOVA result of step size. The results suggested that there was no statistically significant difference between the step size and eccentricity ($p = 0.461$) and all the other network measures showed a significant difference in step size.

Network measures	F	Sig.
d	385.321	0.000
BC	161.177	0.000
C	7.819	0.000
E_{loc}	7.804	0.000
e(v)	0.919	0.461
S	3.730	0.011
SW	31.225	0.000
L	3.730	0.011

Table 7 The one-way ANOVA results of step size ($p<0.05$)

d = Degree, BC = Betweenness Centrality, C = Cluster Coefficient, E_{loc} = Local Efficient, e (v) = Eccentricity, S = Strength, SW = Small-Worldness, L = Characteristics Path Length

7.4 Discussion

In this study, we examined the impact of turning angle, the number of seeds per voxel and step size in fibre tracking on the structural networks using DTI of 10 healthy subjects. We estimated the mean values of network measures in the whole brain to optimise the parameters in fibre tracking of the Connectome Mapper.

We investigated how the different number of seeds, turning angles and step size may influence the estimation of several network measures that represent human structural connectome including degree, strength, centrality, local efficiency, cluster coefficient, eccentricity, and global network measures including small-worldness and characteristics path length. We showed that how the choice of parameters in turning angle, number of seeds per voxel and step size related to network measures. It is important to examine the most useful network measures such as small-worldness, local efficiency, and cluster coefficient.

The results of degree, local efficiency, cluster coefficient, eccentricity, and strength increased when the turning angle, and the number of seeds per voxel increase. This result revealed that strong dependence not suggests given parameters are any more optimal than another except some few network measures.

The results of Pearson correlation suggested that turning angle and the number of seeds can have less impact on most of the network measures except small-worldness since the most of network measures increased when the turning angle and the number of seeds per voxel increase. The correlation between the number of seeds per voxel and all the network measures except small-worldness were strong or moderate positive correlation which determined that the number of seeds did not have an impact on network measures. The step size possesses strong negative correlations with betweenness centrality, cluster coefficient, local efficiency and small-worldness which emphasized that small step size would be appropriate for network measures.

The one-way ANOVA results of the turning angle showed that there were significant difference between five groups in most of the network measures ($p< 0.05$) except small-worldness ($F (4, 45) = 2.277$, $p=0.076$) that suggested small-worldness only can have an effect from the turning angle and there could not be an optimal value in the turning angle related to the network measures except small-worldness. The number of seeds per voxel also could not have any optimal value in most of the network measures except betweenness centrality ($F (4, 45) = 14.608$, $p = 0.084$) and small-worldness ($F (4, 45) =0.842$, $p= 0.506$). The step size also showed that the network measures except eccentricity ($F (4, 45) = 0.919$, $p= 0.461$) would not have any optimal value in network measures in terms of the step size.

The degree and the strength had a similar trend. The mean degree increased when the turning angle ($r= 0.986$, $p=0.000$), number of seeds ($r= 0.735$, $p= 0.000$) and step size ($r= 0.979$, $p= 0.000$) increase. The strength was also increased when the parameters increase. Figure 7.2 shows the graph of degree versus three parameters. This result emphasised that more connections can be obtained when increasing these three parameters. However, the

strength did not follow a linear relationship with the step size. Figure 7.3 (c) shows the strength slightly increased when step size increases (r = 0.434, p=0.002) and the rate of increment is lower with larger step size. The strength is the mean value of total weight of edges in the particular node. For this reason, the strength value did not follow a linear pattern in the graph. The results of the degree and the strength determined that more connections were obtained when parameters increase.

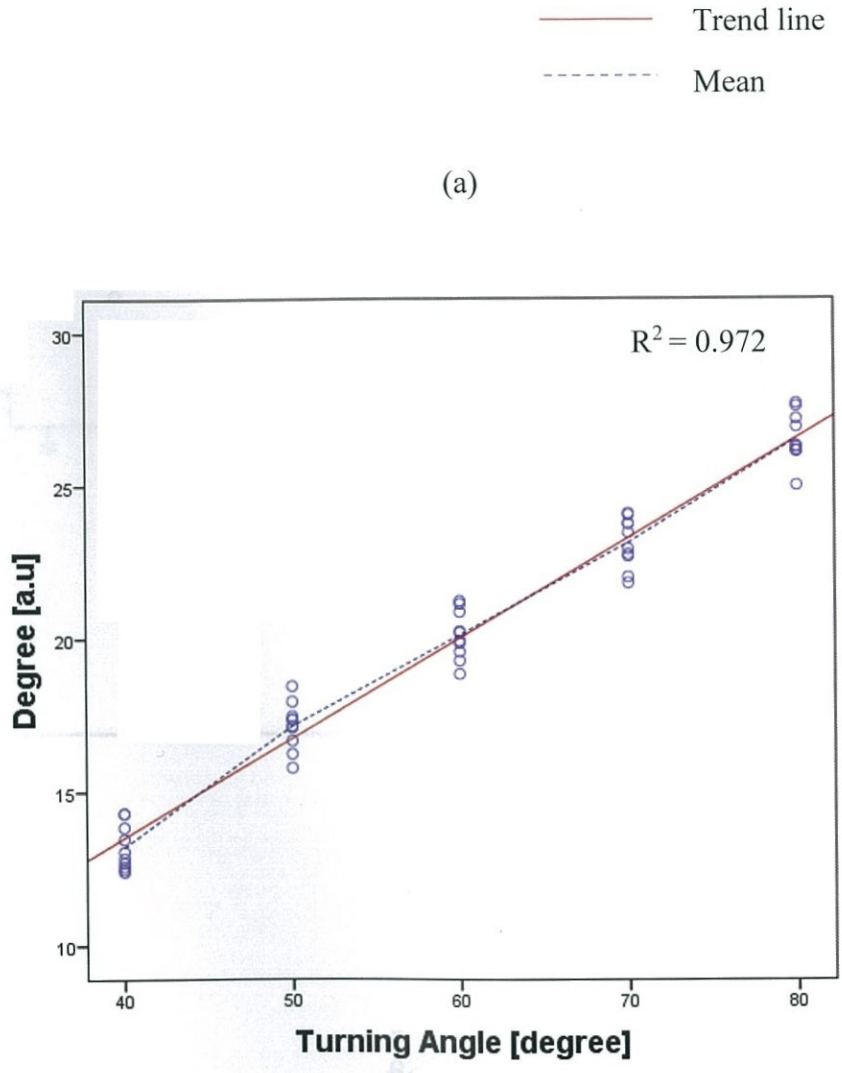

(b)

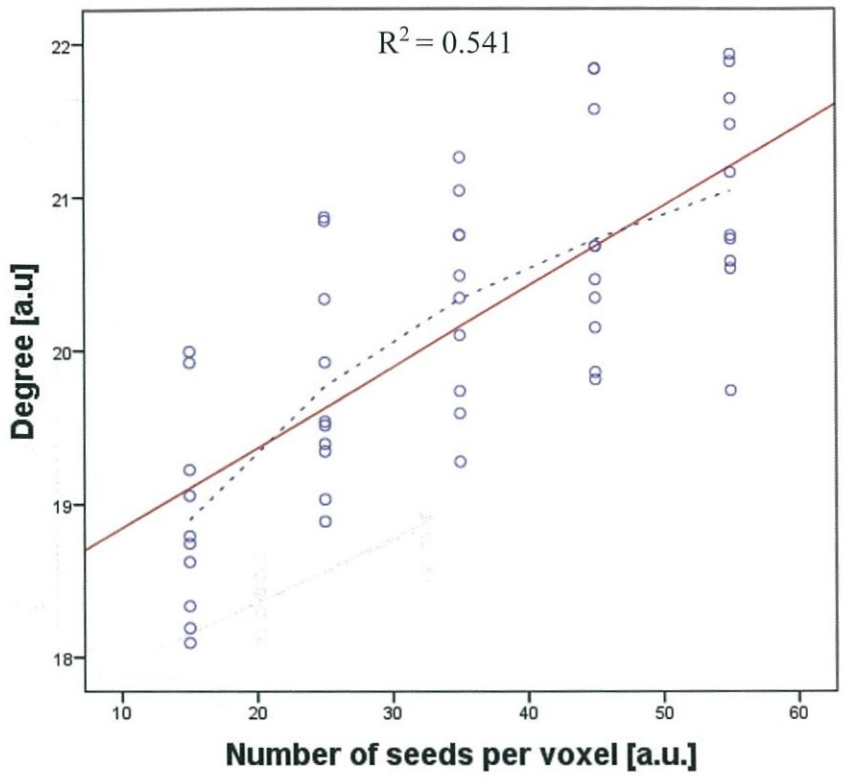
$R^2 = 0.541$
Degree [a.u]
Number of seeds per voxel [a.u.]
22
21
20
19
18
10
20
30
40
50
60

(c)

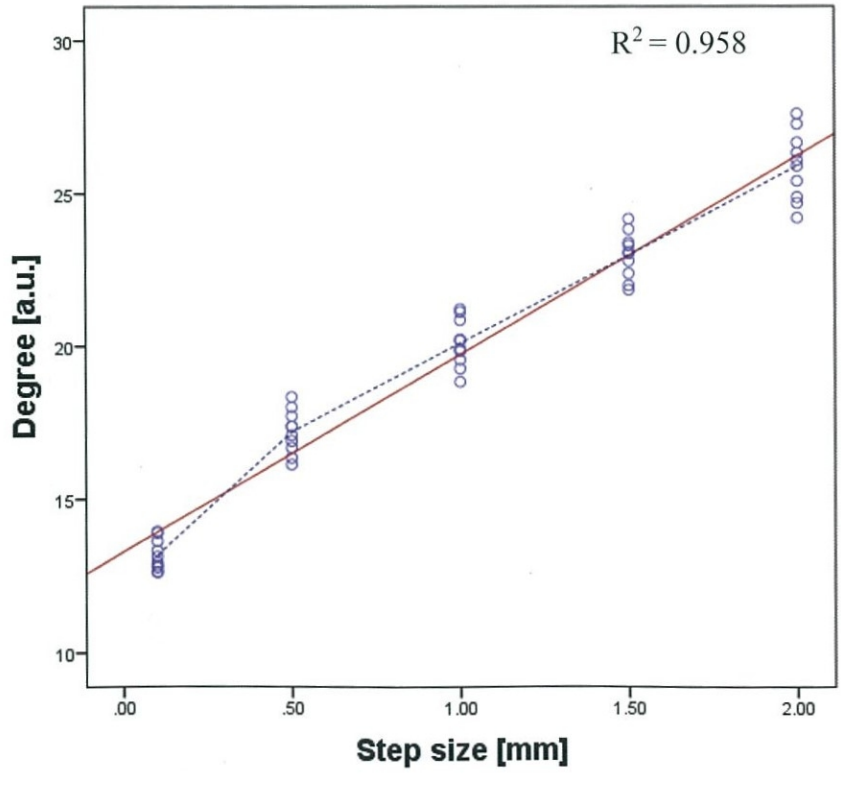
$R^2 = 0.958$
Degree [a.u.]
Step size [mm]
30
25
20
15
10
.00
.50
1.00
1.50
2.00

Figure 7.2 Mean of the degree increase when turning angle, number of seeds per voxel and step size increase.

(a)

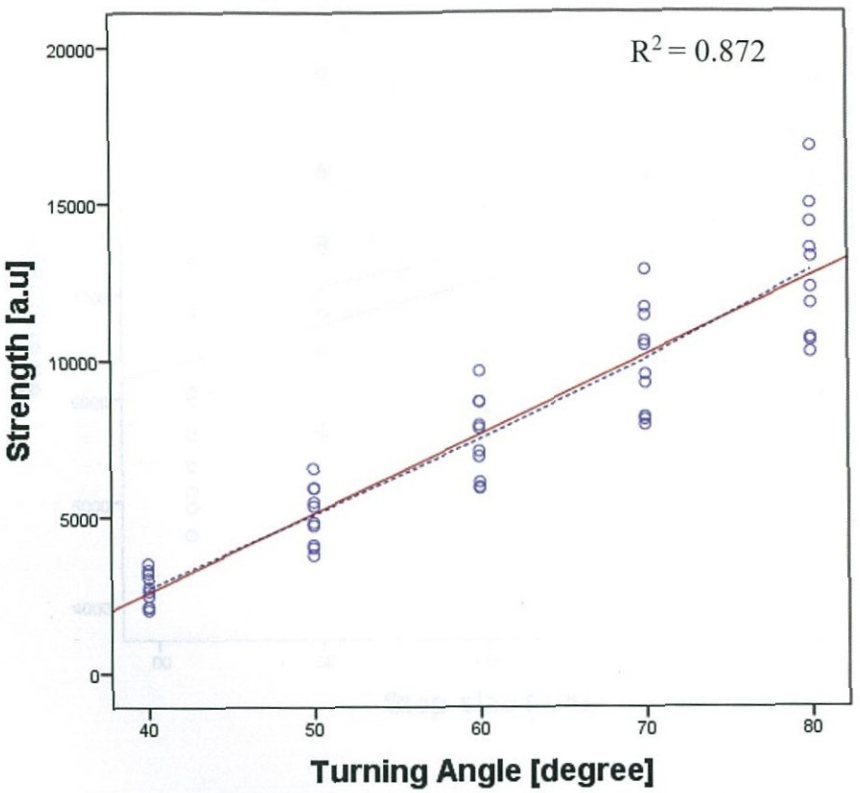

(b)

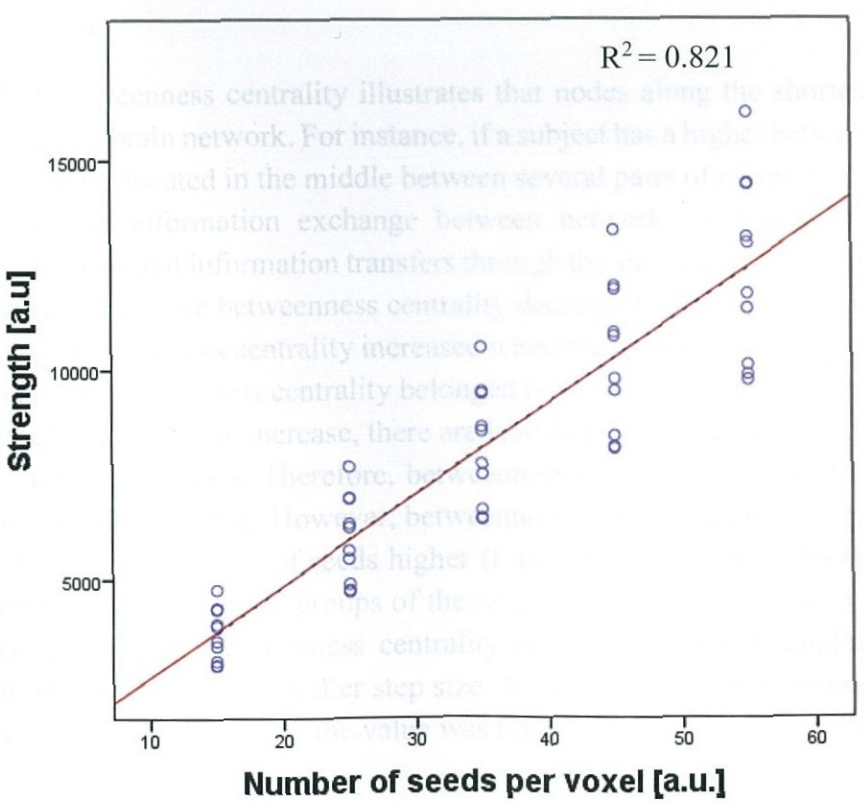

(c)

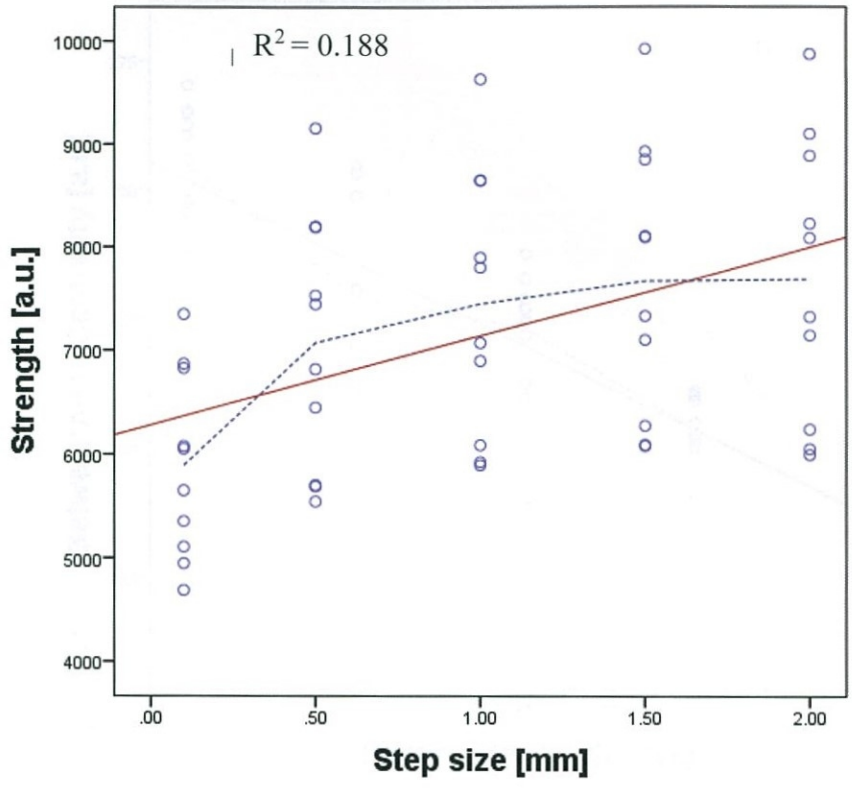

Figure 7.3 Mean of the strength increased when turning angle and number of seeds per voxel increase. (c) The mean strength did not increase linearly when step size increases.

The betweenness centrality illustrates that nodes along the shortest path to be the most central in a brain network. For instance, if a subject has a higher betweenness centrality, and if the node is located in the middle between several pairs of nodes, that reveals the flow and integrity of information exchange between networks is higher. The betweenness centrality deduces that information transfers through the shortest path in a network [27]. Figure 7.4 shows that while the betweenness centrality decreased when turning angle and step size increase, the betweenness centrality increased when the number of seeds per voxel increases and the highest betweenness centrality belonged to 45 seeds per voxel. Generally, when the turning angle and step size increase, there are less shortest path can be seen in networks due to longer fibre trajectories. Therefore, betweenness centrality decreased when the turning angle and step size increase. However, betweenness centrality increased up to 45 seeds and decreased when the number of seeds higher ($F(4, 45) = 2.199$, $p = 0.084$) which could be the optimal group among five groups of the number of seeds in related to the betweenness centrality. The higher betweenness centrality can be obtained in smaller turning angle, higher number of seeds and smaller step size. Although the highest betweenness centrality belonged to 45 seeds per voxel, the value was not emphasised in other network measures.

(a)

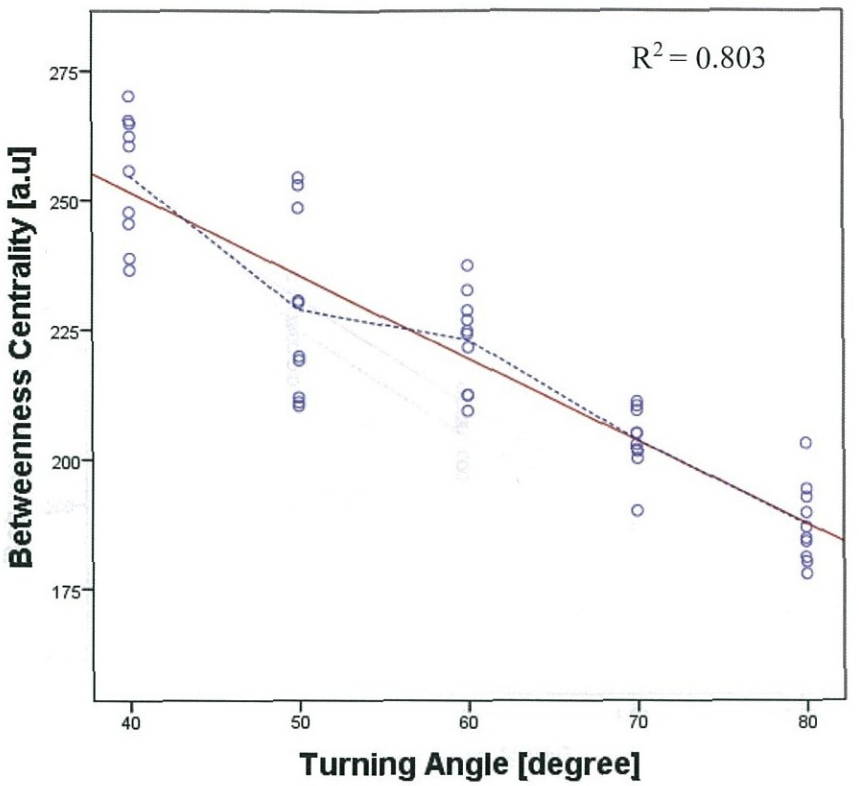
$R^2 = 0.803$
Betweenness Centrality [a.u]
275
250
225
200
175
40
50
60
70
80
Turning Angle [degree]

(b)

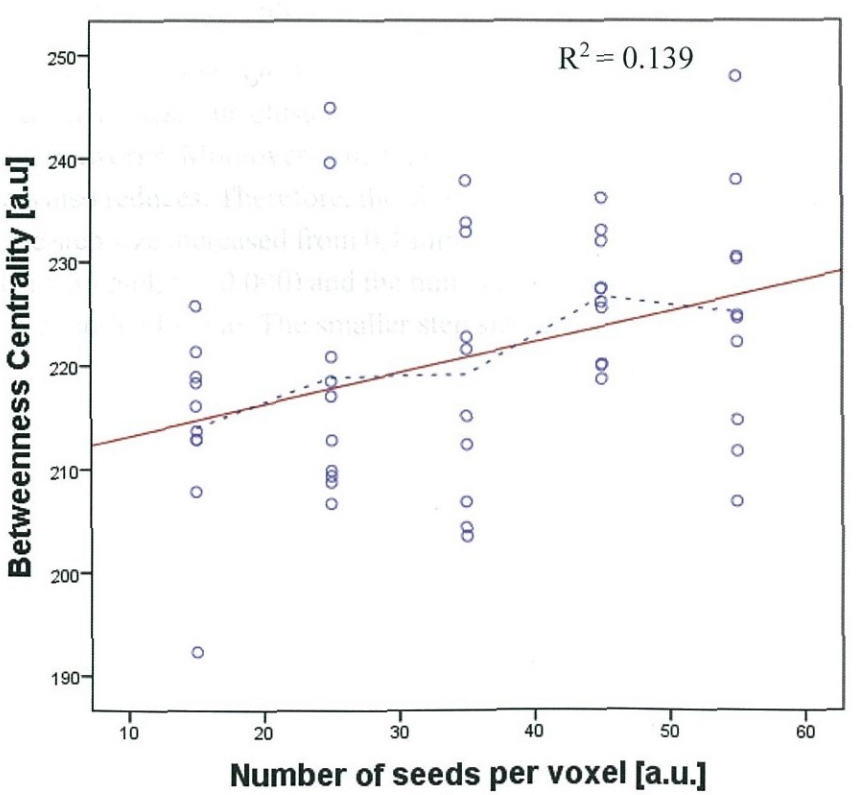
$R^2 = 0.139$
Betweenness Centrality [a.u]
250
240
230
220
210
200
190
10
20
30
40
50
60
Number of seeds per voxel [a.u.]

(c)

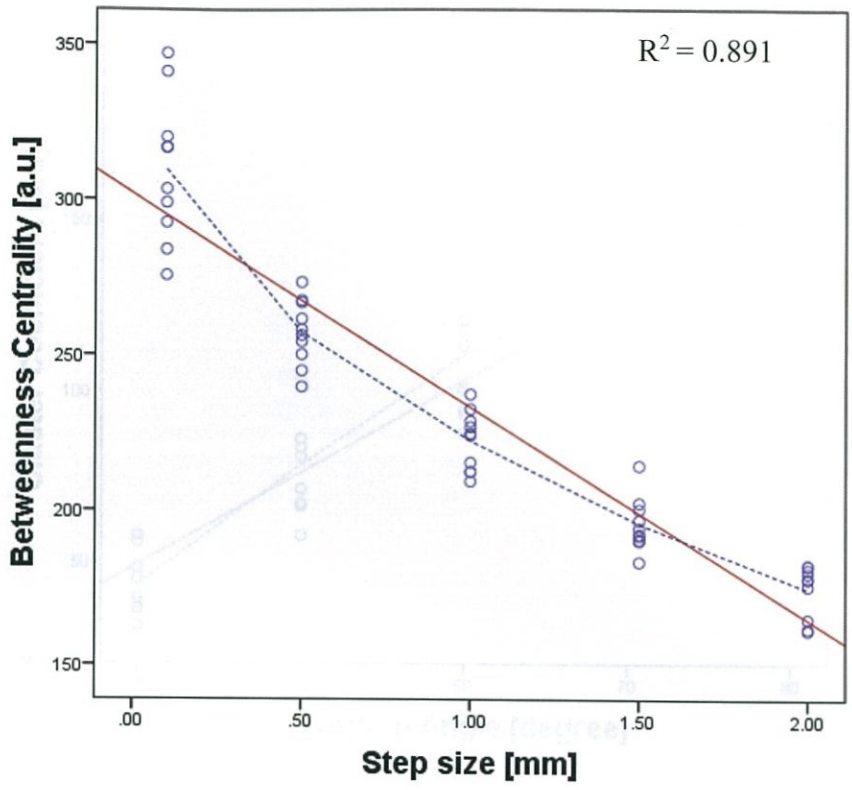

Figure 7.4 (a) (c) Betweenness Centrality decreased when turning angle and step size increase. (b) Betweenness Centrality increased when a number of seeds increases.

Figure 7.5 shows that cluster coefficient increased when turning angle, and the number of seeds increases. The cluster coefficient assumes the abundance of the connected triangle in brain networks. Moreover, when the length of fibre tracts increases the possibility to form clusters also reduces. Therefore, the cluster coefficient ($F(4, 45) = 7.819$, $p = 0.000$) decreased as the step size increased from 0.1 mm to 2 mm. This result illustrated that turning angle ($F(4, 45) = 35.544$, $p = 0.000$) and the number of seeds ($F(4, 45) = 27.953$, $p = 0.000$) did not show any optimal value. The smaller step size is appropriate to obtain higher cluster coefficient.

(a)

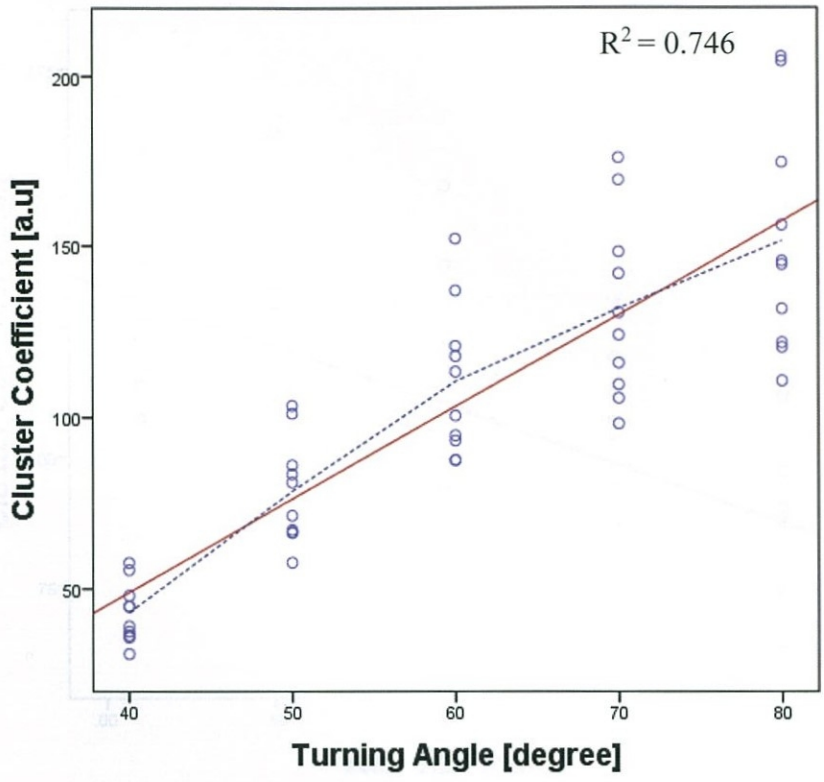
$R^2 = 0.746$
Cluster Coefficient [a.u]
200
150
100
50
40
50
60
70
80
Turning Angle [degree]

(b)

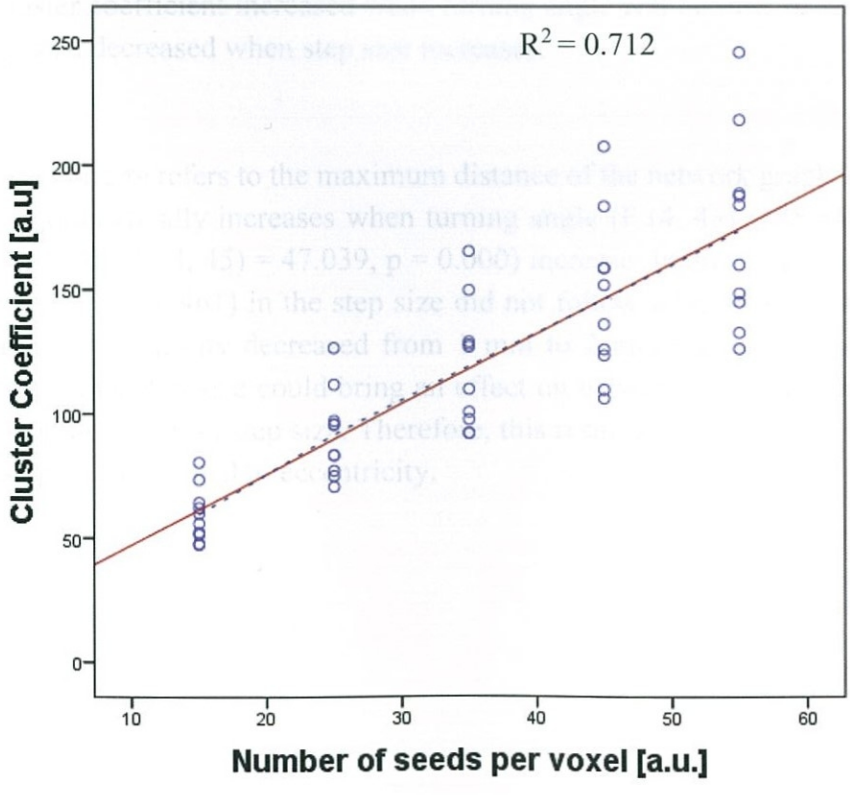
$R^2 = 0.712$
Cluster Coefficient [a.u]
250
200
150
100
50
0
10
20
30
40
50
60
Number of seeds per voxel [a.u.]

(c)

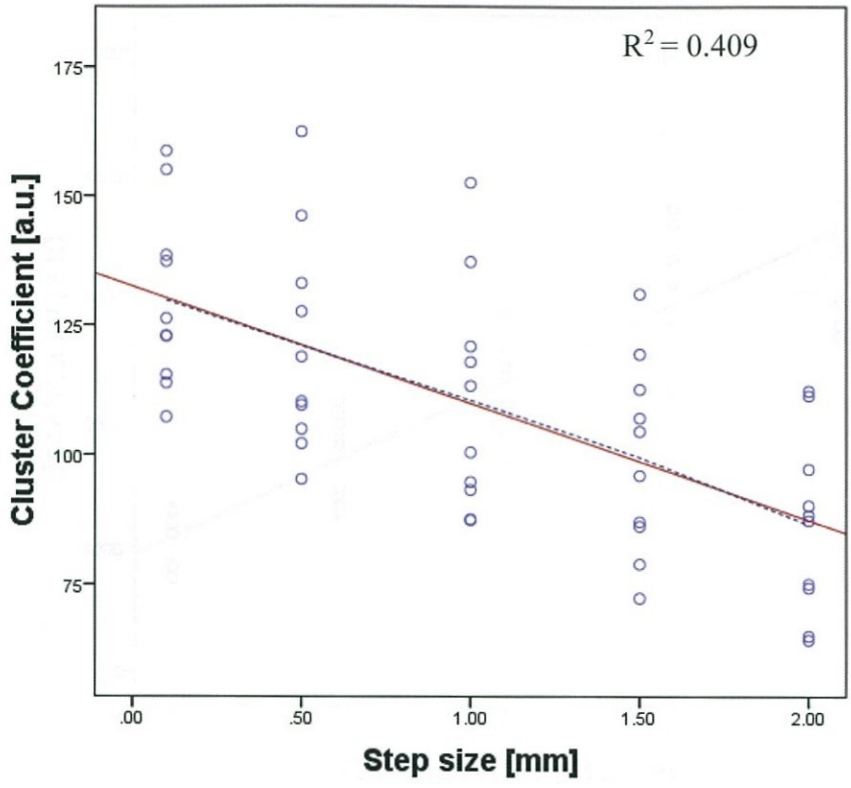

Figure 7.5 Cluster coefficient increased when turning angle and number of seeds per voxel increase. Step size decreased when step size increases.

The eccentricity refers to the maximum distance of the network graph. The length of the fibre tracts dramatically increases when turning angle ($F(4, 45) = 35.544$, $p = 0.000$) and number of seeds ($F(4, 45) = 47.039$, $p = 0.000$) increase. Interestingly the eccentricity ($F(4, 45) = 0.919$, $p = 0.461$) in the step size did not follow a linear trend. Figure 7.6 (c) shows that mean eccentricity decreased from 1 mm to 2 mm step size. The eccentricity results illustrated that step size could bring an effect on network measures and the highest eccentricity belongs to 1 mm step size. Therefore, this result suggested that 1 mm could be the optimal step size in related to eccentricity.

(a)

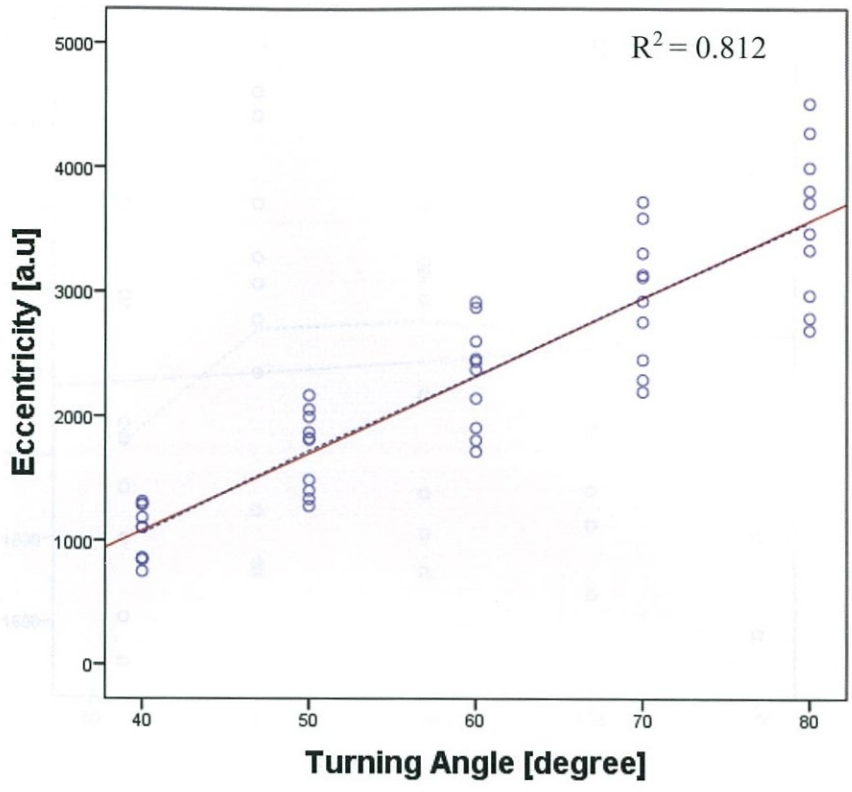
$R^2 = 0.812$
Eccentricity [a.u]
Turning Angle [degree]
0
1000
2000
3000
4000
5000
40
50
60
70
80

(b)

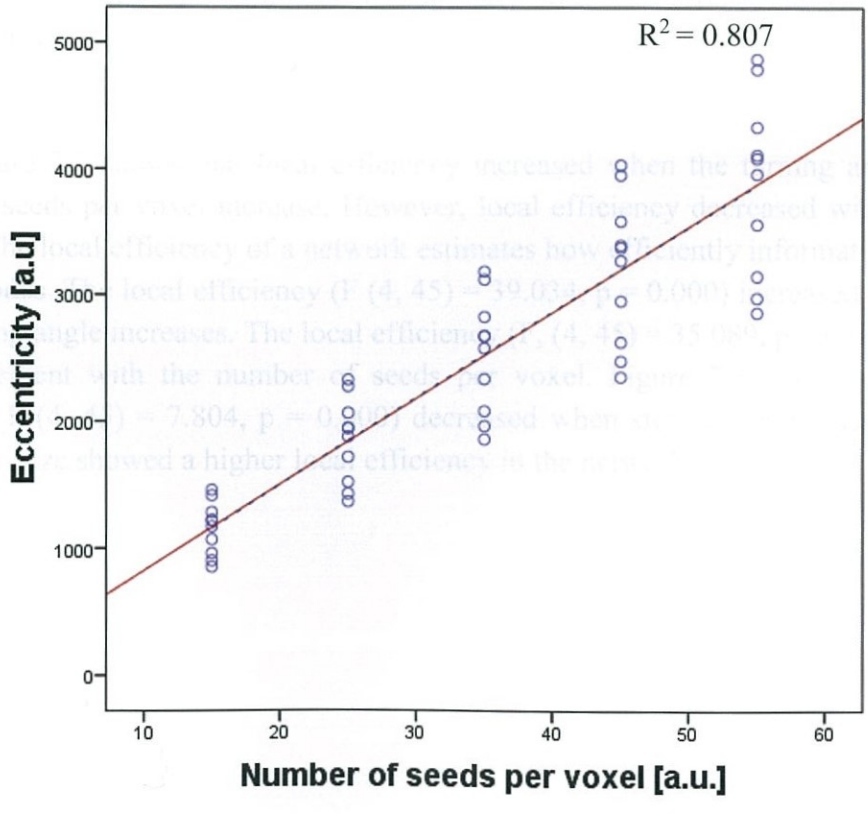
$R^2 = 0.807$
Eccentricity [a.u]
Number of seeds per voxel [a.u.]
0
1000
2000
3000
4000
5000
10
20
30
40
50
60

(c)

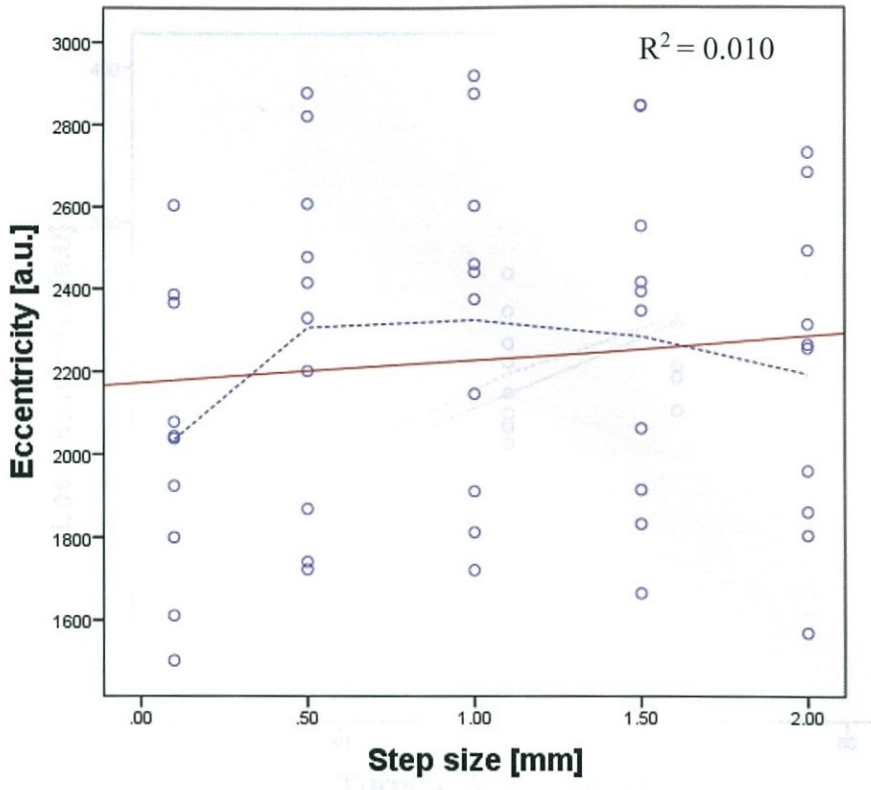

Figure 7.6 The mean eccentricity increased with turning angle and number of seeds per voxel. (c) The mean eccentricity was highest at 1mm step size and decreased when the step size increases further.

Figure 7.7 shows that local efficiency increased when the turning angle and the number of seeds per voxel increase. However, local efficiency decreased with the higher step size. The local efficiency of a network estimates how efficiently information exchange between nodes. The local efficiency ($F(4, 45) = 39.034$, $p = 0.000$) increased dramatically when turning angle increases. The local efficiency ($F, (4, 45) = 35.089$, $p = 0.000$) followed linear increment with the number of seeds per voxel. Figure 7.7 (c) shows the local efficiency ($F(4, 45) = 7.804$, $p = 0.000$) decreased when step size increases. Therefore, smaller step size showed a higher local efficiency in the networks.

(a)

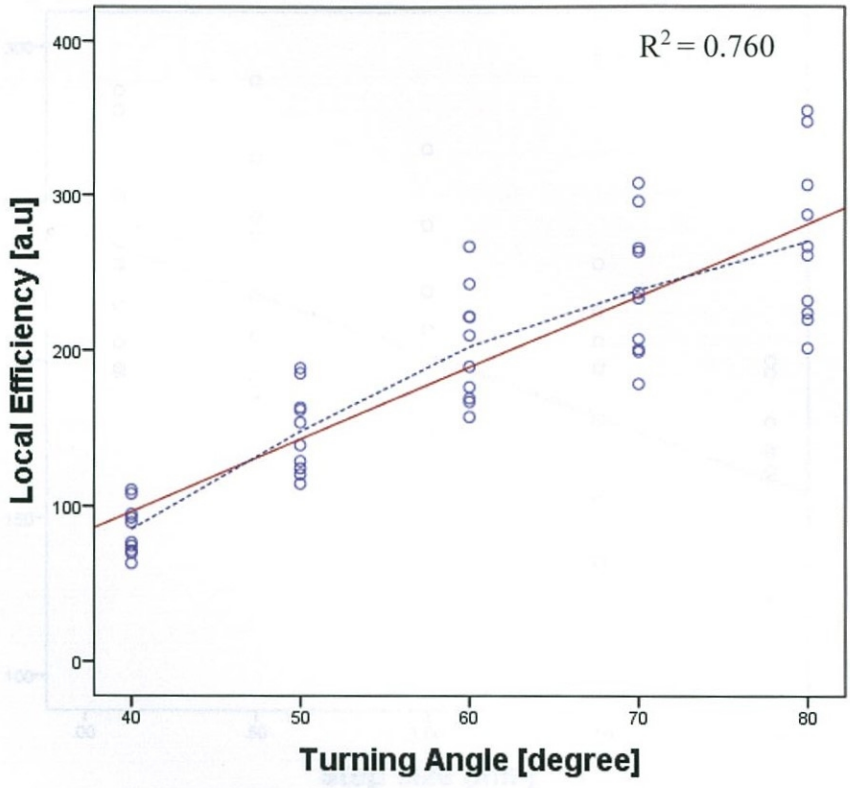
$R^2 = 0.760$
Local Efficiency [a.u]
400
300
200
100
0
40
50
60
70
80
Turning Angle [degree]

(b)

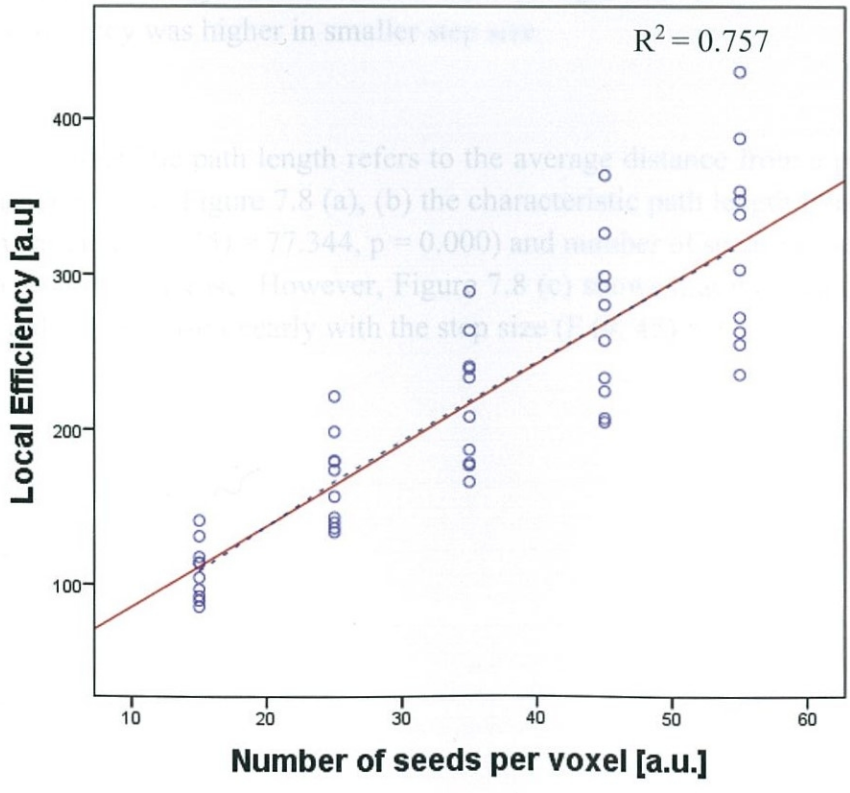
$R^2 = 0.757$
Local Efficiency [a.u]
400
300
200
100
10
20
30
40
50
60
Number of seeds per voxel [a.u.]

(c)

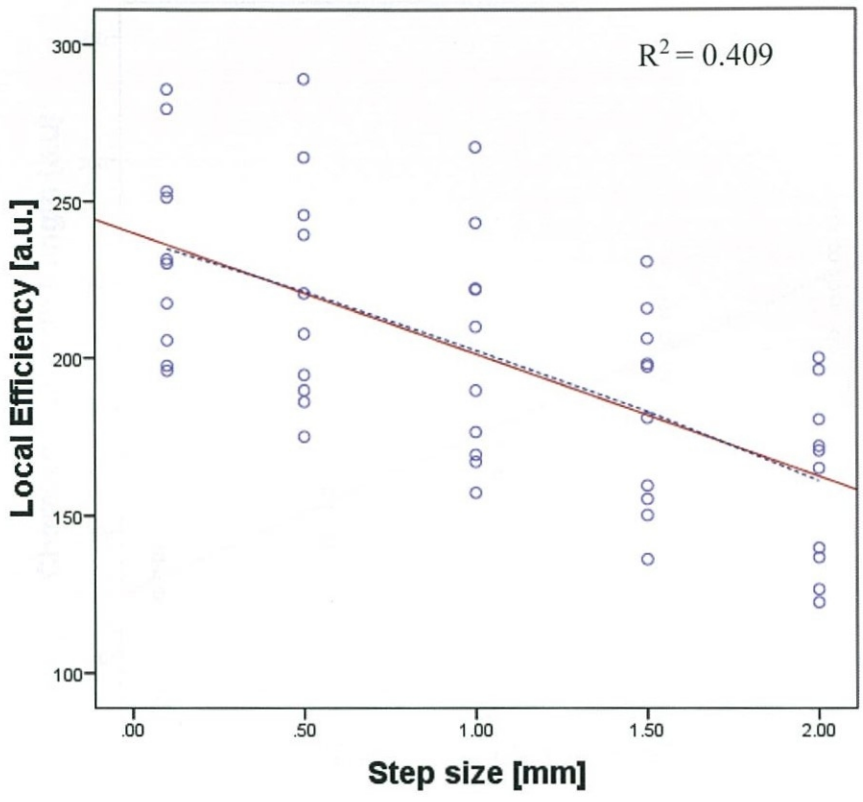

Figure 7.7 Local efficiency increased when turning angle and number of seeds increase. Mean local efficiency was higher in smaller step size.

The characteristic path length refers to the average distance from a particular node to any other node. In the Figure 7.8 (a), (b) the characteristic path length linearly increased when turning angle ($F(4, 45) = 77.344$, $p = 0.000$) and number of seeds per voxel ($F(4, 45) = 51.499$, $p = 0.000$) increase. However, Figure 7.8 (c) shows that the mean characteristic path length did not increase linearly with the step size ($F(4, 45) = 3.730$, $p = 0.011$).

(a)

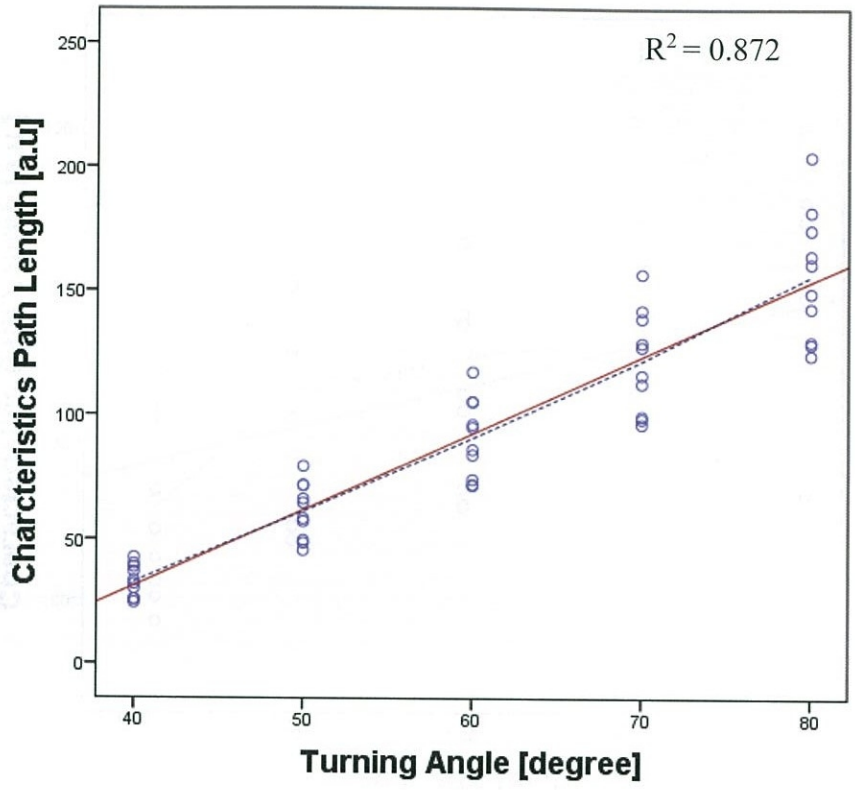
$R^2 = 0.872$
Charcteristics Path Length [a.u]
Turning Angle [degree]
250
200
150
100
50
0
40
50
60
70
80

(b)

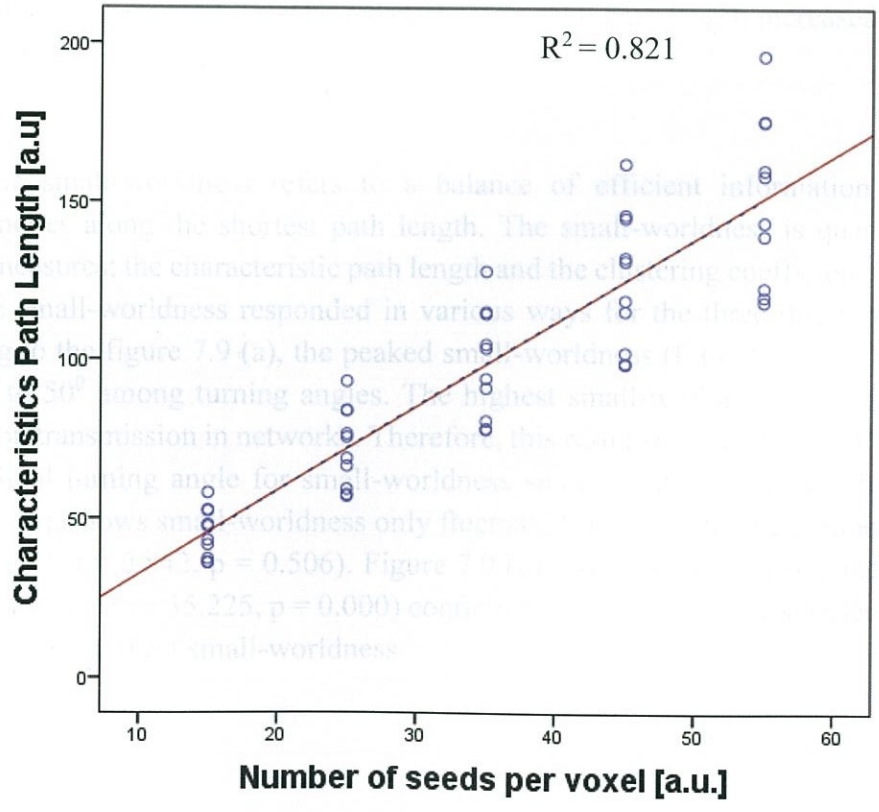
$R^2 = 0.821$
Characteristics Path Length [a.u]
Number of seeds per voxel [a.u.]
200
150
100
50
0
10
20
30
40
50
60

(c)

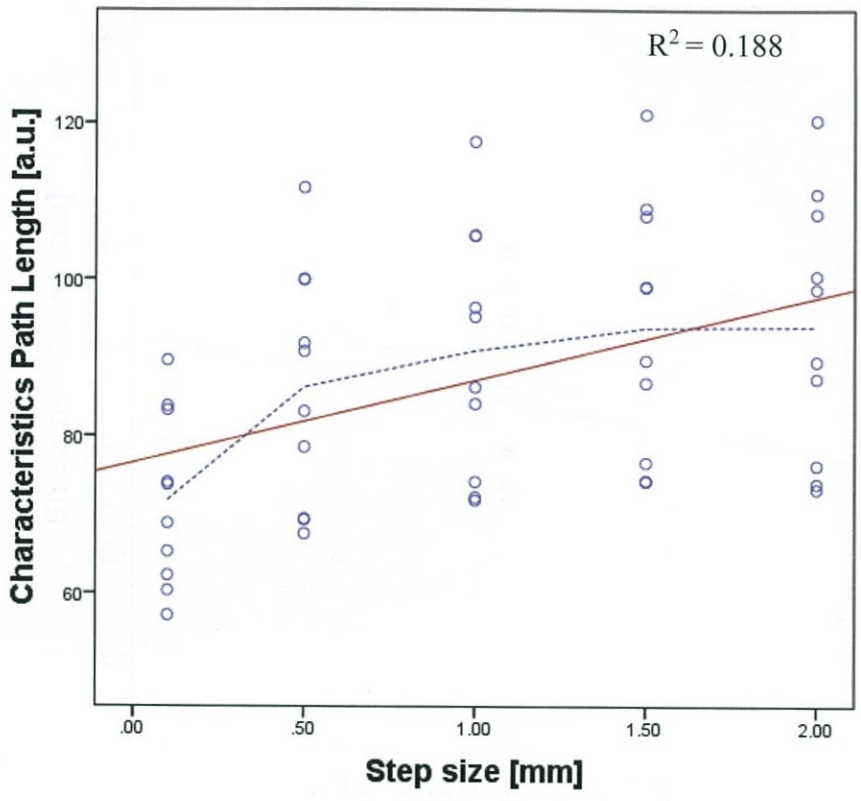

Figure 7.8 (a), (b) The characteristic Path length increased linearly with turning angle and number of seeds per voxel. (c) The mean characteristic path length increased slightly after 0.5mm step size.

The small-worldness refers to a balance of efficient information transmission between nodes along the shortest path length. The small-worldness is quantified by two network measures; the characteristic path length and the clustering coefficient. In the present study, the small-worldness responded in various ways for the three different parameters. According to the figure 7.9 (a), the peaked small-worldness ($F(4, 45) = 2.277$, $p = 0.076$) belonged to 50^0 among turning angles. The highest small-worldness determines efficient information transmission in networks. Therefore, this result suggested that 50^0 is most likely to be optimal turning angle for small-worldness since small-worldness is highest at 50^0. Figure 7.9 (b), shows small-worldness only fluctuated slightly with the number of seeds per voxel ($F(4, 45) = 0.842$, $p = 0.506$). Figure 7.9 (c) shows when step size increases small-worldness ($F(4, 45) = 35.225$, $p = 0.000$) continuously decreased. The smallest step size 0.1 mm showed the highest small-worldness.

(a)

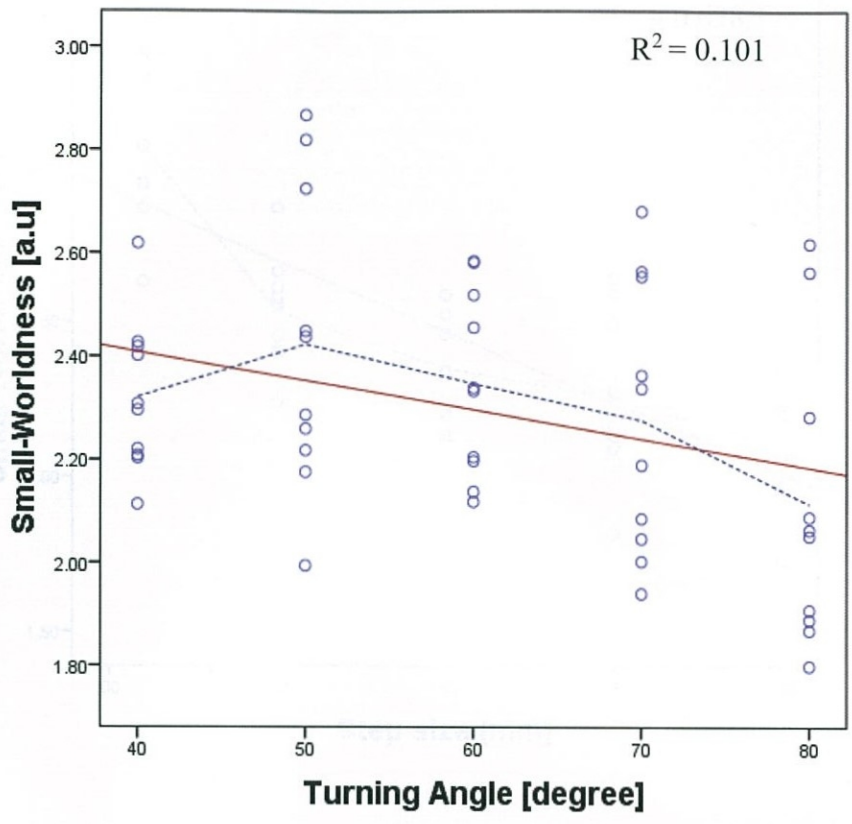
$R^2 = 0.101$
Small-Worldness [a.u]
3.00
2.80
2.60
2.40
2.20
2.00
1.80
40
50
60
70
80
Turning Angle [degree]

(b)

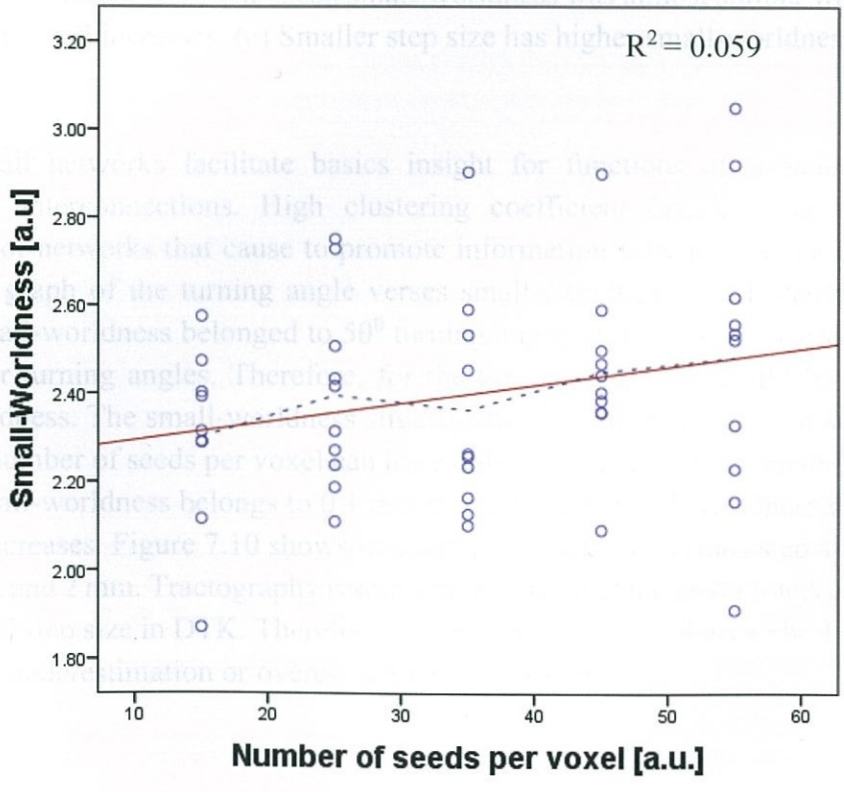
$R^2 = 0.059$
Small-Worldness [a.u]
3.20
3.00
2.80
2.60
2.40
2.20
2.00
1.80
10
20
30
40
50
60
Number of seeds per voxel [a.u.]

(c)

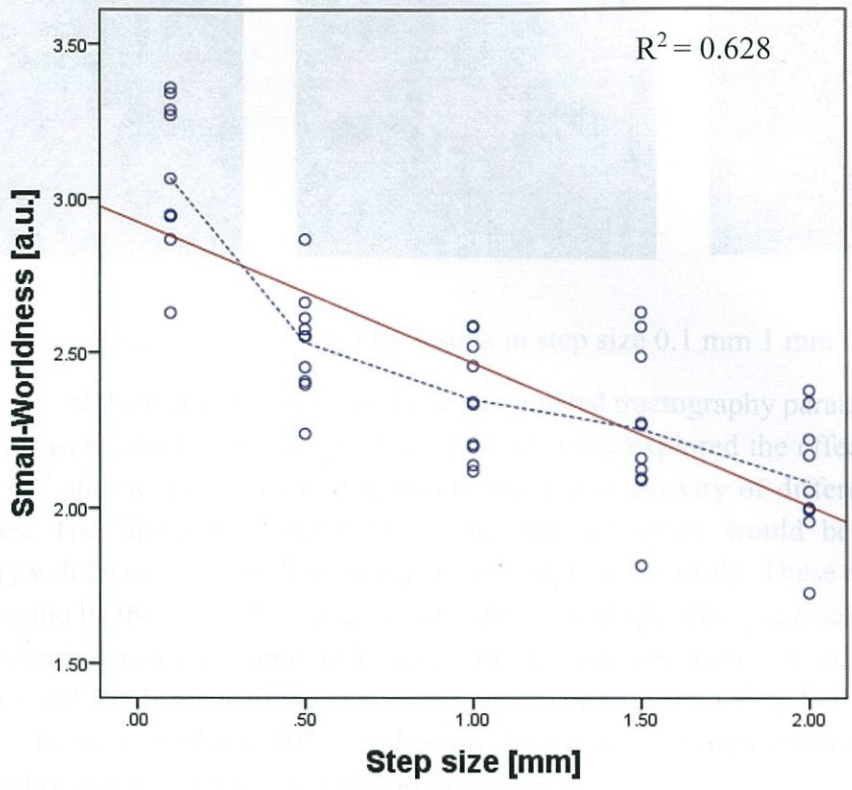

Figure 7.9 (a) The mean Small-worldness peaked at 50^0 turning angle and decreased when turning angle increases. (b) The mean small-worldness was almost similar when the number of seeds per voxel increases. (c) Smaller step size has higher small-worldness.

Small networks facilitate basics insight for functions of complex networks to understand interconnections. High clustering coefficient directly involves the small-worldness of networks that cause to promote information flow in a system. Figure 7.9 (a) shows the graph of the turning angle verses small-worldness which determined that the highest small-worldness belonged to 50^0 turning angle, and the small-worldness decreased with higher turning angles. Therefore, for the turning angle 50^0 could be optimal in the small-worldness. The small-worldness slightly altered with the number of seeds per voxel. Thus, the number of seeds per voxel can have only less impact on the small-worldness. The highest small-worldness belongs to 0.1 mm step size, and small-worldness decreased when step size increases. Figure 7.10 shows tractography results of various step sizes such as 0.1 mm, 1 mm, and 2 mm. Tractography results emphasised that the fewer tracts can be extracted with a small step size in DTK. Therefore, the average step size likely to be 1 mm which can be avoided underestimation or overestimation of fibre tracking.

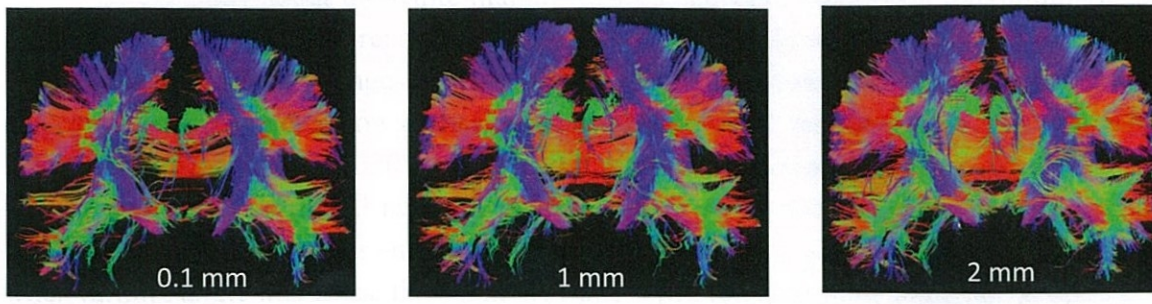

Figure 7.10 Tractography results in step size 0.1 mm 1 mm and 2 mm

Some of the research findings can be generalised tractography parameters with brain network measures in different ways. Thomas et al. have explored the effect of four angles (30^0 45^0 60^0 and 80^0) to examine the specificity and sensitivity of different tractography techniques. The findings of the results said that sensitivity would be increased, and specificity will be decreased while increasing the angular threshold. These results suggested that 45^0 would be the optimal angular threshold due to its specificity and sensitivity depends on the deterministic tractography technique. For instance, results suggested that 60^0 for DTI and Q ball and 45^0 for constrained spherical deconvolution (CSD) [61]. In the present study, small-worldness showed that 50^0 would be the drastic turning angle. However, this turning angle was not significant in other network measures.

The findings of Cheng et al. revealed that the variance of the networks is inversely related to the square root of seed density. Moreover, the author described that stability of structural network measures is increased as the number of seeds increased. Despite, DTI showed a mixed effect from more number of seeds since more seeds would extract more spurious fibres that influence on the nodal degree and edge weights in networks [62]. Our findings revealed that more connections of networks appeared with the higher number of seeds per voxel.

Chamberland et al. have determined that findings of tractography parameters can have an impact on results of graph theory which could be helpful in some clinical settings. This study suggested essential results for crossing regions such as the corpus callosum (CC) and the cingulum (Cg). The author mentioned that the best maximum angles are 60^0 and 65^0 and step size, 1.5 mm and 1 mm for CC and Cg respectively in DTI tractography and these parameters are different for HARDI techniques. Moreover, Chamberland et al. have determined that curvature of fibre bundles is different in each brain region. Thus, optimal tracking parameters can be different for each region. The interpretation of the results could be complicated as slightly different parameters brings various connectivity profiles [24]. In the present study, the whole brain connectivity considered for network measures instead of region-wise analysis. In fact, our results did not suggest any optimal parameter for whole brain tractography in the Connectome Mapper. Therefore, future study should be considered for region-wise analysis. However, the mean eccentricity peaked at 1mm step size in the present study which revealed that 1mm step size (Figure 7.6 (c)) would be the appropriate step size in DTK tractography of the Connectome Mapper.

In the study about the white matter, Tench et al. have mentioned maximum 10^0 per 1 mm step size can provide reasonable curvature anatomically while trajectories experience unexpected directional changes [65]. Bastiani et al. have examined the effect of tractography algorithm and parameters on global network density. The results determined that when turning angle changes from 30^0 to 90^0 tend to double the connections density of networks [60]. We analysed two global network measures such as characteristic path length and the small-worldness for turning angle. While the characteristic path length linearly increased when turning angle increases, the small-worldness peaked at turning angle 50^0 in our study.

The present study suggested that the higher turning angles, higher step size and a higher number of seeds per voxel more likely to extract more connections. The degree and strength increased with three parameters. The local efficiency, cluster coefficient of networks also increased when the number of seeds per voxel and turning angle increase. Although more connections were obtained when step size increases, local efficiency, cluster coefficient, and small-worldness decreased with larger step sizes. Among all network measures, turning angle 50^0 is most appropriate for small-worldness and more competent network measures such as local efficiency or cluster coefficient increased when turning angle increases. Therefore, we suggested that default values in turning angle (60^0) and the number of seeds per voxel (32) would be appropriate for tractography of the Connectome Mapper. Although, higher values in important network measures such as cluster coefficient, local efficiency, and small-worldness, resulted in smaller step size, average 1 mm step size could be acceptable to obtain the better results in tractography since fibre bundles can be under-extracted in smaller step size. Chamberland et al. have mentioned that large step size would have risk of stepping outside the bundle and smaller step size may bring numerical errors and computational burden [24]. The maximum eccentricity determines the structural quality rather than functions in networks. The highest eccentricity belonged to 1 mm step size which is the default step size in tractography in the Connectome Mapper.

This study had a few limitations. Our study was limited by small sample size. Since we used healthy subjects for the study, parameters could be slightly different for patients with pathological conditions. The results of graph theory measures would not solely depend on tractography parameters. Some parameters in other steps of the pipeline process of the Connectome Mapper could interfere with results in networks. The results of network measures depend on subjects as well. There is no option to set the FA value in tractography of the Connectome Mapper related to deterministic tractography. The sensitivity and accuracy of the tractography need to be considered in the future study. Moreover, the brain region-wise analysis would be more critical since scale and curvature of fibre bundles are different from region to region.

7.5 Conclusion

We presented three fibre tracking parameters including the turning angle, step size and the number of seeds per voxel that can impact tractography through structural brain connectivity. Although tractography parameters have exposed to arguments, optimising tractography parameters in an automated pipeline process such as Connectome Mapper using healthy subjects was a novel study. Most network measures such as degree, strength,

local efficiency, and cluster coefficient continuously increased when turning angle and the number of seeds per voxel increase. We showed that turning angle and number of seeds had no optimal value in tractography of the Connectome Mapper except a very few network measures. The results showed that turning angle 50^0 is optimal for small-worldness and 45 seeds per voxel is optimal for betweenness centrality. Since these values were not significant in many cases, suggesting that default values in turning angle 60^0 and 32 seeds per voxel can be used for connectome analysis using the Connectome Mapper. According to the step size results, the most appropriate network measures accomplished with the smaller step size except eccentricity. The 1 mm step size showed the highest eccentricity, and also tractography determined the better quality of tractography belong to 1 mm step size. However, under tracking of white matter fibres can be an issue in smaller step size. Therefore, our study proposed that the default values in turning angles, the number of seeds and step size in the DTK of the Connectome Mapper more likely to be useful in future studies with healthy subjects. Additionally, future study should give careful consideration to the choice of parameters based upon the network measures that will be analysed.

Chapter 8

Summary

DWI provides crucial information about the white matter structures which can be studied non-invasively and *in vivo*. The advancement of MRI offers more sophisticated protocols such as DTI and tractography which have been led to the possibilities in neuroscience to estimate the white matter integrity. Interestingly, combining MRI of the human brain and graph theory analysis have been combined as a robust approach for investigating large-scale networks through brain connectivity such as functional connectivity and structural connectivity. Structural connectivity can be estimated using DTI and associated white matter tractography that enables to identify the white matter pathways that connected brain regions and construct brain network architecture. Network analysis theory such as graph theory is used to form whole brain networks using Tractography.

Most of the structural connectivity studies base on most publicly available tractography methods with the default tractography parameters. However, the scale and curvature of fibre bundles depend on subjects, brain regions, and pathological conditions. Therefore, optimal parameters can be varied dramatically, and it can bring different connectivity profiles and results in different values in network measures. Therefore, access to tractography parameters could be beneficial as it will help to a better understanding of sensitive streamline features.

In this study, we aimed to understand the impact of tractography parameters related to the Connectome Mapper which is used to create connectivity matrices for graph theory analysis. We mainly focused on parameters including the number of seeds, step size and angular threshold in the tractography. Although a few studies have been conducted to optimise turning angle in tractography techniques and step size, our study is a novel study, slightly different since the parameters are related to the tractography in the Connectome Mapper. Additionally, the impact of the number of seeds per voxel on the structural network measures also has not yet been understood.

DTI data were used to construct connectivity matrices using the Connectome Mapper, and the graph theory analysis was applied on connectivity matrices using Brain Connectivity MATLAB toolbox. Connectivity measures of five different number of seeds per voxel, step sizes, and turning angles were analysed for network measures including degree, betweenness centrality, local efficiency, cluster coefficient, eccentricity, strength, small-worldness and characteristic path length.

The results revealed that more fibre tracts could be extracted when turning angle, the number of seeds per voxel and step size increase. Local efficiency, cluster coefficient increased with the higher number of turning angles and a greater number of seeds. The step size showed slightly different results on network measures. Degree, strength and characteristic path length increase with larger step size and betweenness centrality, cluster coefficient, local efficiency decreased when step size is smaller.

Our study investigated that strong dependence not suggest the number of seeds per voxel and turning angle can have more optimal than another. There are more connections can be obtained when increases tractography parameters such as turning angle and number of seeds per voxel. However, smaller step size would bring most appropriate network measures in graph theory rather than larger size step size. Finally, our results suggested that default values in fibre tracking parameters could be appropriate for the future studies with the Connectome Mapper.

Appendix 1 Abbreviations

ADC	Apparent Diffusion Coefficient
B_0	External Magnetic field
BC	Betweenness Centrality
BCT	Brain Connectivity Toolbox
C	Cluster Coefficient
CC	Corpus Callosum
Cg	Cingulum
CMTK	Connectome Mapping Toolkit
CSD	Constrained Spherical Deconvolution
CSF	Cerebrospinal Fluid
DICOM	Digital Imaging and Communication in Medicine
dMRI	Diffusion Magnetic Resonance Imaging
DTK	Diffusion Toolkit
DTI	Diffusion Tensor Imaging
DWI	Diffusion Weighted Imaging
E	Edges
EPI	Echo Planer Imaging
e(V)	Eccentricity
FA maps	Fractional Anisotropy maps
FACT	Fibre Assignment by Continuous Tracking
FID	Free-Induction Decay
fMRI	Functional Magnetic Resonance Imaging
FT	Fourier Transform
G	Graph
GRE	Gradient echo
IR	Inversion Recovery
L	Characteristic Path length
NIfTI	Neuroimaging Informatics Technology Initiative

NMR	Nuclear Magnetic Resonance
MD	Mean diffusivity
MPG	Motion Probing Gradients
MRI	Magnetic Resonance Imaging
Mxy	Transverse magnetisation
Mz	Longitudinal magnetisation
RF	Radio Frequency
ROI	Region of Interest
S	Strength
SE	Spin Echo
SNR	Signal to Noise Ratio
SW	Small-worldness
TE	Echo Time
TR	Repetition Time
V	Nodes

Appendix 2 The Configuration of the Connectome Mapper

The Connectome Mapper was built on Ubuntu 12.04.4 in the virtual machine which is VMware vSphere Client. The manual configuration was supported by one of the resources available on the http://www.nemotos.net/resources/ubuntu-connectome, and the online forum is also available to obtain some help with some feedback, comments and for the asking helps. The latest version of the Connectome Mapper is CMP v2.1.0-beta at www.connectomics.org.

In the first step, VMware VSphere Client 6 should be configured (Figure1), and Ubuntu can be installed on the workstation (Figure2).

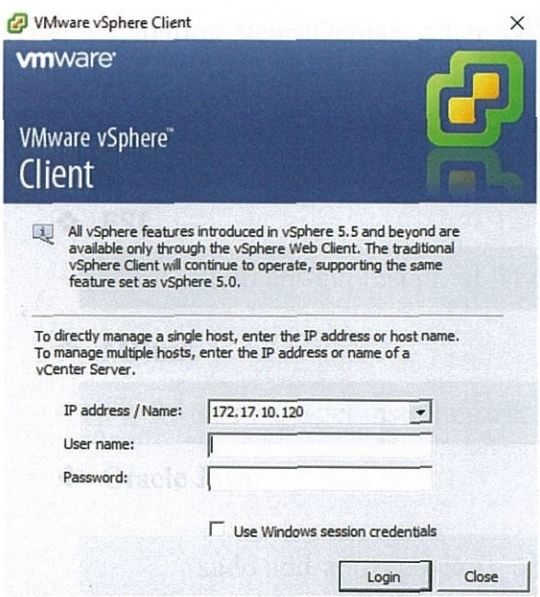

Figure 1.VMware vSphere workstation

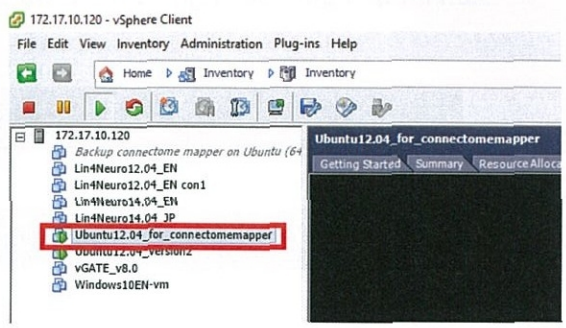

Figure 2. Ubuntu 12.04 on VMware vSphere

The Connectome Mapper installation begins with NeuroDebian installation. The relevant operation system which is Ubuntu 12.04 LTS "Precise Pangolin" (precise) and download server of Japan (Kiyotaka Nemoto) should be chosen, and the command appears for installation (Figure 3). Therefore the following command can be typed on the terminal and user could get the NeuroDebian.

```
wget -O- http://neuro.debian.net/lists/precise.jp.full | sudo tee
/etc/apt/sources.list.d/neurodebian.sources.list
sudo apt-key adv --recv-keys --keyserver hkp://pool.sks-keyservers.net:80
0xA5D32F012649A5A9
```

To update the package "sudo apt-get update" command can be used on the terminal.

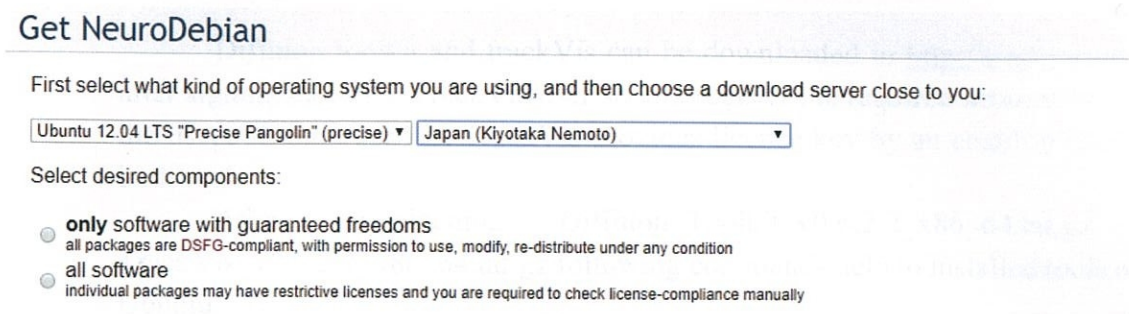

Figure 3. NeuroDebian download

After installation NeuroDebian, other tools can be installed using following commands.

- Connectome Viewer

```
sudo apt-get install connectomeviewer
```

- FSL

```
sudo apt-get install fsl fslview fslview-doc
```

- MRtrix

```
sudo apt-get install mrtrix
```

- Oracle Java

```
sudo add-apt-repository ppa:webupd8team/java
sudo apt-get update
sudo apt-get install oracle-java7-installer
sudo apt-get install oracle-java7-set-default
```

- Lapack

```
sudo apt-get install libblas-dev liblapack-dev libatlas-base-dev
```

- The libraries which need for the Connectome Mapper

```
sudo apt-get install libboost-program-options-dev libnifti-dev
libblitz0-dev
sudo apt-get install libboost-program-options1.48.0
```

- git

```
sudo apt-get install git
```

❖ Diffusion Toolkit and TrackVis

Diffuion toolkit and trackVis can be downloaded in http://trackvis.org/dtk/ after signing up to the TrackVis user should register the required information about the usage of the trackVis. TrackVis provides licence key by an email to download both tools.

After downloading Diffuion_Toolkit_v0.6.2.2_x86_64.tar.gz and TrackVis_v0.5.2.2_x86_64.tar.gz following commands help to installed tools on the Ubuntu.

```
cd /usr/local
sudo tar xvzf /home/foo/Diffusion_Toolkit_v0.6.2.2_x86_64.tar.gz
/usr/local
```

```
cd /usr/local/dtk
sudo tar xvzf /home/foo/ TrackVis_v0.5.2.2_x86_64.tar.gz /usr/local
```

❖ FreeSurfer

FreeSurfer for Linux can be downloaded in the following link.
https://surfer.nmr.mgh.harvard.edu/fswiki/DownloadAndInstall
Installation should be done using following.

The below link is used to access the Downloads before installing the FreeSurfer tool.

```
cd/home/senolab/Downloads
wget ftp://surfer.nmr.mgh.harvard.edu/pub/dist/freesurfer/5.3.0/
freesurfer-Linux-centos4_x86_64-stable-pub-v5.3.0.tar.gz
```

Installation command is here.

```
cd /usr/local
sudo tar xvzf /home/senolab/Downloads/ freesurfer-Linux-
centos4_x86_64-stable-pub-v5.3.0.tar.gz
```

In the FreeSurfer registration, there is a license which can receive through the emails. This licence should be copied to the. license manually.

#----------CUT HERE----------
ruwan@gmail.com
1234
*St0rinGs.
#----------CUT HERE----------

The command is here.

```
cd/usr/local/Freesurfer
sudo gedit .license
```

- Camino

https://sourceforge.net/projects/camino/files/latest/download was used to download the Camino and following command is used for the installation on Ubuntu.

```
unzip camino-code-xxxx(version number)
cd camino-code-xxxx(version number)
make
cd ..
mv camino-code-xxxx(version number) camino
sudo cp -r camino /usr/local
```

- Camino-Trackvis

https://sourceforge.net/projects/camino-trackvis/ was used to download the Camino-Trackvis.

```
tar xvjf camino-trackvis-0.2.8.1.tar.bz2
cd camino-trackvis-0.2.8.1.tar.bz2
 ./build.sh
cd ..
sudo cp -r camino-trackvis-0.2.8.1 /usr/local
```

- MITK-Diffusion

MITK was downloaded and installed using these commands.

```
cd /home/foo/Downloads
wget http://mitk.org/download/releases/MITK-Diffusion-
2013.09/Linux/MITK-Diffusion-2013.09.04-linux64.tar.gz
cd /usr/local
sudo tar xvzf /home/foo/Downloads/MITK-Diffusion-2013.09.04-
linux64.tar.gz
```

After all the installation, tools should be checked for the proper installation using the command on terminal.

```
cd/home/senolab
gedit / .bashrc
```

```
#FSL
. /etc/fsl/fsl.sh
#MRtrix
export MRTRIX=/usr/lib/mrtrix/bin
#Diffusion toolkit
export DTDIR=/usr/local/dtk
export DSI_PATH=/usr/local/dtk/matrices
#Freesurfer
Export FREESURFER_HOME=/usr/local/freesurfer
source $FREESURFER_HOME/SetUpFreeSurfer.sh
#Camino
export MANPATH=/usr/local/camino/man:$MANPATH
export CAMINODIR=/usr/local/camino/bin
#Camino-trackvis
export CAMINO2TRK=/usr/local/camino-trackvis-0.2.8.1/bin
#MITK
export MITK=/usr/local/MITK-2013.12.00-linux64
#MITK Diffusion
export MITKDIFFUSION=/usr/local/MITK-Diffusion-2013.09.04-linux64
#Update PATH
export PATH="${DTDIR}:${MRTRIX}:${CAMINODIR}:${CAMINO2TRK}:
 ${MITK}:${MITKDIFFUSION}:${PATH}"
```

❖ Nipype

The Connectome Mapper is needed for a modified version of Nipype.

```
cd
git clone git://github.com/LTS5/nipype.git
cd nipype
sudo python setup.py install
```

❖ Connectome Mapper

https://github.com/LTS5/cmp_nipype/releases was used to download the Connectome Mapper.

Installation can be done by following commands.

```
cd
git clone git://github.com/LTS5/cmp_nipype.git
cd cmp_nipype
sudo python setup.py install
```

The Connectome Mapper installion can be checked by typing following command on the terminal. (Figure 4)

```
connectomemapper
```

The successful installation can be evidenced with the Connectome Mapper graphical use interphase. (Figure 5)

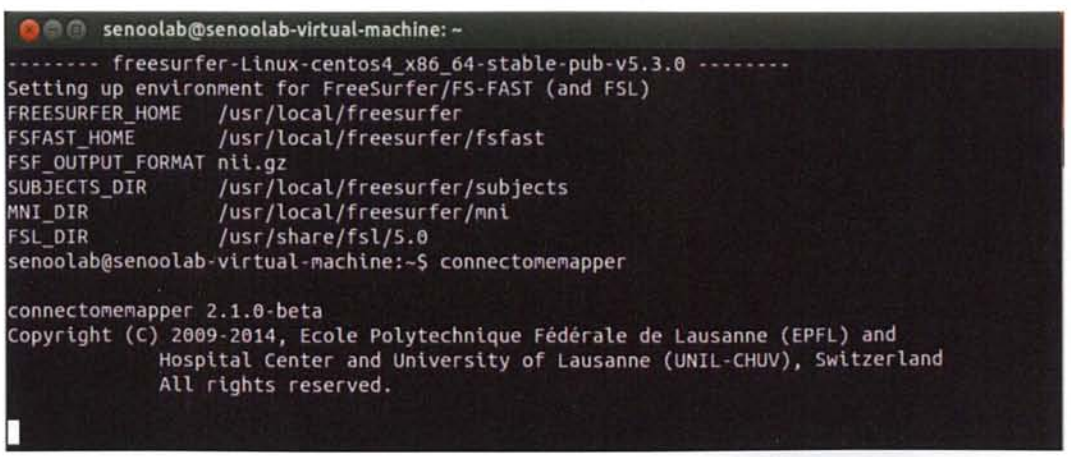

Figure 4. Connectome Mapper code on the terminal

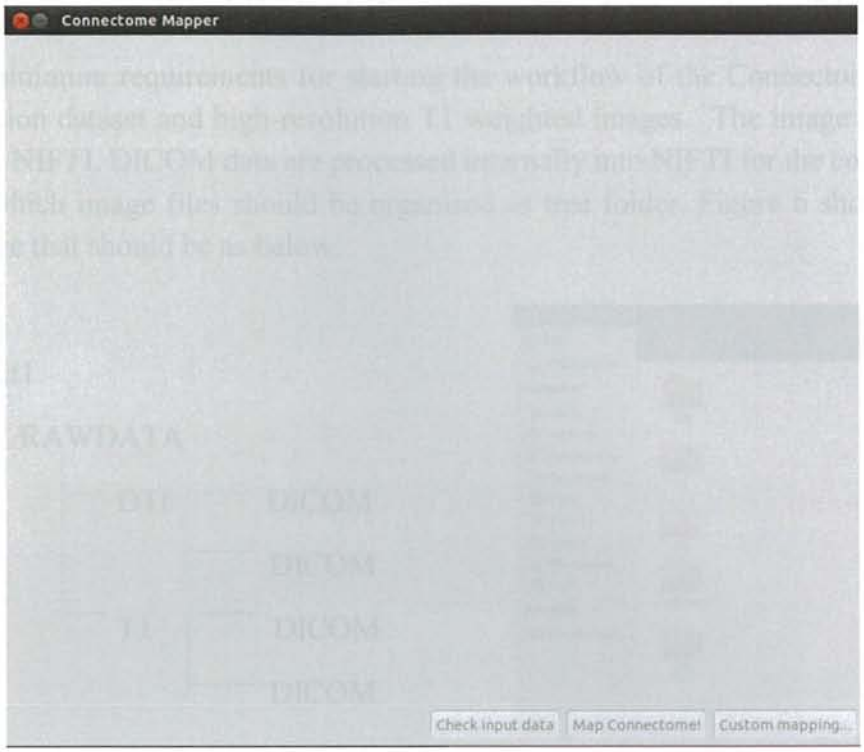

Figure 5.GUI of the Connectome Mapper

Appendix 3 The Workflow of Pipeline in the Connectome Mapper

The minimum requirements for starting the workflow of the Connectome Mapper are one diffusion dataset and high-resolution T1 weighted images. The image format can be DICOM or NIFTI. DICOM data are processed internally into NIFTI for the convenience. The folders which image files should be organised as tree folder. Figure 6 shows the the folder structure that should be as below.

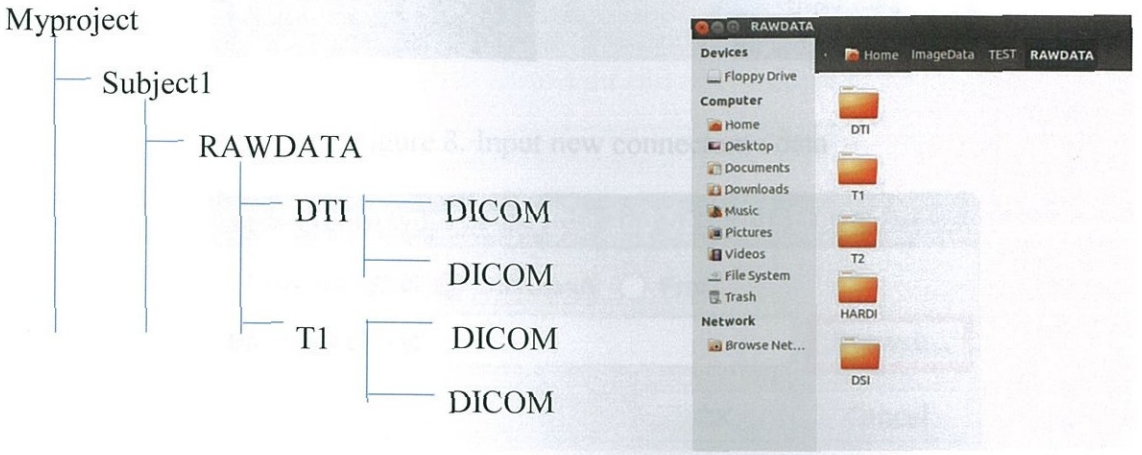

Figure 6. Folder arrangement of input data

The hierarchical files are created when starting time at the workflow. Figure 7 shows the folders that created at the beginning after started the workflow of the Connectome Mapper.

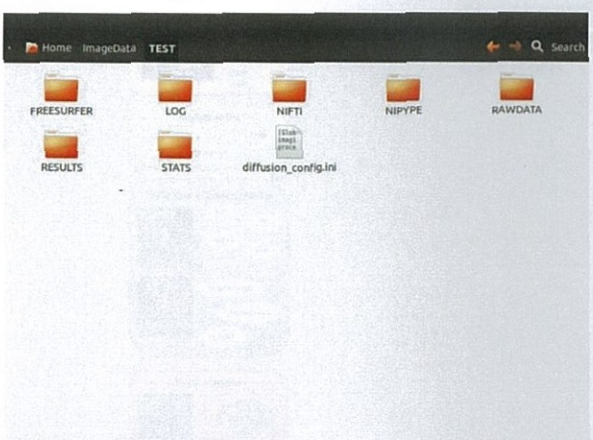

Figure 7. The files created at the beginning of the workflow

The DTI and T1 data can be input into the Connectome Mapper pipeline using the 'new connectome data' option in the GUI of the Connectome Mapper (Figure 8). The browsed data (Figure 9) should be checked for accuracy since the incorrect data will not be

able to process in the Connectome Mapper. After completing the check input data, a dialogue box will be appeared to notify whether inputs are successful or not (Figure 11).

Figure 8. Input new connectome data

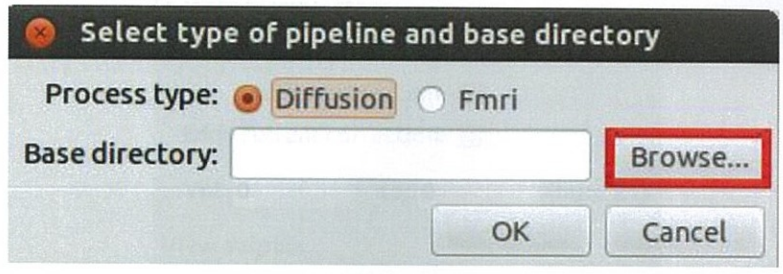

Figure 9. Selection of data type

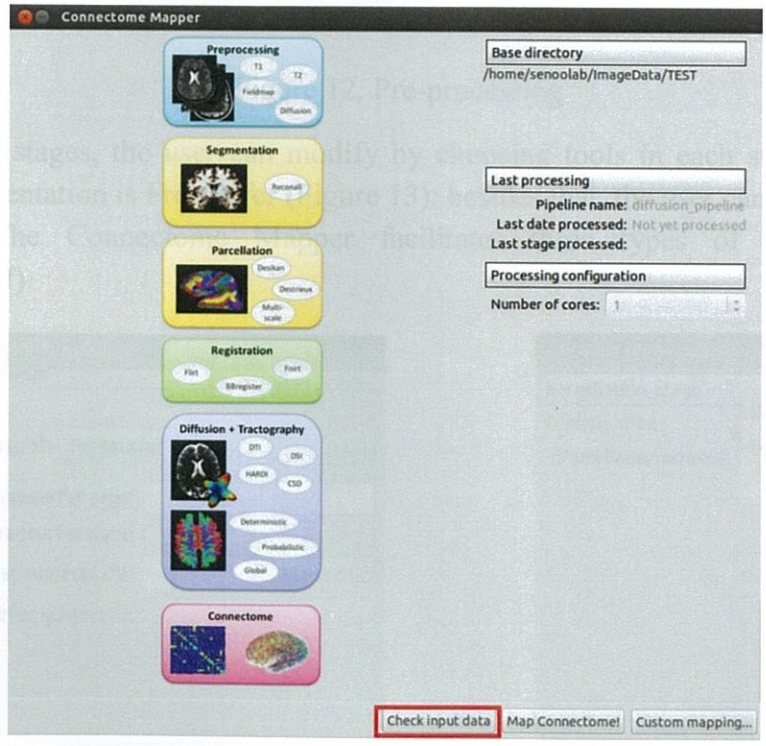

Figure 10. Checking Input data

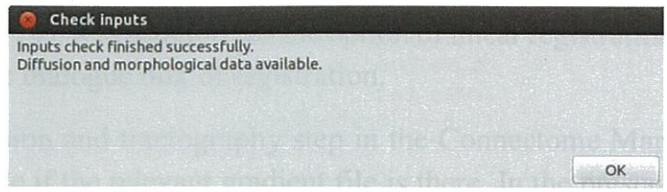

Figure 11. Dialogue box which appears after checking inputs

Once the diffusion type set, pipeline enables to start with pre-processing. The user needs to put a check on the options of motion correction and eddy current corrections.

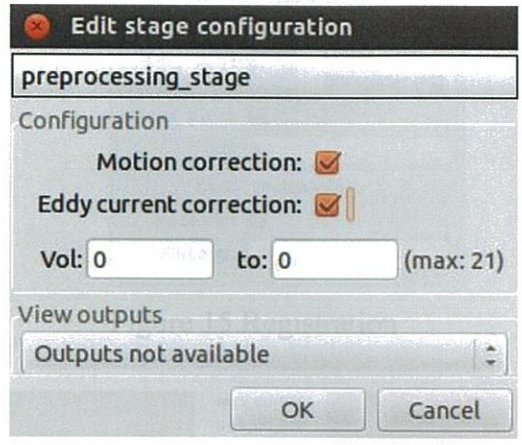

Figure 12. Pre-processing

All the stages, the user can modify by choosing tools in each stage. The default option of segmentation is Freesurfer (Figure 13); besides that, the user can select the option of custom. The Connectome Mapper facilitates three types of output such as (norm/aseg/surf).

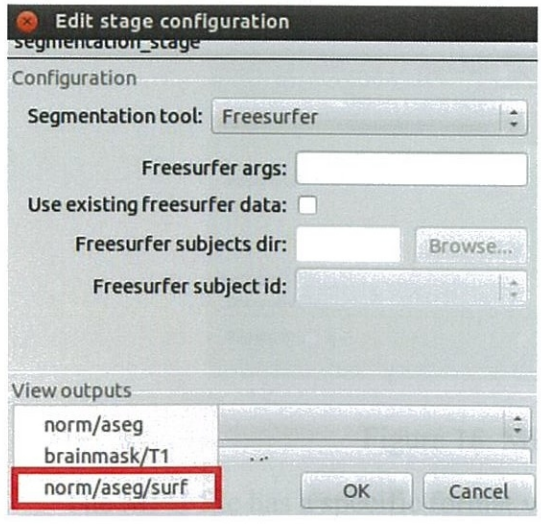

Figure 13. Segmentation

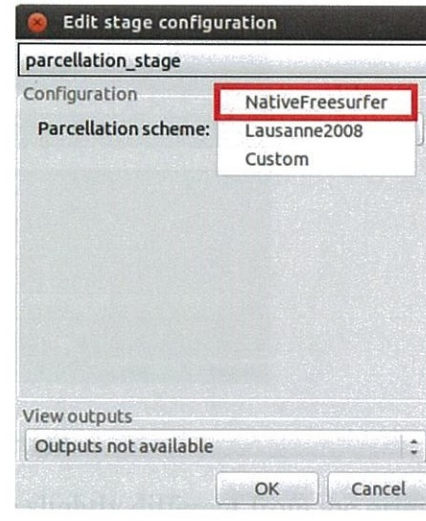

Figure 14. Parcellation

Parcellation has three options including nativeFreesurfer, Laussane 2008 and custom parcellation (Figure 14). Registration has the option of linear registration and BB registration. Figure 15 shows the dialogue box of registration.

In the diffusion and tractography step in the Connectome Mapper, the user should browse the MPG file if the relevant gradient file is there. In the present study, MRI images were obtained from a Hitachi scanner. Thus, the gradient file was manually browsed using the custom option in the DTK (Figure 16).

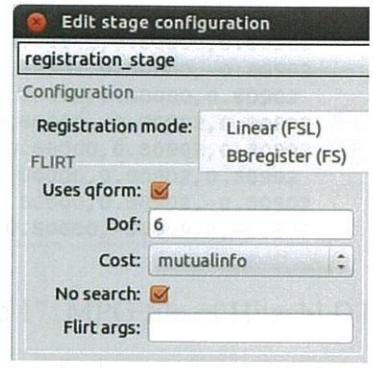

Figure 15.Registration

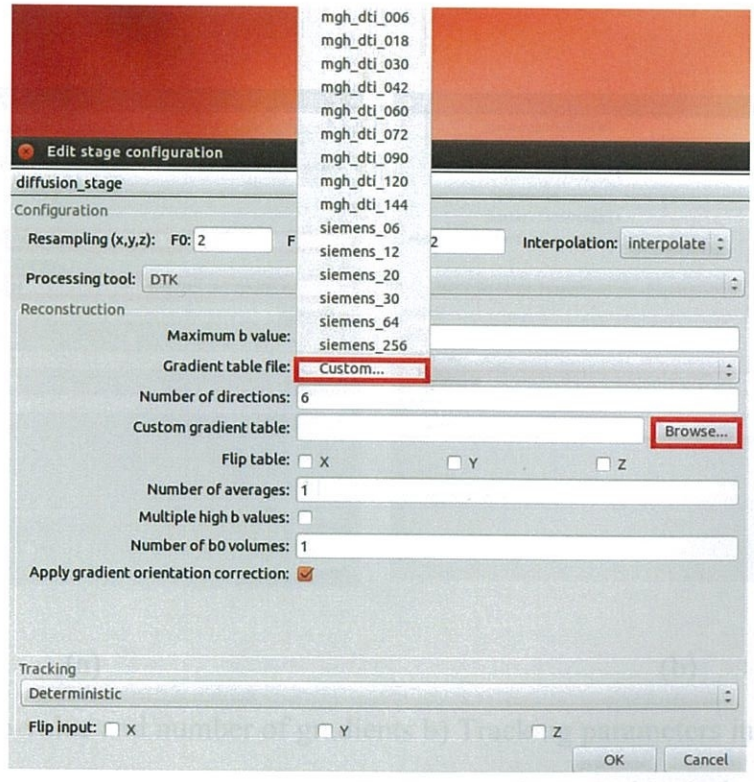

Figure 16. MPG file selection

The MPG file has a specific format which can be slightly different from the original format. In our study, we used the MPG file (Figure 17) that created by the Hitachi Medical system. However, the creating MPG file can be done using dcm2nii or MRIconvert tools.

```
0.00000,0.00000,0.00000
-0.00000,1.00000,0.00000
1.00000,0.00000,0.00000
-0.00000,0.00000,1.00000
0.52573,0.00000,-0.85065
-0.52573,0.00000,-0.85065
0.85065,0.52573,0.00000
-0.00000,-0.85065,0.52573
-0.00000,-0.85065,-0.52573
-0.80902,0.30902,-0.50000
0.80902,0.30902,-0.50000
-0.80902,-0.30902,-0.50000
-0.80902,0.30902,0.50000
0.30902,-0.50000,0.80902
-0.30902,0.50000,0.80902
0.30902,0.50000,-0.80902
0.30902,0.50000,0.80902
0.50000,-0.80902,0.30902
-0.50000,0.80902,0.30902
0.50000,0.80902,0.30902
0.50000,0.80902,-0.30902
-0.50000,-0.80902,-0.30902
```

Figure 17. MPG file of Hitachi DTI

The user should mention the details which are related to the images in this stages such as maximum b-value and the number of gradients. Figure 18 shows the configuration of DTK.

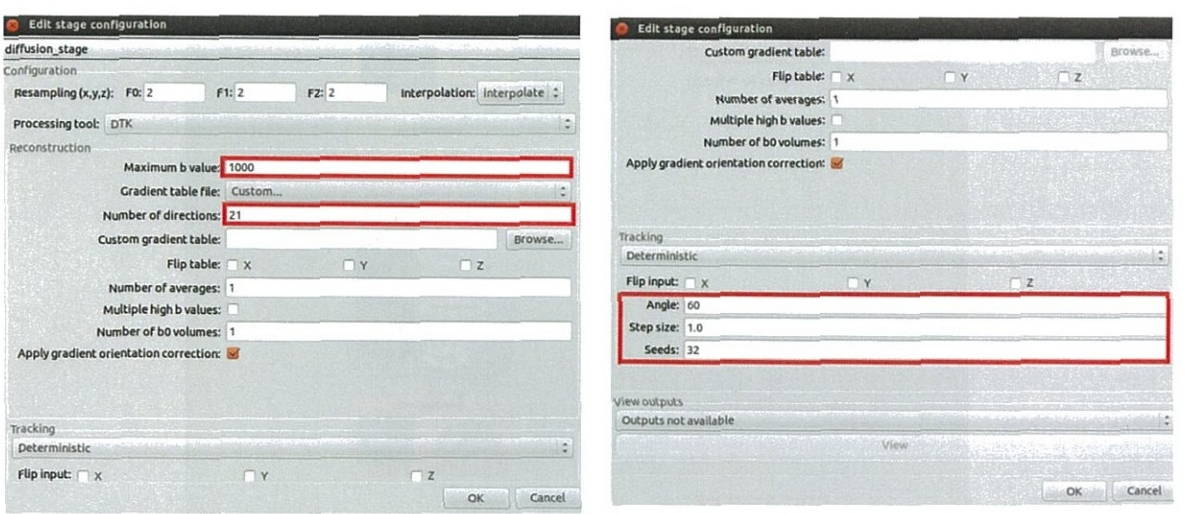

(a) (b)

Figure 18 a) b-value and number of gradients b) Tracking parameters in the DTK

In the DTK, the user can select the parameters such as angle, step size, and number of seeds. Figure 18 b) shows the tracking options in the DTK.

The final stage of connectome used to create connectivity matrices as mat files in MATLAB. These connectivity matrices can be stored as Gpickle in python, CFF or Graphml files as well. Figure 19 shows the available options to store the results.

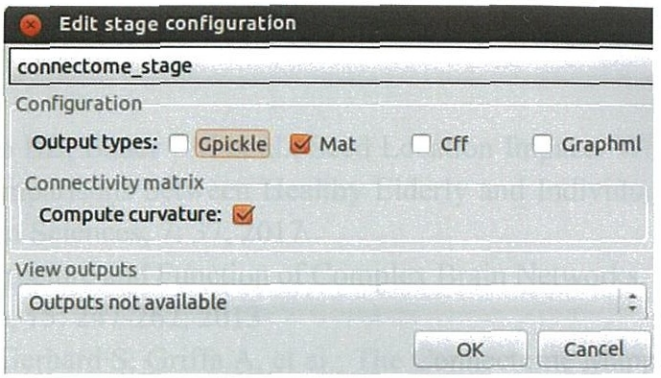

Figure 19. Connectome Stage

When the pipeline stages configured, the user can run the map connectome button on the GUI (Figure 20).

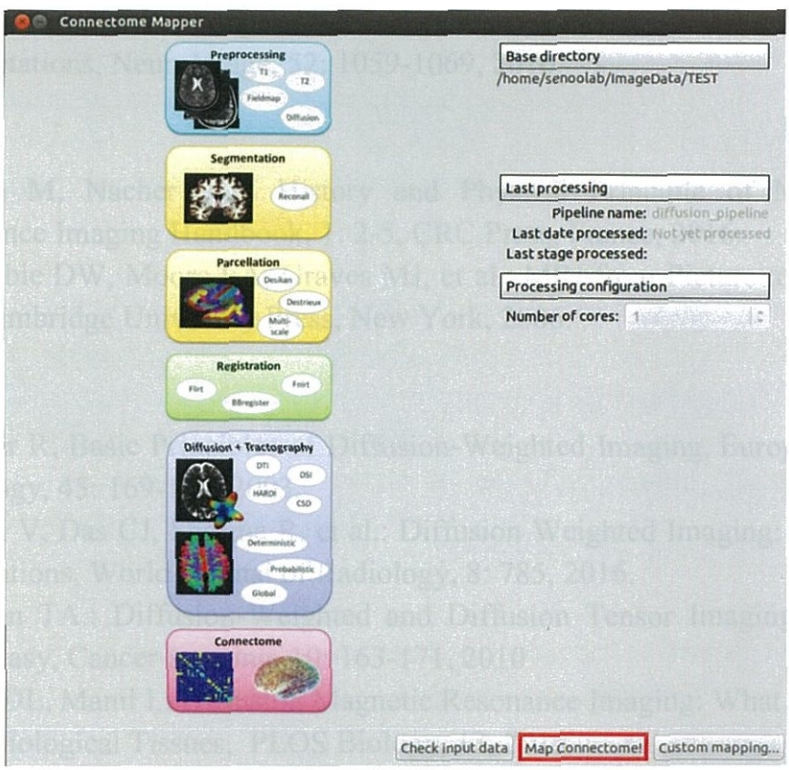

Figure 20. Start the mapping of the connectome

References

Chapter 1

1. Zajac L, Koo BB, Bauer CM et al.: Seed Location Impacts Whole-Brain Structural Network Comparisons between Healthy Elderly and Individuals with Alzheimer's disease, Brain Sciences, 7: 37, 2017.
2. Sporns o.: Structure and Function of Complex Brain Networks, Dialogues in clinical neuroscience, 15: 247-262, 2013
3. Daducci A, Gerhard S, Griffa A, et al.: The Connectome Mapper: An Open-Source Processing Pipeline to Map Connectomes with MRI, PLoS ONE, 7, 2012.
4. Chen H, Liu T, Zhao Y, et al.: Optimization of Large-Scale Mouse Brain Connectome via Joint Evaluation of DTI and Neuron Tracing Data, NeuroImage, 115: 202-213, 2015.
5. Duda JT, Cook PA, Gee J: Reproducibility of Graph Metrics of Human Brain Structural Networks, Frontiers in Neuroinformatics, 8: 2014.
6. Rubinov M, Olaf S: Complex Network Measures of Brain Connectivity: Uses and Interpretations, NeuroImage, 52: 1059-1069, 2010.

Chapter 2

7. Hayden M, Nacher P-J.: History and Physical Principle of MRI, Magnetic Resonance Imaging Handbook, 1: 2-5, CRC Press, France, 2016.
8. McRobbie DW, Moore EA, Graves MJ, et al.: MRI from Picture to Proton, 2: 30-345, Cambridge University Press, New York, 2006.

Chapter 3

9. Bammer R, Basic Principles of Diffusion-Weighted Imaging, European Journal of Radiology, 45: 169-184, 2003.
10. Baliyan V, Das CJ, Sharma R, et al.: Diffusion Weighted Imaging: Technique and Applications, World Journal of Radiology, 8: 785, 2016.
11. Huisman TA.: Diffusion-Weighted and Diffusion Tensor Imaging of the Brain, Made Easy, Cancer Imaging, 10: 163-171, 2010
12. Bihan DL, Mami I,: Diffusion Magnetic Resonance Imaging: What Water Tells Us about Biological Tissues, PLOS Biology, 13, 2015.
13. Chilla GS, Tan CH, Xu C, et al.: Diffusion Weighted Magnetic Resonance Imaging and its Recent Trend—a Survey, Quantitative Imaging in Medicine and Surgery, 5: 407-422, 2015.
14. Huisman TA,: Diffusion-Weighted Imaging: Basic Concepts and Application in Cerebral Stroke and Head Trauma, Clinical Imaging, 28: 153-155, 2004.
15. Bihan, DL,: Apparent Diffusion Coefficient and Beyond: What Diffusion MR Imaging Can Tell Us about Tissue Structure, Radiology, 268: 318-322, 2013.
16. Werring DJ Toosy AT, Clark CA, et al.: Diffusion Tensor Imaging Can Detect and Quantify Corticospinal Tract Degeneration after Stroke, Journal of Neurology, Neurosurgery & Psychiatry, 69: 269-272, 2000.

17. Aa NEVD, Leemans A, Northington FJ et al.: Does Diffusion Tensor Imaging-Based Tractography at 3 Months of Age Contribute to the Prediction of Motor Outcome After Perinatal Arterial Ischemic Stroke?, Stroke, 42: 3410-3414, 2011.
18. Mukherjee P, Berman JI, Chung SW, et al.: Diffusion Tensor MR Imaging and Fiber Tractography: Theoretic Underpinnings, American Journal of Neuroradiology, 29: 632-641, 2008.
19. Lindenberg R, Seitz RJ. : Impact of White Matter Damage After Stroke, Neuroimaging - Methods, 2012.
20. O'Donnell LJ, Westin C.: An Introduction to Diffusion Tensor Image Analysis, Neurosurgery Clinics of North America, 22: 185-196, 2011.
21. Kunimatsu, A, Aoki S, Masutani Y, et al.; Three-Dimensional White Matter Tractography by Diffusion Tensor Imaging in Ischaemic Stroke Involving the Corticospinal Tract, Neuroradiology, 45: 532-535, 2003.
22. Jellison BJ, Field AS, Medow J, et al.: Diffusion Tesnsor Imaging of Cerebral White Matter:A Pictorial Review of Physics, Fiber Tract Anatomy, and Tumor Imaging patterns, American Journal of Neuroradiology, 25: 356-369, 2004.
23. Yamada K, Sakai K, Akazawa K, et al.: MR Tractography: A Review of Its Clinical Applications, Magnetic Resonance in Medical Sciences, 8: 165-174, 2009.
24. Chamberland M, Whittngstall K, Fortin D, et al.: Real-Time Multi-Peak Tractography for Instantaneous Connectivity Display, Frontiers in Neuroinformatics, 8: 2014.
25. Essayed, WI, Zhang F, Unadkat P, et al.: White Matter Tractography for Neurosurgical Planning: A Topography-Based Review of the Current State of the Art, NeuroImage: Clinical, 15: 659-672, 2017.
26. Mori S, Ziji PCMV.: Fibre Tracking:Principles and Strategiew-A Technical Review, NMR in Biomedicine, 15: 468-480, 2002.
27. Takemura H, Caiafa CF, Wandell B, et al.:Ensemble Tractography, PLOS Computational Biology, 12, 2016.

Chapter 4

28. Fallani, FDV, Richiardi J, Chavez M, et al.: Graph Analysis of Functional Brain Networks: Practical Issues in Translational Neuroscience, Philosophical Transactions of the Royal Society B: Biological Sciences, 369: 20130521-20130521, 2014.
29. Biggs, NL, Lloyd EK, Wilson, RJ: Graph Theory: New York, USA: Oxford University press Inc, 1736- 1936. 1976.
30. Alexanderson, GL: About the Cover: Euler and Königsbergs Bridges: A Historical View, Bulletin of the American Mathematical Society, 43: 567-574, 2006.
31. Leonhard E: Solutio Problematis ad Geometriam Situs Pertinentis, Commentarii Academiae Scientiarum Imperialis Petropolitanae 8, Opera Omnia, 7: 128-140 ,1976.
32. Stam CJ, Reijneveld J: Graph Theoretical Analysis of Complex Networks in the Brain, Nonlinear Biomedical Physics, 1:3, 2007.
33. Solomonoff R, Anatol R: Connectivity of Random Nets, The Structure and Dynamics of Networks, 2011.

34. Watts DJ, Strogatz SH.: Collective Dynamics of Small-World Networks, The Structure and Dynamics of Networks, 2011.
35. Barabási A.: Emergence of Scaling in Random Networks, Science, 286:509-512, 1999.
36. Bullmore ET, Bassett DS.: Brain Graphs: Graphical Models of the Human Brain Connectome, Annual Review of Clinical Psychology, 7: 113-140, 2011.
37. Barun U, Plichta MM, Esslinger C, et al.: Test–Retest Reliability of Resting-State Connectivity Network Characteristics Using FMRI and Graph Theoretical Measures, NeuroImage, 59: 1404-1412, 2012.
38. He Y, Evans A.: Graph Theoretical Modeling of Brain Connectivity, Current Opinion in Neurology, 23: 341 350, 2010.
39. Guye M, Bettus G, Bartolomei F, et al.: Graph Theoretical Analysis of Structural and Functional Connectivity MRI in Normal and Pathological Brain Networks, Magnetic Resonance Materials in Physics, Biology and Medicine, 23: 409-421, 2010.
40. Humphries MD, Gurney K.: Network 'Small-World-Ness': A Quantitative Method for Determining Canonical Network Equivalence, PLoS ONE, 3, 2008.
41. Liao X, Vasilakos AV, He Y.: Small-world Human Brain Networks: perspectives and Challenges, Neuroscience and Biobehavioral Reviews, 77: 286-300, 2017
42. Wang J, Zuo X, He Y.: Graph-Based Network Analysis of Resting-State Functional MRI, Frontiers in Systems Neuroscience, 4:16, 2010.
43. Hage P, Harary F: Eccentricity and Centrality in Networks, Social Networks, 17: 57-63, 1995.
44. Onnela J-P, Saramaki J, Kertesz J, et al.: Intensity and Coherence of Motifs in Weighted Complex Networks, Physical Review E, 71, 2005.

Chapter 5

45. Rachid D: Computational Brain Connectivity Mapping: A Core Health and Scientific Challenge, Medical Image Analysis, 33: 122-126, 2016.
46. Lang EW, Tome AM, Keck IR, et al.: Brain Connectivity Analysis: A Short Survey, Computational Intelligence and Neuroscience, 2012:121, 2012.
47. Sporns O, Tononi G, Kotter R, et al.: The Human Connectome: A Structural Description of the Human Brain, PLoS Computational Biology, 1, 2005.
48. Eliassen JC, Boespflug EL, Lamy M, et al.: Brain-Mapping Techniques for Evaluating Poststroke Recovery and Rehabilitation: A Review, Topics in Stroke Rehabilitation, 15: 427-450, 2008.
49. Bullmore E, Olaf Sporns.: Complex Brain Networks: Graph Theoretical Analysis of Structural and Functional Systems, Nature Reviews Neuroscience, 10:186-198, 2009.
50. Fischi-Gomez E, Munoz-Moreno E, Vasung L, et al.: Brain Network Characterization of High-Risk Preterm-Born School-Age Children, NeuroImage: Clinical, 11:195-209, 2016.

51. Fischi-Gómez E, Vasung L, Meskaldji DE.: Structural Brain Connectivity in School-Age Preterm Infants Provides Evidence for Impaired Networks Relevant for Higher Order Cognitive Skills and Social Cognition, Cerebral Cortex, 25:2793-2805, 2014.
52. Szalkai B, Varga B, Grolmusz.: Brain Size Bias Compensated Graph-Theoretical Parameters Are Also Better in Women's Structural Connectomes, Brain Imaging and Behavior, 12: 663 673, 2017.
53. Kerepesi C, Szalkai B, Varga B et al.: Comparative Connectomics: Mapping the Inter-Individual Variability of Connections within the Regions of the Human Brain, Neuroscience Letters, 662:17-21, 2018
54. Szalkai B, Szalkai B, Grolmusz V.: Graph Theoretical Analysis Reveals: Women's Brains Are Better Connected than Men's, Plos One, 10, 2015.
55. Kim M, Park H.: Structural Connectivity Profile of Scans without Evidence of Dopaminergic Deficit (SWEDD) Patients Compared to Normal Controls and Parkinson's Disease Patients, SpringerPlus, 5: 1421, 2016.

Chapter 6

56. Rodrigues NB, Mithani K, Meng Y.:The Emerging Role of Tractography in Deep Brain Stimulatation:Basic Principles and Current Applications, Brain Sciences, 8, 2017.
57. Jeurissen B, Descoteaux M, Mori S, et al.: Diffusion MRI Fiber Tractography of the Brain." NMR in Biomedicine, 2017.
58. Moldrich RX, Pannek K, Hoch R, et al.: Comparative Mouse Brain Tractography of Diffusion Magentic Resonance Imaging, Neuroimage, 51: 1027-1036, 2010.
59. Liao R, Ning L, Chen Z, et al.: Performance of Unscented Kalman Filter Tractography in Edema: Analysis of the Two-Tensor Model, NeuroImage: Clinical, 15: 819-831, 2017.
60. Bastiani M, Shah NJ, Goebel R, et al.: Human Cortical Connectome Reconstruction from Diffusion Weighted MRI: The Effect of Tractography Algorithm, NeuroImage, 62:1732-1749, 2012.
61. Thomas C, Ye FQ, Irfanoglu MO, et al.: Anatomical Accuracy of Brain Connections Derived from Diffusion MRI Tractography Is Inherently Limited, Proceedings of the National Academy of Sciences, 111: 16574-16579, 2014.
62. Cheng H, Wang Y, Sheng J, et al.: Optimization of Seed Density in DTI Tractography for Structural Networks, Journal of Neuroscience Methods, 203: 264-272, 2012.

Chapter 7

63. Cao Q, Shu N, An L, et al.: Probabilistic Diffusion Tractography and Graph Theory Analysis Reveal Abnormal White Matter Structural Connectivity Networks in Drug-naïve Boys with Attention Deficit/Hyperactivity Disorders, The journal of neurosciences, 33: 10676-10687, 2013.

64. Zalesky A, Fornito A, Harding IH, et al.: Whole-Brain Anatomical Networks: Does the Choice of Nodes Matter?, NeuroImage, 50: 970-983, 2010.
65. Tench, CR, Morgan PS, Wilson M, et al.: White Matter Mapping Using Diffusion Tensor MRI, Magnetic Resonance in Medicine, 47: 967-972, 2002.

Acknowledgment

Foremost, I would like to express my sincere gratitude to my supervisor Professor Atsushi Senoo of the Department of Radiological Sciences at Graduate school of Human Health Sciences, Tokyo Metropolitan University for the continuous support of my master study and research, for his patience, motivation, enthusiasm and immense knowledge. His guidance helped me in all the time of research and writing of the thesis.

This study was supported by the research grant for the Tokyo Metropolitan City Diplomacy scholarship students. I thank the University for providing the financial support that greatly assisted the research.

I appreciate and grateful for all the academic staff for sharing knowledge during my master course classes. I would like to extend my thanks to all the staff of the International House at Tokyo Metropolitan University for supporting in various ways.

I would also like to thank Ueda Ryo, Goh Narufumi, Uchida Wataru, Watanabe Hanae, Takenaka Uki, Saitoh Yuya and other lab mates for supporting and being with me all the time. The wonderful memories in the Senoo lab will be in my mind forever. Besides, I like to specially mention and thank my colleagues, Suren Mahrajan, Salma Suman, Yeasir Arfat, Thuy Linh and Mike Sy for helping me get through two years of graduate school.

I especially like to mention Panduka Neluwala, Dr.Menaka Hindagolla, Dr.Janaka Marasinghe for helping me keep things perspective.

I must express my gratitude to Ramith Dayaratne, my husband for his continued support and encouragement.

Finally, I must express my very profound gratitude to my parents and my family members, Sri Lankan friends and, relatives for providing me with unfailing support and continuous encouragement throughout my years of study.